SYNTHESIS AND CHARACTERIZATION OF LAYERED DOUBLE HYDROXIDES (LDHs) AND EVALUATION OF THEIR ADSORBENT, ANTIMICROBIAL AND THERMOKINETIC PROPERTIES

by

APUCHU R SANGTAM

Submitted to

NAGALAND UNIVERSITY

In Partial Fulfilment of the Requirements for Award of the Degree of

DOCTOR OF PHILOSOPHY IN CHEMISTRY

DEPARTMENT OF CHEMISTRY

NAGALAND UNIVERSITY

LUMAMI-798627

NAGALAND, INDIA

2022

DEDICATED

To

My

PARENTS

(*Ihtpa Ko Üwa***)**

BROTHERS AND SISTERS

(*Ihmong, Ihfü Ko Ihnerüti***)**

ACKNOWLEDGEMENT

I express my sincere gratitude to my supervisor **Prof. Upasana Bora Sinha**, for her immense support and inspiration throughout my research, without which it would be impossible. Her constant encouragement and valuable suggestions helped me a lot in exercising my research skills beyond what is measurable and made me a potential contributor in my specialized fields.

I would also like to express my deep gratitude to my co-supervisor, **Dr. Rajib Lochan Goswamee**, for the entire field of my research and for allowing me the facilities accessible for the smooth conduct of my research. His constant support and encouragement have significantly molded me into greater success in my research subject.

I extend my gratitude to all the teaching faculties of the chemistry department, Nagaland University, **Prof. Upasana Bora Sinha (HoD)**, **Prof. M. Indira Devi**, **Prof. Dipak Sinha**, **Dr. I. Tovishe Phucho**, **Dr. M. Prabhakar**, **Dr. Nurul Alam Choudhary**, and **Dr. Seram Dushila Devi** for their encouragement and support.

I would also like to thank Nagaland University for providing me with the UGC NON-NET fellowship for financial help in my research.

I would also like to convey my special thanks to **Dr. Chubakaam Pongener** and **Dr. Aola Supong** for their kind support and interactions in my research.

Taking this opportunity, I convey my special thanks to my research labmates, **Dr. Kekholeho Richa**, **Ms. Naruti Longkumer**, **Ms. Ritupurna Karmaker**, **Mr. Basanta Singha**, **Mrs. Angunou Kheiya**, **Ms. Narola Imchen, Ms. Penlisola Longkumer, and Mr. Partha Pratim Gogoi** for their immense love, support, encouragement, and friendship.

Further, I thank all the non-teaching faculties of the chemistry department and other scholar friends for their continuous support and friendship.

Last but not least, I express my deep sense of emotions and gratitude to almighty God for the long research journey and his enormous blessings. Also, my parents, brothers, sisters, and relatives for their constant love, support, and prayers till the completion of my Ph.D. research.

Apuchu R Sangtam

नागालैण्ड विश्वविद्यालय
NAGALAND UNIVERSITY
(केंद्रीय विश्वविद्यालय) / (A Central University)
मुख्यालय : लुमामी, जिला : जुन्हेबोटो (नागालैण्ड) – 798 627
Hqrs: Lumami, Dist: Zunheboto, Nagaland – 798 627
Department of Chemistry

DECLARATION

I, **Mr. Apuchu R Sangtam**, bearing Ph.D. registration No. **Ph.D/CHE/00006**, dated **30/08/2016**, hereby declare that the content of my thesis entitled **"Synthesis and characterization of layered double hydroxides (LDHs) and evaluation of their adsorbent, antimicrobial and thermo-kinetic properties"** is the record of work done by me, that the content of this thesis did not form the basis of the award of any previous degree to me or to the best of my knowledge to anybody else, and that the thesis has not been submitted by me for any research degree in any other university or institute.

This Ph.D. thesis is submitted in compliance with the UGC Regulation 2016 dated May 05, 2016 (Minimum Standard and Procedure for Award of M.Phil./Ph.D. Degree) to Nagaland University for the degree of Doctorate of Philosophy in Chemistry.

(Apuchu R Sangtam)

(Upasana Bora Sinha)	**(Upasana Bora Sinha)**	**(Rajib Lochan Goswamme)**
Head	**Supervisor**	**Co-supervisor**
Department of Chemistry		
Nagaland University		

नागालैण्ड विश्वविद्यालय
NAGALAND UNIVERSITY
(केंद्रीय विश्वविद्यालय) / (A Central University)
मुख्यालय : लुमामी, जिला : जुन्हेबोटो (नागालैण्ड) – 798 627
Hqrs: Lumami, Dist: Zunheboto, Nagaland – 798 627
Department of Chemistry

CERTIFICATE

This is to certify that **Mr. Apuchu R Sangtam**, a registered research scholar for a Ph.D. degree in Chemistry at Nagaland University, has carried out his research work under our guidance and supervision. His thesis entitled **"Synthesis and characterization of layered double hydroxides (LDHs) and evaluation of their adsorbent, antimicrobial and thermo-kinetic properties"** is being forwarded for submission for the Ph.D. (Science) degree of this University. It is certified that he has fulfilled all the requirements according to the rules of this University regarding investigations embodied in his thesis and the work described in this thesis is original and has not been submitted for any other degree or diploma in this or any other University.

(Upasana Bora Sinha)

Supervisor

(Rajib Lochan Goswamee)

Co-supervisor

नागालैण्ड विश्वविद्यालय
NAGALAND UNIVERSITY
(केंद्रीय विश्वविद्यालय) / (A Central University)
मुख्यालय : लुमामी, जिला : जुन्हेबोटो (नागालैण्ड) – 798 627
Hqrs: Lumami, Dist: Zunheboto, Nagaland – 798 627
Department of Chemistry

COURSE COMPLETION CERTIFICATE

This is to certify that **Mr. Apuchu R Sangtam**, a registered Research Scholar for Ph.D. degree in Chemistry under Nagaland University, bearing Ph.D. Registration No. **Ph.D./CHE/00006,** has satisfactorily completed all the courses offered in the Pre-Ph.D Course Work Programme in the Department of Chemistry, Nagaland University, Hqrs. Lumami.

The course includes:

CHEM-601 Research Methodology

CHEM-602 Advance in Chemistry

CHEM-603 Literature Review, Report Writing, and Presentation.

Upasana

(Upasana Bora Sinha)
Head
Department of Chemistry
Nagaland University

NAGALAND UNIVERSITY

HEAD QUARTERS : LUMAMI

Ph. D COURSE WORK EXAMINATION

This is to certify that Mr/Ms..... **Apuchu R. Sangtam** .....

of Nagaland University bearing Roll No..... **1/16** .....*is qualified in the Ph.D Course Work Examination*

in the Department of..... **Chemistry** ....., *Nagaland University held in the Year 20.....* **17** .....

Head of Department
Head
Department of Chemistry
Nagaland University

Dean
School of Sciences

Dean
School of Sciences
Nagaland University
HQ: Lumami Nagaland

नागालैण्ड विश्वविद्यालय
NAGALAND UNIVERSITY
(केंद्रीय विश्वविद्यालय) / (A Central University)
मुख्यालय : लुमामी, जिला : जुन्हेबोटो (नागालैण्ड) – 798 627
Hqrs: Lumami, Dist: Zunheboto, Nagaland – 798 627
Department of Chemistry

Ph.D. Thesis Certificate on Plagiarism check

Name of the research scholar	Apuchu R Sangtam
Ph.D. registration number	Ph.D/CHE/00006
Title of Ph.D. thesis	**Synthesis and characterization of layered double hydroxides (LDHs) and evaluation of their adsorbent, antimicrobial and thermokinetic properties**
Name & institutional address of the supervisor	Prof. Upasana Bora Sinha Department of Chemistry Nagaland University, Lumami-798627
Name of the department and school	Department of Chemistry, School of Sciences
Date of submission	16/12/2022
Date of plagiarism check	16/12/2022
Percentage of similarity detected by the **URKUND** software	6%

I hereby declare that/certify that the Ph.D thesis submitted by me is complete in all respect as per the guidelines of Nagaland University (NU) for this purpose. I also certify that the thesis (soft copy) has been checked for plagiarism using **URKUND** similarity check software. It is also certified that the contents of the electronic version of the thesis are the same as the final hard copy of the thesis. A copy of the report generated by the **URKUND** software is also enclosed.

Apuchu

Place: (Name & signature of the Scholar)

Date:

Upasana

Name & signature of the Supervisor:

List of figures

List of tables

CONTENTS

Chapter 3B: Applications of adsorption study on 2,4-DNP removal from aqueous solution: A theoretical study complemented by first principle DFT Monte-Carlo approach.

Chapter 4A: Synthesis and Characterization of a novel Co(II)-Co(III) LDH and Ac@Co(II)-Co(III) LDH nanohybrid

Chapter 6: Summary and Conclusion

Appendix:

CHAPTER 1

Introduction

This chapter gives an overview of the layered double hydroxide (LDHs). The salient points of this section cover the detail of the general introduction, properties, crystal structures, and the scope of current research applications.

1. Introduction

1.1. Layered double hydroxide (LDHs)

Layered double hydroxides (LDHs), also known as "Hydrotalcite-like compounds (HTlc)", "Hydrotalcite-type compounds (HTtc)", and "Anionic clays", are the most commonly used terminology to describe a wide range of layered materials. In Sweden, around 1842 was the first attempt to describe hydrotalcite as having a similar appearance to that of the clay-like powder, which is composed of hydroxycarbonate of magnesium and aluminum. Later, several hydrotalcite were reported, including that of magnesium and iron, and because of their likeness to gold, they are called pyroaurite. The first chemical formula of hydrotalcite was put forward by E. Manasse around 1915 in Italy to represent one of the naturally occurring layered materials called anionic clays. He considered carbonate ions as essential ions that exist in between two hydroxide layers[1,2]. Thus, "LDHs" is used as a representative term to designate those common terms in the present context. The unique feature of the LDHs properties and their structure is that these materials are distinct from "cationic clays", where the structures are composed of positively charged metal hydroxide sheets with interlayer anions localized between them[3]. In the actual chemical composition of LDHs, the term layered hydroxycarbonates of magnesium and aluminum called "Hydrotalcite" has been used to denote the di- and trivalent magnesium and aluminum, and the "carbonate" considered the basic interlayer ions. Hence, the importance of such mineral has a general formula [$Mg_6Al_2(OH)_{16}$ $CO_3 \times 4H_2O$], which is used to designate the layered hydroxide materials. Mg, Al, OH, CO_3, and H_2O denote magnesium, aluminum, hydroxides, carbonates, and water molecules[2].

Likewise, the chemical composition and general formula of the synthetic LDHs can be expressed as; $[M^{2+}_{1-x}M^{3+}_{x}(OH)_2]^{x+}(A^{n-})_{x/n} \times yH_2O$. M^{2+} and M^{3+} denote di- and trivalent metallic cations (M^{2+} = Mg, Ca, Ni, Fe, Co, Zn, etc., and M^{3+} = Al, Fe, Co, Cr etc.). A^{n-} and

yH_2O represent interlayer anions and the overall charge density of LDH layers, and water as a neutral molecule. Also, the subscripts x denote the di- and trivalent metallic ratios of LDHs i.e, $x = M^{II}/M^{II} + M^{III}$[4]. The fascinating feature of LDHs structure is that the overall electrical charge sometimes results in excess positive charges triggered by partial substitution of M^{2+}/M^{3+} cations. Simultaneously, the excess charge is compensated by charge-balancing anionic species present in the interlayer domain. Hence, in a solid state, the overall charge becomes electrically neutral[5]. For the sake of simplicity, one can presume that the stacking pattern of LDHs structure commonly exhibits that of the brucite-like mineral i.e., $Mg(OH)_2$ or $Al(OH)_3$ type, in which the hydroxyl groups (OH) are octahedrally coordinated to bimetallic LDH cations. Depending upon the flexibility or interchangeability nature of LDH, the structure can be tuned into different unusual combinations, which results in a binary, trinary, or ternary LDH system[6]. The exchangeable property of LDHs is due to weak forces like covalent bonds, Van der Waals, or hydrogen bonding in the interlayer domain[7]. In the present research context, several reported literature about the LDH combination to produce hybrid LDH material or intercalated LDH nanocomposite has proven to be the leading topic for vast applications[5].

Some unique properties of LDHs are excellent catalytic, electrochemical, magnetic, photocatalytic, intercalation, high thermal stability, high ion-exchange capacity, and high surface areas with high positive charges. Another potential or attractive property of LDHs that differs from cationic clays is the reconstruction of their structure after undergoing structural transformation, called the “memory effect”[8]. Furthermore, it is well known that LDHs also act as a “nanoreactor center” in the selected confined region. Because of these, they act as a selective anion scavengers, ions-exchanger, polymer stabilizers etc[9]. In recently reported literature, all of these properties could be better achieved after calcination

reactions. Because of these, LDHs play an important role in diverse chemical applications like electrochemical, adsorption, catalytic, intercalation, antimicrobial, sensors, photochemistry, water splitting mechanism, flame retardant, biomedical, fuel cells, drug delivery, agriculture etc[3,5]. Generally, LDHs are three-dimensional (3D) inorganic layered nanocomposites characterized by regular hexagonal, monoclinic or rhombohedral stacking placed on top of each other, similar to the graphene layers[10]. Hence, it shows a polytypism in crystal geometry. Moreover, it is well known that LDHs are recognized as multifunctional nanomaterials that fall under a nano range of micro, meso, or in some cases, macro-size[11]. The diversity of pores depends on the precursors and methods used in the study, which needs control synthesis procedures. Hence, the study of LDHs gains potential applications in the fields of inorganic material science or nanoscience.

1.2. Crystal structures of LDHs

As stated, the basic structure of LDHs is similar to that of the naturally occurring brucite-like anionic clays where the hydroxyl groups are octahedrally coordinated to the bimetallic LDHs forming a plane of paper-like sheets and thereby create a layer-by-layer assembly. The crystal structures of hydrotalcite and brucite are shown in Figure 1.1[12,13]. The brucite structure consists of a hexagonal closed-packing configuration of OH ions, and when M^{2+} occupies the alternate octahedral sites, the overall LDHs structure becomes neutral. Another important point to note is that the LDHs are built up with high positive hydroxyl ions due to the isomorphous substitution of divalent species by trivalent cations. The excess positive charges developed by metal hydroxide sheets are counterbalanced by the intercalated anionic species. In comparison, it is seen that the structure bears a resemblance to each other in terms of the geometry and atomic arrangements along ZX crystallographic axes[14]. Moreover, the position of metal hydroxide sheets is vertically arranged on top of other, separated by the space containing a region called interlayer space.

The distance (angstrom or nanometer) between the two metal hydroxide sheets containing space is called interlayer/interdomain/interlamellar spacing. Also, the two metal hydroxide sheets have several intercalated ions or molecules, which affects the orientations of bimetallic hydroxide layers, called interplanar or d-spacing (d_{00l}). This d-spacing determines the orientation and distance between the two-layer separation of LDHs nanosheets, represented by crystallographic planes[15].

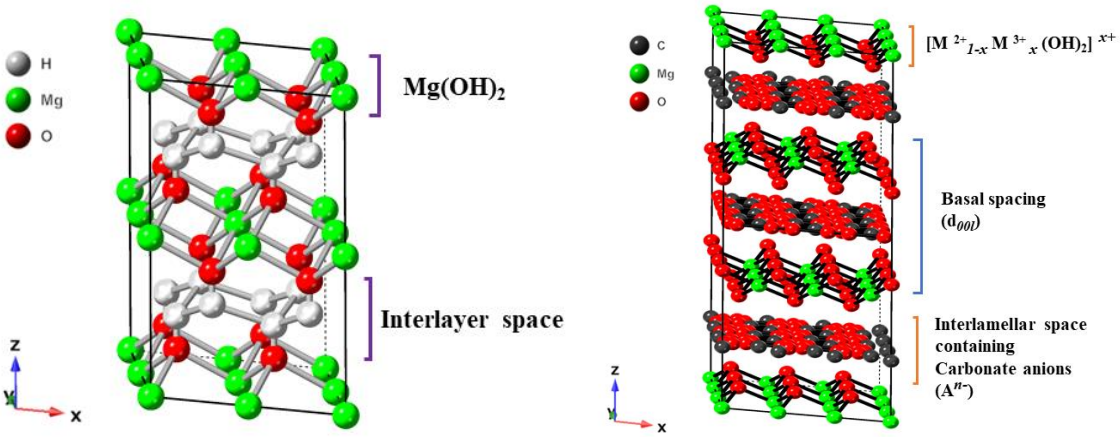

(a) **(b)**

Figure 1.1. Showing crystal structures of **(a)** Brucite at 2×2×2 supercell and **(b)** Hydrotalcite at 3×3×1 supercell

Due to the isomorphous substitution of some of the Mg^{2+} ions by Al^{3+} cations, the overall structure of LDHs results in positively charged sheets in the octahedral configuration. To maintain electrical neutrality, some of the interlayer anions, such as CO_3^{2-}, halides, polyatomic etc. are essential[16]. Similar to brucite structure, the stacking pattern of LDHs sheets follows the sequence of the hexagonal type, i.e. $[AcBZAcB]_n$ where A, B represent the hydroxide layers, c represents the layers of bimetallic cations, and Z represents the interlayer anions and neutral molecules[4]. It should be noted that the d-spacing or basal spacing of the hydroxide layers does not always remain the same. It is due to the nature of metallic cations or the number of interlamellar anions that exist in the host LDH layers[17]. However, the value of lattice parameters such as *a*, *b*, or *c* and cell

angles α, β, γ must lie in the same approximated range by taking hydrotalcite as a common reference. In the present context, several reported literature contains information where the change in lattice constants varies with the change in precursors or intercalated anions for hybrids LDHs nanocomposite[18]. Some of the important factors that could affect the crystallographic parameters are the change in atomic radii of di- and trivalent cations[10]. Another critical factor affecting the crystal geometry of LDHs is the Jahn-Teller distortion for the octahedral complexes. The effects are more susceptible to those metals in the first-row transition series followed by the second series[19].

1.2.1. Flattening of octahedral LDHs structure and geometry distortion caused by the Jahn-Teller effect

It is known that the crystal geometry of LDHs does not always show a regular octahedron arrangement of hydroxyl groups around the central metals. However, due to some imperfection in the spatial orientation of LDHs atoms, sometimes it crystallizes into different geometry[20]. Two important factors critically affect the geometry of LDHs *viz.* pseudo-stacking caused by the arrangement of LDHs atoms and the Jahn-Teller distortion. Both factors lead to the flattening of octahedral units and, as a result, reduce the symmetry of LDHs crystal from O_h to D_{3d} subgroup[21]. Figure 1.2. and Figure 1.3. shows the Jahn-Teller effect that might occur on LDHs crystals and compression of the octahedral unit to D_{3d} point group[1,22]. LDHs containing transition elements with more unpaired d-electrons would most likely undergo a distortion. Figure 1.2. illustrates the distortion caused by Jahn-Teller effect having only a d^4 configuration. However, the effect is less likely in LDHs containing a d^5 high spin state. This is because distortion will not occur when there is no net energy change in e_g orbitals, having two degenerate states (dz^2, dx^2-y^2). Subsequently, in order to stabilize the degenerate states of the orbital, the t_{2g} orbital should remain energy neutral because the distortion takes place only in e_g energy states.

Another important factor for imperfection in LDHs structure is the elongation and compression of octahedral units. These two occur parallelly with and without z components. When the stabilization of d-degenerate orbitals (lowering in energy) occurs along z-components, causing elongation, and conversely, without z-components, causes compression of octahedron LDHs geometry[10].

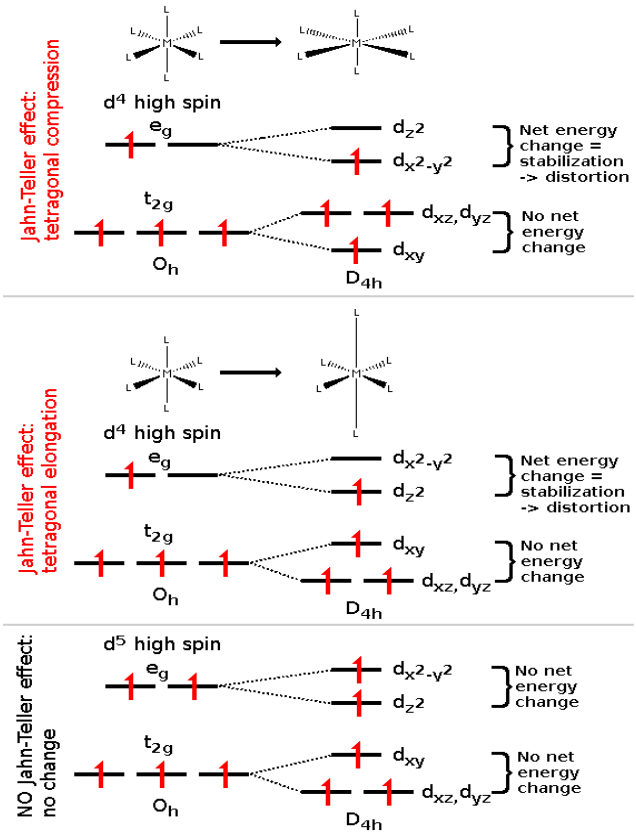

Figure 1.2. Illustration of Jahn-Teller effect on LDHs geometry

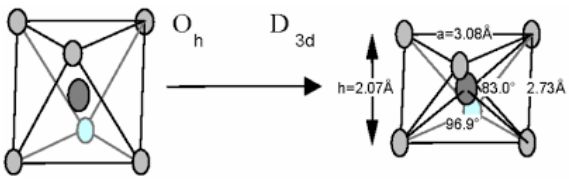

Figure 1.3. Flattening of octahedral (Oh) to D3d point group symmetry

Jahn-Teller distortion is more pronounced in the case of octahedral and tetrahedral complexes[23]. Because of such an effect in the non-linear system, the geometry of LDHs undergoes distortion and reduces its symmetry. Transition metals are commonly known to exhibit variable oxidation states from +1 up to +8 in their d-subshells. Ligands generally

stabilize them at six-coordinate points to satisfy the octahedral valency. Because of this, the d-orbitals of transition metals containing unpaired electrons (high-spin) experience distortion caused by the Jahn-Teller effect. Studies have proved that the Jahn-Teller effect of LDHs can be seen in the transition metals containing copper, nickel, zinc, chromium, iron, cobalt, and some alkaline metals like magnesium, calcium, and aluminum due to the degeneracy of the octahedral LDHs complex[24]. Jahn-Teller effect is an important phenomenon for determining the stability of complexes because it deals with the distortion and electronic excitation in the degeneracy of orbitals.

1.3. Pseudo-stacking among LDHs polytype

It is known that the stacking pattern of LDHs sheets generally takes the form of either two-layered hexagonal ($2H_1$) or three-layered rhombohedral ($3R_1$) polytypes. Studies have shown that the sequence of stacking patterns of LDHs is random, and they usually deviate from the ideal structures[25]. The factors affecting the stacking faults could be the synthesis procedure, nature of interlayer ion/molecules that reside in the LDH layers, symmetry and mode of coordination of the intercalated species, electronic charge, size or atomic radii of atoms that could result in pseudo-stacking of LDHs structure[26]. There are three possible ways in which the two-layered hexagonal stacking sequence could be arranged;...AbC=CbA=AbC... $2H_1$, ...AbC~AcB~AbC... $2H_2$, ...AbC~BcA=AbC... $2H_3$ In the case of the $2H_1$ polytype, the cations all occupy b positions, whereas for the other two polytypes, the cations alternate between b and c sites. It should be noted that the interlayers in the $2H_1$ polytype are all prismatic, and those in the $2H_2$ polytype are all octahedral, whilst in the $2H_3$ polytype, both types of interlayers are present. In the case of three-layered rhombohedral LDH, nine possible polytypes could be observed. Two of these have rhombohedral symmetry (3R):...AbC=CaB=BcA=AbC... $3R_1$ ...AbC~BcA~CaB~AbC... $3R_2$ whilst the remaining seven have hexagonal symmetry:

...AbC~AcB~AcB~AbC... $3H_1$ ...AbC~AcB~CaB~AbC... $3H_2$

...AbC~AcB=BcA~AbC... $3H_3$ ...AbC~AbC=CbA=AbC... $3H_4$

...AbC~AcB=BaC~AbC... $3H_5$ ...AbC~AcB~CbA=AbC... $3H_6$

...AbC~AbA~BcA=AbC...$3H_7$

From the above polytypes, the cations are homogenously distributed over a, b and c sites in the case of the $3R_1$, $3R_2$, and $3H_2$ polytypes. For the $3R_1$ polytype, the interlayers are all prismatic, and in the case of $3R_2$, $3H_1$, and $3H_2$, they are all octahedral; other polytypes involve both types of interlayers. Some authors have also described the large number of possible six-layer polytypes, some of which have rhombohedral symmetry (6R) and the remainder hexagonal symmetry (6H)[10].

1.4. Powder X-ray diffraction (PXRD) studies

PXRD is considered an important tool for solving the complex crystal system or visualizing the polymorphism among LDHs. As stated, the stacking pattern in most of the LDHs sheets results in non-uniform basal spacing (Å), and reports have shown that it is not possible to presume the correct orientation of all the reflections peaks obtained from XRD measurement or the diffraction planes at each Bragg's positions (2 theta). In most cases, the diffraction planes of (*hkl*) values such as (*00l*), (*10l*), (*01l*), (*11l*) etc. result in the broadening of XRD peaks or peaks become narrow[10,27]. As said, there are various possible ways of undergoing pseudo-stacking on LDH layers, which results in the mismatch of the correct LDHs sequence. Another important factor in distinguishing whether it is rhombohedral or hexagonal geometry is the systematic absences[28]. For instance, the selection rules of the miller index when (hkl) value gives rise to unless -h+k+l=3n (reflections systematically absent), crystallizes to rhombohedral crystal and conversely when it is dominated by strong reflection, where -h+k+ #3n, crystallizes into hexagonal symmetry, wherein n is called an integer and h, k, and l are the hexagonal miller

indices. Reports have shown that a monoclinic crystal system of LDHs is also possible[29]. In such a crystal system, the LDHs result in uniform composition of di- and trivalent metal hydroxide sheets, however irregular orientation of LDHs interlayer species. As a result, it gives one of the 3R rhombohedral polytypes with the space group C2/m. The complete stacking sequence results in ...=Ac1B=Ba1C=Cb1A=… type and with the lattice parameters a = 5.266, b = 9.114, c = 7.766 Å[3]. Sometimes, it is important to have a close view of lattice parameters obtained after indexing and retrieved refinement studies (R_F), because this will undoubtedly give information about the crystal system. Therefore, to ascertain the stacking sequence/layers arrangement/geometry of LDHs, one has to have a close look in terms of diffraction lines, peaks intensity, d-spacing values, or lattice parameters by taking the Mg-Al hydrotalcite as a common reference[30]. In other words, if the synthesized compounds are new, one must follow certain criteria for solving the crystal structures. As previously stated, LDHs exhibit polytypism, which means they possess polytype structures in terms of stacking sequence and crystal geometry. Therefore, the orientation of metal hydroxide layers might result in non-uniform stacking despite it crystallizes into the same space group. To understand this, the Mg-Al hydrotalcite can be used as a standard reference. In such a case, it crystallizes into two possible geometry; hexagonal (2R) and rhombohedral (3R). The possible lattice parameters i.e., a=b= 3.05-3.07, and c= 23.22-23.3, with the diffraction angles α=90, β=90 and γ=120[31]. However, depending on the type of precursors used, the lattice parameters may vary from atom to atom. The most crucial factor may be associated with synthesis procedures for obtaining the hybrid LDHs composite and the introduction of guest molecules grafted into host LDHs molecules. Besides, some factors like heat or temperature might result in a change in the polytype of LDHs. At high temperatures might affect the crystallinity, morphology, and geometry[32].

1.5. Nature of M(II) and M(III) cations

The M^{2+}/M^{3+} cations determine the key formation of LDHs. Table 1.1 shows the possible combination of M^{2+} and M^{3+} cations in terms of size and ionic radii. For instance, Be^{2+} is too small for octahedral coordination. Ba^{2+} and Ca^{2+} are comparatively large with beryllium and magnesium atoms.

Table 1.1. Ionic radii of some divalent and trivalent cations (Å)

M^{2+}	Be 0.30	**Mg** **0.65**	Cu 0.69	Ni 0.72	Co 0.74	Zn 0.74	Fe 0.76	Mn 0.80	Cd 0.97	Ca 0.98
M^{3+}	**Al** **0.60**	Ga 0.62	Ni 0.62	Co 0.63	Fe 0.64	Mn 0.66	Cr 0.69	V 0.74	Ti 0.76	In 0.81

From Table 1.1, the trends in metallic radii increase from left to right. Fundamentally, it should be noted that a larger or small ionic radius value is incompatible with di and trivalent LDH formation. Therefore, to make a possible combination of LDH, the size of di- and trivalent metallic radii should not deviate enormously. Therefore, the best way to view this is to closely consider the Mg-Al LDH system in terms of size or ionic radius. In this LDH combination, the size of ionic radii of the bimetallic Mg and Al cations look close in proximity, and the size of M^{2+} cations should be slightly greater than M^{3+} cations for octahedral coordination[2]. Also, it has been known that a pure LDH could be obtained in the divalent and trivalent metallic ratio $x = M^{III}/M^{II} + M^{III}$, which has to be equal to $0.2 \leq x \leq 0.4$. For x value more than the measurable limit results in other unusual LDH structures[10]. In some cases, monovalent and trivalent Li-Al LDH combination is also reported. The difference with other LDHs is the high charge density in the case of lithium-aluminium LDH[33].

1.6. Nature and impact of interlayer ions

The study of layered double hydroxides is an exciting subject. The reason because of its high ion-exchange properties, flexibility, or tunable structure, one can opt for the choice of interest. The interlayer or inter-domain ions of LDHs can vary from ions to molecules. Polyatomic ions such as CO_3^{2-}, NO_3, PO_4, SO_4, OH, ClO_3, [Fe(CN)], CrO_4 etc. are the common ions that can be introduced in the bimetallic LDHs layer. Also, Inorganic halide ions such as F, Cl, Br, I and organic molecules or macromolecules like DNA/RNA, proteins, carbohydrates, lipids, fats, drugs etc. can be selectively intercalated or exchanged in the layers. It is well known that carbonate ions are considered the inherent interlayer ions in the bimetallic LDHs layers[3,5].

The impacts of interlamellar ions or molecules of LDHs are of great interest and have a potential application in the field of nanoscience, which would result in a unique nanostructured material in terms of morphology and enhanced applications[16]. In recent times, studies have shown that the grafting of guest molecules results in intercalated or hybrid LDH nanocomposite. Studies have shown that the introduction of guest molecules into LDH layers changes crystal morphology[17]. Because of these reasons, there is a slight change in lattice parameters or diffraction planes[34]. Thus, the intercalation of various organic or inorganic species in LDHs interlayer domain can be extensively used for several nanoscience applications.

1.7. Computational/theoretical applications

Chemistry is the study of how particles behave, react, and the interaction of ions/molecules takes place. These interactions of particles or reactions can be best visualized and described by some basic or sophisticated solid-state computing software. A computation or theoretical simulation studies are essential in defining the electronic structure of materials (solids). In the present context, molecular dynamics or quantum-

based computational models are considered important modules for understanding materials' properties at macroscopic or atomic levels[35]. The simulation of the electronic structure of materials, including energy minimization, orbitals energy calculation, band structure and band gap energy, rotational/translational/vibrational frequencies, electronic charges, etc. are considered essential parameters for understanding the complex system of materials[36]. Various modules have been popularized in the present day. The most popular ones are DMol^3, forcite, CASTEP, Gaussian, quantitative structure-activity relationship (QSAR), sorption, and many more[37]. All these modules have different uses based on the target of the study. Most importantly, these are based on first-principle density functional theory (DFT) at a molecular or quantum dynamic level. Nowadays, a plane wave basis set and pseudopotential methods are the most popular ones used in DFT quantum computing research to understand the dynamics of the electronic structure of solids[38]. Besides, many solid-state chemistry/physics programs such as gromacs, LAMMPS, desmond, spartan, ABINIT, VASP, quantum espresso, SIESTA etc. are some of the basic software packages used in modern days[39]. In the present studies, the molecular dynamics (MD) involving DmoL^3, Monte-Carlo, Forcite, and Gaussian were successively carried out to understand the adsorbate-substrate interaction mechanism, binding energy, hydrophobic and hydrophilic nature, and orbital energy calculations[40,41]. In any simulation studies, the successive timeline for structure solution always starts with designing the molecular structure and proper atomic inputs, followed by energy minimization and interaction of matters. During such a process, some important energy input parameters involving energy correlation exchange functionals (χ_c), symmetry, atomic charge, basis sets, core electron treatment, approximation, electronic properties etc are essential[42]. Therefore, one must properly specify the required energy inputs for better results. Currently, the use of expensive energy correlation functional or basis sets has

become a powerful choice for obtaining high-accuracy results, despite long operating conditions. For instance, the use of PBEO, B3LYP, HSEO3, HSEO6 produces better approximation than LDA and GGA exchange functional[43]. Once the energy minimization is done, the electronic structure in terms of properties like band structure, phonons, orbitals, electronic excitations, the density of states, electrostatics, frequency, NMR etc. can be enumerated.

1.8. Layered double hydroxide as potential adsorbents

Questions about water treatment were considered the most difficult in the past decades. At the same time, the solutions to the question did not meet certain criteria due to the limited number of techniques available in the back days. Moreover, the focus on designing or developing new functionalized materials was inadequate to overcome such problems[44,45]. Fortunately, in this modern era, constant research on developing new techniques, low cost and efficient materials has led to wide applicability for the particular topic under study. Layered double hydroxides (LDHs) are considered to be nano adsorbents[46]. Several novel LDHs hybrid nanocomposites have developed in the present days, which are well-characterized nanosorbents that could be used in the study of environmental remediation of contaminants or harmful gases present in the atmosphere[47,48]. Therefore, it can be used extensively for scavenging various chemical species. The ability of the materials to act as potential adsorbent depends on the nature of the surface and chemical properties. Because LDHs are characterized by their layer structure and built up with a high positive charge, the adsorbent properties are affected by surface adsorption or ion-exchange mechanisms[49]. The fact that LDHs act as potential nano adsorbents can adsorb the anionic species in several ways. It is because the structure of LDHs is composed of di- and trivalent metal hydroxide sheets, and also, the layers consist of the anions which reside in the LDHs domain[50]. Therefore, it can potentially

adsorb any pollutants within the two layers, i.e. through interlayer ions due to hydrogen bonding interactions, or on the main hydroxide layers, i.e. on the metal hydroxide sheets. Another potential property of LDHs is the high surface area and diverse pore morphology[51]. It is known that LDHs are nanostructured materials with several different pores. Several reports also presented that the adsorption or ion-exchange properties of the LDH can also be enhanced by making hybrid nanocomposites. For instance, the use of organic or inorganic substrates as guest ions or molecules can improve the adsorption properties of LDHs. Likewise, in the present situation, researchers put efforts into making a hybrid LDHs composite for better performance[52]. These enhanced properties of LDHs not only help scavenge pollutants or unwanted species but also help in drug intercalation or transport of ions/ molecules. Furthermore, another crucial property of LDHs is the 'reconstruction ability' or 'memory effect'[53]. This phenomenon helps LDHs to reuse or re-adsorbed the anionic species after undergoing structural changes. Several removal techniques like membrane filtration, ion-exchange, coagulation, electrochemical oxidation, osmosis, biological process etc., have been widely used in the few decades[11,54]. However, due to some disadvantages like incomplete removal, expensive, long operating conditions, and loss of recycling ability of adsorbents. On the other hand, adsorption is a low-cost and efficient removal technique widely used[55]. Another advantage of the technique is that it is generally inexpensive, easy to operate, and does not need extreme control experiments.

1.9. Layered double hydroxides as antimicrobial or bactericidal agents

It is well known that LDHs are good antimicrobial or antibacterial agents. As aforementioned, LDHs are built up of high positive charge, and interlayer ions or anions increase the exchange capacity with other chemical species. Also, due to the presence of active di- and trivalent metallic species, the interaction of most LDHs molecules with

microbial cells shows a significant effect on microbial inhibition activity[56,57]. Studies have shown that LDHs due to its small size nanoparticles have a direct inhibition effect on microbial cells[58]. There are several ways of inhibiting bacterial growth such as the nature of antimicrobial metallic elements, particle size, oxidative stress or reactive radicals etc. Metals like aluminum, titanium, and tin show less antimicrobial activity. However, LDHs produce a synergistic effect against the host cells and therefore, it acts as strong antimicrobial or biocidal agents[59]. LDHs show such properties due to the transition metals in their composition. It is generally known that transition metals act excellent antimicrobial property due to the release of di- or trivalent cations and exhibits variable oxidation states[60]. Basically, LDHs contain mixed metal hydroxide sheets with some intercalated anions. Besides this, some guest ions or molecules could be introduced between the layered structure. The purpose of guest ions intercalation is to establish the additive effect, which makes LDHs a potential candidate for microbial activity[61]. In addition, various factors enhance the antimicrobial activity of LDHs. Some of the factors include di and trivalent metallic LDHs ratio, particle size, particle charge, pore size or volumes, and also the nature of anionic species present in the LDHs[59]. Several reports of LDHs as antimicrobial towards bacterial strains (gram-positive & gram-negative) showed that LDHs containing transition elements showed excellent bacterial inhibition properties. The mechanism of bacterial inhibition or killing is because of the factors like small particle size, oxidative stress and nature of antibacterial metallic elements etc[62].

1.10. Thermokinetic properties of layered double hydroxides

Kinetic-based thermal reactions called ‘thermokinetics’ is an essential phenomenon for understanding the kinetics of thermal reactions of solids, described by some reaction models or mechanisms[63]. In thermal analysis, information such as crystal growth or nucleation, polymerization, glass transition, melting, and phase changes are essential for

understanding solid materials' degradation properties[64]. In recent decades, the study of the thermal decomposition of LDHs was necessary for obtaining the kinetic parameters such as activation energy (KJ mol^{-1}) and pre exponential factor (A/S^{-1})[65]. However, due to some drawbacks associated with the TGA/DSC data analysis or the kinetic models, the reliability in evaluating the kinetic factors was not enough or considered in accurate. In the modern context, with the evolution of various thermal methods, analytical techniques, and kinetic models, the study of the thermal properties of materials is quite challenging. Another disadvantage associated with it is the use of single isothermal heating data rather than non-isothermal heating data[66]. The non-isothermal heating programme is applicable for those materials with complex overlapping DSC/TGA heating curves. However, when it comes to the accuracy in determining reaction models or mechanisms, it is recommended to use non-isothermal data rather than isothermal with multiple heating rates[67]. Nowadays, people use multiple heating data non-isothermally to increase the accuracy of describing the thermal degradation governed by multiple reaction mechanisms. The kinetic models are well-known established models in describing the thermal reaction mechanisms[68]. It is generally known that LDHs are the inorganic layered nanocomposite that is thermally stable up to 198-200 ^{o}C. The first weight loss is usually accompanied by the removal of moisture content in the LDHs matrix. In real situations, the kinetics of the thermal decomposition mechanism starts from the second and third degradation steps. This is due to the presence of kinetics flaws at the temperature until 200 ^{o}C[69,70]. Fundamentally, it can be stated that LDHs nanocomposites are generally controlled by the number of multiple thermal degradation steps as well as undergo a kinetically complex process[71]. In previously reported literature, the determination of kinetic degradation steps was based on a single heating TGA/DSC data, where such information does not seem to be so useful. In the present studies, the focus is on the thorough thermal degradation

investigation and further explanation of the understanding of the kinetics of overlapping TGA curves. This is because sometimes the thermal degradation of LDHs undergoes a multistep reaction and is usually governed by the number of additional peaks components called the pseudo-components[72]. Hence, the current studies are on the thorough structural degradation investigation of some of the selected LDHs.

1.11. Aims and objectives of the present research

In the present research, the aim of synthesizing the compounds using an environmentally benign process (green solvents) is the main target in our study. Because this will benefit the usage of less toxic chemicals rather than more hazardous ones, which could be economical, low energy usage, cost-efficient, and less operating conditions. Furthermore, the as-synthesized LDHs product has been used to address some primary objectives such as novel nanoadsorbent, kinetic-based thermal reaction models, antimicrobial agents, intercalation chemistry, leaching phenomena, crystallography, classical mechanics or quantum computation, and so on. To our knowledge, no known reports have been investigated using our presently synthesized LDHs for the applications in particular.

References

[1] V. Rives, Layered Double Hydroxides: Present and Future, 2001.

[2] F. Cavani, F. Trifirò, A. Vaccari, Hydrotalcite-type anionic clays: Preparation, properties and applications., Catal Today. 11 (1991). https://doi.org/10.1016/0920-5861(91)80068-K.

[3] J. He, M. Wei, B. Li, Y. Kang, D.G. Evans, X. Duan, Preparation of layered double hydroxides, Struct Bond. 119 (2005). https://doi.org/10.1007/430_006.

[4] Q. Wang, D. Ohare, Recent advances in the synthesis and application of layered double hydroxide (LDH) nanosheets, Chem Rev. 112 (2012). https://doi.org/10.1021/cr200434v.

[5] S. Daniel, S. Thomas, Layered double hydroxides: fundamentals to applications, in: Layered Double Hydroxide Polymer Nanocomposites, 2020. https://doi.org/10.1016/b978-0-08-101903-0.00001-5.

[6] M.B. Poudel, H.J. Kim, Confinement of Zn-Mg-Al-layered double hydroxide and α-Fe2O3 nanorods on hollow porous carbon nanofibers: A free-standing electrode for solid-state symmetric supercapacitors, Chemical Engineering Journal. 429 (2022). https://doi.org/10.1016/j.cej.2021.132345.

[7] X.J. Zhao, Y.Q. Zhu, S.M. Xu, H.M. Liu, P. Yin, Y.L. Feng, H. Yan, Anion exchange behavior of MIIAl layered double hydroxides: a molecular dynamics and DFT study, Physical Chemistry Chemical Physics. 22 (2020). https://doi.org/10.1039/d0cp02537b.

[8] S. Xu, J. Zhao, Q. Yu, X. Qiu, K. Sasaki, Effect of Natural Organic Matter Model Compounds on the Structure Memory Effect of Different Layered Double

Hydroxides, ACS Earth Space Chem. 3 (2019). https://doi.org/10.1021/acsearthspacechem.9b00175.

[9] A. Chatterjee, P. Bharadiya, D. Hansora, Layered double hydroxide based bionanocomposites, Appl Clay Sci. 177 (2019). https://doi.org/10.1016/j.clay.2019.04.022.

[10] D.G. Evans, R.C.T. Slade, Structural aspects of layered double hydroxides, Struct Bond. 119 (2005). https://doi.org/10.1007/430_005.

[11] A. R.Sangtam, P. Saikia, R. L. Goswamee, D. Sinha, U. B. Sinha, Environmental chemical engineering. 10 (2022). https://doi.org/10.1016/j.jece.2022.108378.

[12] E.S.Zhitova, S. v. Krivovichev, I. Pekov, H.C. Greenwell, Crystal chemistry of natural layered double hydroxides. 5. Single-crystal structure refinement of hydrotalcite, [Mg6Al2(OH)16](CO3)(H2O)4, Mineral Mag. 83 (2019). https://doi.org/10.1180/mgm.2018.145.

[13] X. Guo, T. Yoshino, T. Okuchi, N. Tomioka, H-D interdiffusion in brucite at pressures up to 15 GPa, American Mineralogist. 98 (2013). https://doi.org/10.2138/am.2013.4550.

[14] Z.P. Xu, H.C. Zeng, Interconversion of Brucite-like and Hydrotalcite-like Phases in Cobalt Hydroxide Compounds, Chemistry of Materials. 11 (1999). https://doi.org/10.1021/cm980420b.

[15] X. Lu, U.R. Gabinet, C.L. Ritt, X. Feng, A. Deshmukh, K. Kawabata, M. Kaneda, S.M. Hashmi, C.O. Osuji, M. Elimelech, Relating Selectivity and Separation Performance of Lamellar Two-Dimensional Molybdenum Disulfide (MoS2)

Membranes to Nanosheet Stacking Behavior, Environ Sci Technol. 54 (2020). https://doi.org/10.1021/acs.est.0c02364.

[16] A.I. Khan, D. O'Hare, Intercalation chemistry of layered double hydroxides: Recent developments and applications, in: J Mater Chem, 2002. https://doi.org/10.1039/b204076j.

[17] G.R. Williams, T.G. Dunbar, A.J. Beer, A.M. Fogg, D. O'Hare, Intercalation chemistry of the novel layered double hydroxides [MAl 4(OH)12](NO3)2·yH 2O (M = Zn, Cu, Ni and Co). 2: Selective intercalation chemistry, J Mater Chem. 16 (2006). https://doi.org/10.1039/b514875h.

[18] H.S. Panda, R. Srivastava, D. Bahadur, In-vitro release kinetics and stability of anticardiovascular drugs-intercalated layered double hydroxide nanohybrids, Journal of Physical Chemistry B. 113 (2009). https://doi.org/10.1021/jp905440e.

[19] J. Liu, P. Yao, Z.M. Ni, Y. Li, W. Shi, Jahn-Teller effect of Cu-Mg-Al layered double hydroxides, WuliHuaxueXuebao/ Acta Physico - ChimicaSinica. 27 (2011). https://doi.org/10.3866/pku.whxb20110923.

[20] L. Pachayappan, S. Nagendran, P.V. Kamath, Polytypism in Alumite-like Layered Double Hydroxides of M (Zn2+, Ni2+) and Al: A Structural Transformation from Monoclinic to Orthorhombic Symmetry, Cryst Growth Des. 20 (2020). https://doi.org/10.1021/acs.cgd.0c00081.

[21] L. Wu, B. Peng, Q. Li, Q. Wang, X. Yan, K. Li, Q. Lin, Effects of Cu2+ incorporation on ZnAl-layered double hydroxide, New Journal of Chemistry. 44 (2020). https://doi.org/10.1039/d0nj00278j.

[21] https://en.wikipedia.org/wiki/Jahn%E2%80%93Teller_effect.

[23] M.A. Halcrow, Jahn–Teller distortions in transition metal compounds, and their importance in functional molecular and inorganic materials, Chem Soc Rev. 42 (2013). https://doi.org/10.1039/c2cs35253b.

[24] R. Freitag, J. Conradie, Understanding the Jahn-Teller effect in octahedral transition-metal complexes: A molecular orbital view of the Mn(β-diketonato)3 complex, J Chem Educ. 90 (2013). https://doi.org/10.1021/ed400370p.

[25] S. Radha, P.V. Kamath, Polytype selection and structural disorder mediated by intercalated sulfate ions among the layered double hydroxides of Zn with Al and Cr, Cryst Growth Des. 9 (2009). https://doi.org/10.1021/cg801259n.

[26] W.A. Slawiński, A.O. Sjåstad, H. Fjellvåg, Stacking Faults and Polytypes for Layered Double Hydroxides: What Can We Learn from Simulated and Experimental X-ray Powder Diffraction Data?,Inorg Chem. 55 (2016). https://doi.org/10.1021/acs.inorgchem.6b02247.

[27] G.S. Thomas, P.V. Kamath, Line broadening in the PXRD patterns of layered hydroxides: The relative effects of crystallite size and structural disorder, Journal of Chemical Sciences. 118 (2006). https://doi.org/10.1007/BF02708774.

[28] M. Vucelic, G.D. Moggridge, W. Jones, Thermal properties of terephthalate- and benzoate-intercalated LDH, Journal of Physical Chemistry. 99 (1995). https://doi.org/10.1021/j100020a068.

[29] S.V. Krivovichev, V.N. Yakovenchuk, E.S. Zhitova, A.A. Zolotarev, Y.A. Pakhomovsky, G.Yu. Ivanyuk, Crystal chemistry of natural layered double hydroxides. 2. Quintinite-1 M : first evidence of a monoclinic polytype in M 2+ - M 3+ layered double hydroxides , Mineral Mag. 74 (2010). https://doi.org/10.1180/minmag.2010.074.5.833.

[30] A.V. Radha, P.V. Kamath, C. Shivakumara, Order and disorder among the layered double hydroxides: combined Rietveld and DIFFaX approach, Acta Crystallogr B. 63 (2007). https://doi.org/10.1107/S010876810700122X.

[31] M. Bellotto, B. Rebours, O. Clause, J. Lynch, D. Bazin, E. Elkaïm, A reexamination of hydrotalcite crystal chemistry, Journal of Physical Chemistry. 100 (1996). https://doi.org/10.1021/jp960039j.

[32] A. de Roy, C. Forano, J.P. Besse, Layered Double Hydroxides: Synthesis and Post-Synthesis Modification, 2015.

[33] S. Britto, P.V. Kamath, Polytypism in the lithium-aluminum layered double hydroxides: The [LiAl2(OH)6]+ layer as a structural synthon, Inorg Chem. 50 (2011). https://doi.org/10.1021/ic200312g.

[34] C. Jaubertie, M.J. Holgado, M.S. San Roman, V. Rives, Structural characterization and delamination of lactate-intercalated Zn,Al-layered double hydroxides, Chemistry of Materials. 18 (2006). https://doi.org/10.1021/cm060512y.

[35] S.G. Louie, Y.H. Chan, F.H. da Jornada, Z. Li, D.Y. Qiu, Discovering and understanding materials through computation, Nat Mater. 20 (2021). https://doi.org/10.1038/s41563-021-01015-1.

[36] W. Kohn, A.D. Becke, R.G. Parr, Density functional theory of electronic structure, Journal of Physical Chemistry. 100 (1996). https://doi.org/10.1021/jp960669l.

[37] E.E. Ebenso, C. Verma, L.O. Olasunkanmi, E.D. Akpan, D.K. Verma, H. Lgaz, L. Guo, S. Kaya, M.A. Quraishi, Molecular modelling of compounds used for corrosion inhibition studies: a review, Physical Chemistry Chemical Physics. 23 (2021). https://doi.org/10.1039/d1cp00244a.

[38] V. Milman, K. Refson, S.J. Clark, C.J. Pickard, J.R. Yates, S.P. Gao, P.J. Hasnip, M.I.J. Probert, A. Perlov, M.D. Segall, Electron and vibrational spectroscopies using DFT, plane waves and pseudopotentials: CASTEP implementation, Journal of Molecular Structure: THEOCHEM. 954 (2010). https://doi.org/10.1016/j.theochem.2009.12.040.

[39] https://en.wikipedia.org/wiki/List_of_quantum_chemistry_and_solid state_physics_software.

[40] M. Ramezanzadeh, G. Bahlakeh, Z. Sanaei, B. Ramezanzadeh, Studying the Urticadioica leaves extract inhibition effect on the mild steel corrosion in 1 M HCl solution: Complementary experimental, ab initio quantum mechanics, Monte Carlo and molecular dynamics studies, J Mol Liq. 272 (2018). https://doi.org/10.1016/j.molliq.2018.09.059.

[41] M. Ramezanzadeh, G. Bahlakeh, B. Ramezanzadeh, Study of the synergistic effect of Mangifera indica leaves extract and zinc ions on the mild steel corrosion inhibition in simulated seawater: Computational and electrochemical studies, J Mol Liq. 292 (2019). https://doi.org/10.1016/j.molliq.2019.111387.

[42] https://globex.coe.pku.edu.cn/file/upload/201807/16/1259524417.pdf.

[43] H. Yan, B. Nie, C. Peng, P. Liu, X. Wang, F. Yin, J. Gong, Y. Wei, S. Lin, Molecular Model Construction of Low-Quality Coal and Molecular Simulation of Chemical Bond Energy Combined with Materials Studio, Energy and Fuels. 35 (2021). https://doi.org/10.1021/acs.energyfuels.1c02658.

[44] E.O. Ezugbe, S. Rathilal, Membrane technologies in wastewater treatment: A review, Membranes (Basel). 10 (2020). https://doi.org/10.3390/membranes10050089.

[45] S.N. Zulkifli, H.A. Rahim, W.J. Lau, Detection of contaminants in water supply: A review on state-of-the-art monitoring technologies and their applications, Sens Actuators B Chem. 255 (2018). https://doi.org/10.1016/j.snb.2017.09.078.

[46] M. Daud, A. Hai, F. Banat, M.B. Wazir, M. Habib, G. Bharath, M.A. Al-Harthi, A review on the recent advances, challenges and future aspect of layered double hydroxides (LDH)– Containing hybrids as promising adsorbents for dyes removal, J Mol Liq. 288 (2019). https://doi.org/10.1016/j.molliq.2019.110989.

[47] R.K. Gautam, A.K. Singh, I. Tiwari, Nanoscale layered double hydroxide modified hybrid nanomaterials for wastewater treatment: A review, J Mol Liq. 350 (2022). https://doi.org/10.1016/j.molliq.2022.118505.

[48] Q. Shi, X. Zhang, Y. Yang, J. Huang, X. Fu, T. Wang, X. Liu, A. Sun, J. Ge, J. Shen, Y. Zhou, Z. Liu, 3D hierarchical architecture collaborating with 2D/2D interface interaction in NiAl-LDH/Ti3C2 nanocomposite for efficient and selective photoconversion of CO2, Journal of Energy Chemistry. 59 (2021). https://doi.org/10.1016/j.jechem.2020.10.038.

[49] Y. Xie, X. Yuan, Z. Wu, G. Zeng, L. Jiang, X. Peng, H. Li, Adsorption behavior and mechanism of Mg/Fe layered double hydroxide with Fe3O4-carbon spheres on the removal of Pb(II) and Cu(II), J Colloid Interface Sci. 536 (2019). https://doi.org/10.1016/j.jcis.2018.10.066.

[50] G. Darmograi, B. Prelot, G. Layrac, D. Tichit, G. Martin-Gassin, F. Salles, J. Zajac, Study of Adsorption and Intercalation of Orange-Type Dyes into Mg-Al Layered Double Hydroxide, Journal of Physical Chemistry C. 119 (2015). https://doi.org/10.1021/acs.jpcc.5b05510.

[51] M. Laipan, J. Yu, R. Zhu, J. Zhu, A.T. Smith, H. He, D. O'Hare, L. Sun, Functionalized layered double hydroxides for innovative applications, Mater Horiz. 7 (2020). https://doi.org/10.1039/c9mh01494b.

[52] Y. Guo, Z. Zhu, Y. Qiu, J. Zhao, Enhanced adsorption of acid brown 14 dye on calcined Mg/Fe layered double hydroxide with memory effect, Chemical Engineering Journal. 219 (2013). https://doi.org/10.1016/j.cej.2012.12.084.

[53] Z. Gao, K. Sasaki, X. Qiu, Structural Memory Effect of Mg-Al and Zn-Al layered Double Hydroxides in the Presence of Different Natural Humic Acids: Process and Mechanism, Langmuir. 34 (2018). https://doi.org/10.1021/acs.langmuir.8b00059.

[54] A. Ahmad, S.H. Mohd-Setapar, C.S. Chuong, A. Khatoon, W.A. Wani, R. Kumar, M. Rafatullah, Recent advances in new generation dye removal technologies: Novel search for approaches to reprocess wastewater, RSC Adv. 5 (2015). https://doi.org/10.1039/c4ra16959j.

[55] M. Rafatullah, O. Sulaiman, R. Hashim, A. Ahmad, Adsorption of methylene blue on low-cost adsorbents: A review, J Hazard Mater. 177 (2010). https://doi.org/10.1016/j.jhazmat.2009.12.047.

[56] M. Li, L. Li, S. Lin, Efficient antimicrobial properties of layered double hydroxide assembled with transition metals via a facile preparation method, Chinese Chemical Letters. 31 (2020). https://doi.org/10.1016/j.cclet.2019.09.047.

[57] Y. Zhao, C.J. Wang, W. Gao, B. Li, Q. Wang, L. Zheng, M. Wei, D.G. Evans, X. Duan, D. O'Hare, Synthesis and antimicrobial activity of ZnTi-layered double hydroxide nanosheets, J Mater Chem B. 1 (2013). https://doi.org/10.1039/c3tb21059f.

[58] N. Rasouli, M. Movahedi, M. Doudi, Synthesis and characterization of inorganic mixed metal oxide nanoparticles derived from Zn–Al layered double hydroxide and their antibacterial activity, Surfaces and Interfaces. 6 (2017). https://doi.org/10.1016/j.surfin.2016.11.007.

[59] A.R. Sangtam, K. Richa, P. Saikia, N. Longkumer, U.B.Sinha, R. L.Goswamee, Synthesis and characterization of Co(II)–Co(III) LDH and Ac@Co(II)–Co(III) LDH nanohybrid and study of its application as bactericidal agents, J Results in Chemistry. 4 (2022). https://doi.org/10.1016/j.rechem.2022.100671.

[60] J. Awassa, D. Cornu, S. Soulé, C. Carteret, C. Ruby, S. El-Kirat-Chatel, Divalent metal release and antimicrobial effects of layered double hydroxides, Appl Clay Sci. 216 (2022). https://doi.org/10.1016/j.clay.2021.106369.

[61] H.M. Cheng, X.W. Gao, K. Zhang, X.R. Wang, W. Zhou, S.J. Li, X.L. Cao, D.P. Yan, A novel antimicrobial composite: ZnAl-hydrotalcite with: P -hydroxybenzoic acid intercalation and its possible application as a food packaging material, New Journal of Chemistry. 43 (2019). https://doi.org/10.1039/c9nj03943k.

[62] Y.N. Slavin, J. Asnis, U.O. Häfeli, H. Bach, Metal nanoparticles: Understanding the mechanisms behind antibacterial activity, J Nanobiotechnology. 15 (2017). https://doi.org/10.1186/s12951-017-0308-z.

[63] A. Auroux, Calorimetry and Thermal Methods in Catalysis, 2013.

[64] S. Rashidi, N. Karimi, B. Sunden, K.C. Kim, A.G. Olabi, O. Mahian, Progress and challenges on the thermal management of electrochemical energy conversion and storage technologies: Fuel cells, electrolysers, and supercapacitors, Prog Energy Combust Sci. 88 (2022). https://doi.org/10.1016/j.pecs.2021.100966.

[65] A. Khawam, D.R. Flanagan, Solid-state kinetic models: Basics and mathematical fundamentals, Journal of Physical Chemistry B. 110 (2006). https://doi.org/10.1021/jp062746a.

[66] S. Vyazovkin, A.K. Burnham, L. Favergeon, N. Koga, E. Moukhina, L.A. Pérez-Maqueda, N. Sbirrazzuoli, ICTAC Kinetics Committee recommendations for analysis of multi-step kinetics, Thermochim Acta. 689 (2020). https://doi.org/10.1016/j.tca.2020.178597.

[67] S. Vyazovkin, C.A. Wight, Isothermal and non-isothermal kinetics of thermally stimulated reactions of solids, Int Rev Phys Chem. 17 (1998). https://doi.org/10.1080/014423598230108.

[68] Q. Yu, Y. Liu, H. Sui, J. Sun, J. Li, Kinetic Analysis of Overlapping Multistep Thermal Decomposition of 2,6-Diamino-3,5-dinitropyrazine-1-oxide (LLM-105), Journal of Physical Chemistry C. 122 (2018). https://doi.org/10.1021/acs.jpcc.8b07817.

[69] P. Saikia, N.B. Allou, A. Borah, R.L. Goswamee, Iso-conversional kinetics study on thermal degradation of Ni-Al layered double hydroxide synthesized by 'soft chemical' sol-gel method, Mater Chem Phys. 186 (2017). https://doi.org/10.1016/j.matchemphys.2016.10.028.

[70] L. Wang, Z. Lü, F. Li, X. Duan, Study on the mechanism and kinetics of the thermal decomposition of Ni/Al layered double hydroxide nitrate, Ind Eng Chem Res. 47 (2008). https://doi.org/10.1021/ie800609c.

[71] A. Perejón, P.E. Sánchez-Jiménez, J.M. Criado, L.A. Pérez-Maqueda, Kinetic analysis of complex solid-state reactions. A new deconvolution procedure, Journal of Physical Chemistry B. 115 (2011). https://doi.org/10.1021/jp110895z.

[72] S. Pinzi, C. Buratti, P. Bartocci, G. Marseglia, F. Fantozzi, M. Barbanera, A simplified method for kinetic modeling of coffee silver skin pyrolysis by coupling pseudo-components peaks deconvolution analysis and model free-isoconversional methods, Fuel. 278 (2020). https://doi.org/10.1016/j.fuel.2020.118260.

CHAPTER 2

Materials and methods

This chapter outlines the importance of the precursors, characterization techniques, and the basic methodology employed in the present research.

2.1. Introduction

In recent decades, several LDHs synthesis methods have been reported. Depending on the types, nature, and targets of the study, LDHs can be prepared. Nowadays, LDHs can be synthesized by two different methods: direct and indirect. Some conventional direct/indirect preparative methods, including co-precipitation, hydrothermal, ion exchange, urea hydrolysis, salt-oxide, Sol-Gel, memory/rehydration etc. are widely known.

2.2. Preparation of layered double hydroxides(LDHs)

2.2.1. Recent synthesis methods

2.2.1.1. Co-precipitation method

Overall the synthetic methods available, the co-precipitation procedure is among the most commonly used method. In recent days, a number of hydrotalcite have been produced using this method. The reason being the co-precipitation method is a facile and generally inexpensive method. However, every method has its advantages and disadvantages. For instance, pure LDH phase in the given permissible metallic ratios is not strictly required in the co-precipitation method, and considering the presence of other ionic species may be necessary. Moreover, due to non-homogenous precipitation or fluctuations in pH values, co-precipitation does not seem to be the case for obtaining pure LDH. To overcome the drawbacks of this, the metal hydroxides should be allowed to precipitate either at low or high supersaturation with certain defined pH. Generally, it is known that at low supersaturation, the crystal growth dominates then it nucleates, and at high supersaturation, crystal nucleation occurs faster, resulting in small-size crystals. However, it should be noted that the fluctuations in pH values *viz.* supersaturation at high, low, and constant pH has to be carefully examined. For instance, the formation of LDH crystals at increasing pH cannot be achieved since the trivalent cations precipitate at low pH. On the other hand, the precipitation of metal hydroxide at decreasing pH seems to be a suitable

choice. In present situations, researchers prefer to synthesize LDH materials at constant pH. This is because the LDHs synthesized at constant pH show a well-hydrolyzed homogenous phase. However, other disadvantages of the co-precipitation is that the morphology of the LDHs synthesized using the co-precipitation method shows poor crystallinity. Also, this method leads to the uncontrol intercalation of atmospheric carbon dioxide (CO_2) into LDHs structure, which might hinder the desired counter ions required to be intercalated[1,2].

2.2.1.2. Hydrothermal/ solvothermal method

In a hydrothermal (water as solvent)/solvothermal method (organic solvent), a suspension of metal oxides or hydroxides containing M^{2+} and M^{3+} cations is carried out at high temperature and pressure. The hydro/solvothermal method is similar to the co-precipitation method, which involves the addition of a strong alkali base (precipitating agent) into the aqueous phase containing a di- and trivalent mixture. The final mixture is then thermally treated and aged for certain minutes or hours. The advantage of the method is that the synthesized product of LDHs results in high crystal formation and eliminates the toxic by-products. Secondly, a transformation of amorphous to a crystalline product could be achieved by this method. However, the disadvantages of the method are as follows: the synthesized product might not result in the specified molar ratios, which needs further experimental optimization. The synthesized product results in diverse surface morphology; however, it is a long operational technique and uses an expensive autoclave, high temperature, production of wastewater, highly concentrated alkali base, and difficulty in observing crystal growth inside the steel tube[3,4].

2.2.1.3. Urea hydrolysis method

The urea hydrolysis method is similar to the co-precipitation method, where urea (CH_4N_2O) is used as the primary precipitating agent. Unlike other synthetic methods, the

urea method yields LDH with carbonate (CO_3^{2-}) as counter anions. The required synthesized parameters such as di- and trivalent ratio, temperature, pH, and aging time are often adjusted under the hydrothermal condition to control the urea hydrolysis rate, which results in LDH with controllable size, morphology, and crystallinity. The advantage of the method over the co-precipitation method is the high crystallinity with uniform LDH particle sizes. However, the drawbacks of the method are the uncontrollable precipitation of carbonate from the atmospheric condition than the amount of the interlayer anions needed to be adsorbed by LDHs molecule[2,5].

2.2.1.4. Induced hydrolysis method

The induced hydrolysis method can be achieved in two steps. The first step involves the precipitation of M^{3+} ions in an aqueous solution by adding an alkali base. Subsequently, the trivalent precipitate is slowly added to the solution containing divalent salts at constant pH, thereby inducing a controlled release of M^{3+} ions in the solution[6,7]. The advantage of the method is that the synthesized compound shows a well-hydrolyzed LDH phase. The major drawbacks of the method involve long operation procedures, poor crystallinity, irregular LDH morphology, non-uniform particle size, and fluctuations in di- and trivalent metallic ratios.

2.2.1.5. Sol-Gel synthesis

Sol-Gel is simply a hydrolysis method. During the process, sol to gel-like characteristics are transformed, and the appearance of pseudo-solids is seen. The formation of LDHs occurs through hydrolysis of the di- and trivalent cations in the presence of strong acids (HCl or HNO_3) or water and the anions to be intercalated such as carbonate ions, sulfate, organic or inorganic anions[1,8]. The pH is a crucial factor for the precipitation of hydroxide to take place. Moreover, to obtain the well-hydrolyzed crystal structure and well-organized pores morphology, the effect of drying conditions (air, heat or desiccator) is

very much important. The drawbacks of it might be less crystallinity or high pore diversity arrangement, however, it takes a good control particle size.

2.2.1.6. Salt-oxide (or hydroxide method)

A salt-oxide method is a simple solid-liquid method. It involves the addition of divalent oxide suspension into the solution containing trivalent hydroxide solution. The pH of the mixture should be kept slightly acidic to occur the slow hydrolysis or precipitation of divalent metal cations. The anions to be intercalated must be able to form a soluble salt with the trivalent cations and should be stable in an acidic medium[9]. The method is particularly used when co-precipitation is difficult to achieve. The main drawbacks associated with it are that it sometimes results in insoluble salt (by-product), and the obtained LDHs possess a slight acidic character rather than the formation of more OH ions. Moreover, the LDHs product obtained may have poor morphology or non-homogenous precipitate of di and trivalent metallic hydroxides.

2.2.1.7. Electrochemical deposition method

In this method, the formation of LDHs occurs through the electrical reduction of acid ions (mostly nitrate, chloride, and sulfate ions) on the working electrode with the increase in pH value, which induces the precipitation of LDH films. The method is useful for depositing LDH films of any desired thickness, morphology, and film density on a metal substrate [2]. The limitations of the method includes use high energy consumption, expensive technique, non-benign, and poor LDHs morphology.

2.2.1.8. Ion exchange method

An ion exchange is considered the most widely used and is an indirect method of synthesis of LDHs. It is useful when the co-precipitation method is infeasible for the di- and trivalent cations. In the actual procedure, the pre-synthesized or an aqueous solution containing LDH ions is allowed to exchange with the salt solution of anions to be

intercalated. On the other hand, the guest ions are allowed to exchange with the interlayer anions present in the LDH layers, which produces the anions pillared LDHs[3,7]. The disadvantages of the method include long experimental procedures, and the major drawbacks lie in the incomplete exchange of guest ions with the interlayer anions. Moreover, the exchange reaction sometimes results in unpredictable chemical reactions or fluctuation in di- and trivalent metallic LDHs ratios.

2.2.1.9. Rehydration or memory effect

The fascinating property of LDHs is their ability to undergo reconstruction of the original structure, called the 'memory effect'. In such a method, the collapse of LDHs structure brought by calcination at around 400-500 ^{o}C could be regenerated with water or mild organic solvents. To make the reactions happen, the overall rehydration reaction should be carried in an inert atmosphere to prevent interfering ions. In the actual synthesis method, the formation of LDHs layer or newly incorporated anionic species occurs through ion-exchange mechanisms[2,3]. This method is useful for obtaining several LDH combinations containing various organic or inorganic intercalated species. The disadvantage of the method is that sometimes the regenerated LDHs structure results in loss of crystallinity or non-homogenous crystallization due to the non-selective adsorption of various ions/molecules.

2.2.1.10. Delamination methods

The delamination methods of LDHs synthesis are considered to be the most challenging approaches in modern days. The method can be achieved by two approaches *viz.* 'top-down' and 'bottom-up'. The 'top-down' is the most widely used approach. In this method, the modification of LDHs with organic or inorganic substrates is carried out by intercalation or ion exchange process. In recent days, most researchers have had difficulty achieving these two approaches. The difficulty in such approaches is due to the

significantly high charge density of LDHs. Therefore, to overcome these, the most important criterion is the selection of suitable solvents to delaminate the lamellar sheets. In 'bottom-up' synthesis, co-precipitation of di- and trivalent LDH ions are first carried out in the aqueous phase, followed by intercalation of organic substrates in the oil phase. At this point, the LDHs act as nanoreactor centers with anions, and as a result, the LDHs solids are delaminated to form a single layer[10]. The advantages/disadvantage of this method is that this method is considered as a novel engineering method for obtaining the LDHs layers with different delaminated/exfoliated forms, however, it is a long operating process, and sometimes results in non-efficient adhesion of required anionic species around the nanosheets region.

2.2.1.11. Other methods

Besides the aforementioned synthetic routes, other methods of LDHs synthesis routes such as aging, surface, Chimiedouce, in-situ film growth, and templated synthesis, are also known[3].

2.2.2. Present synthesis method

2.2.2.1. Metal acetylacetonates as a precursor for the synthesis of LDHs

Metal acetylacetonates are coordination complexes derived from polyatomic acetylacetonate anions. The most interesting feature of acetylacetonate anions ($C_5H_7O_2^-$) is that it acts as a chelating ligand, in which oxygen atoms bind to the metals forming a six-membered chelate ring[11]. Another important feature of acetylacetonate anion is that it acts as an equilibrium keto-enol tautomerism[12]. The general synthesis reactions of M(acac) involve the reaction of metal salts (base) with acetylacetone in an aqueous medium. This can be represented as:

$$\mathbf{M^{m+} + m\ Hacac} \xrightleftharpoons{\text{Hydrolysis}} \mathbf{M(acac)_m + m\ H^+} \quad \ldots\ldots (1)$$

From equation 1, it can be seen that the metal cations act as electropositive, forming the dissociated protons (H^+) and M(acac) complex as the main product. Figure 2.1. represents the schematic diagram of equilibrium keto-enol tautomerism and the formation of acetylacetonate complexes. The enol form of acac in the polar aprotic solvent is more stable than the keto form due to intramolecular hydrogen bonding, which leads to the formation of highly stable six-membered rings. Conversely, in the polar protic solvents, the keto form of the carbonyl (C=O) groups form hydrogen bonds, which reduces the intramolecular hydrogen bonding of the enol form. Basically, in the formation of M(acac), the acetylacetonate anion acts as a denticity of ligands[13]. Moreover, because of the oxygens and protons dissociation ability or simply electronegativity, the metal cations bindwith the acac molecule, forming the metal-coordinated acac complexes. Another important property of M(acac) is that the acetyl group (methyl), upon hydrolysis, can easily lose and forms a metal hydroxides precipitate, and because of this volatile property, many di- and trivalent M(acac) react to form unique structures, called mixed metal hydroxides[14]. In the present study, the hydrolysis reaction of metal alkoxides was carried out in a non-aqueous medium rather than an aqueous solution. The idea of this is to ignore any unwanted by-products during the chemical reactions. Hence, unlike other precursors, M(acac) are comparatively less toxic, volatile (acetyl group), inexpensive, thermally stable (transition metals), highly soluble in non-aqueous solvents rather than aqueous solution, and can be easily hydrolyzed at moderate temperatures (75-95°C)[15]. In terms of properties and usefulness, M(acac) shows excellent bonding andcatalytic behavior for the preparation and transformation of various organic and inorganic substrates. Moreover, due to the hydrolyzableor volatile properties as a result of the calcination process, M(acac) could easily lose its acetyl group and form the oxide precipitate. The metal oxides obtained are versatile, which can further produce metal nanocomposites[16].

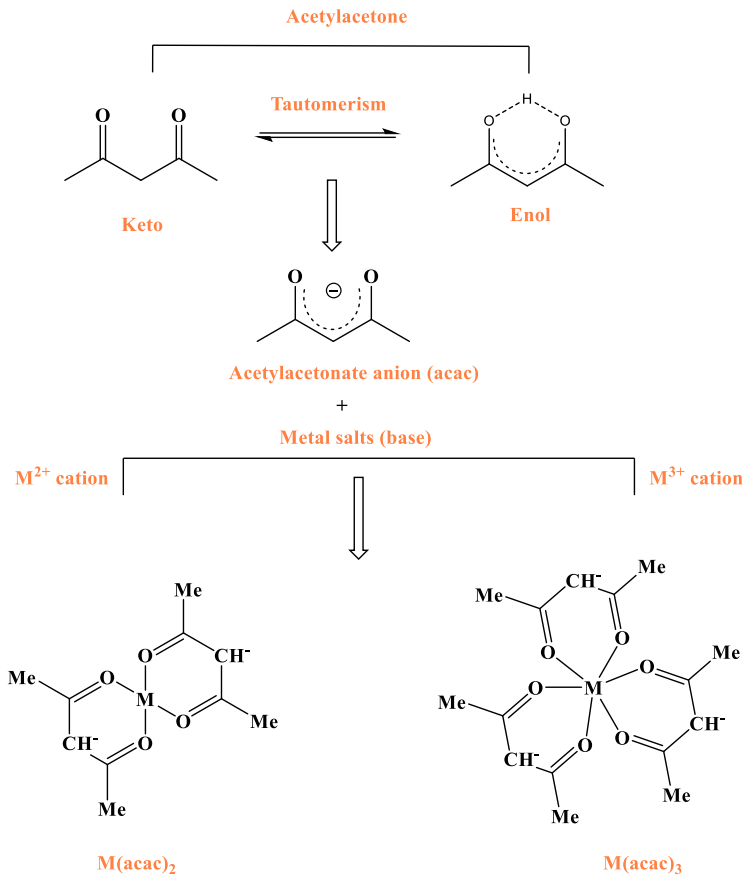

Figure 2.1. Schematic diagram showing keto-enol tautomerism and formation of metal acetylacetonate complexes

Besides properties and advantages, a wide application of M(acac) has been reported, such as semiconductors, antioxidants, antimicrobials, optics, polymer science, drug delivery, catalysts (homogenous/heterogenous catalysis) for various organic transformations like polymerization, hydrogenation, isomerization, coupling reactions etc. Various industrial applications were reported, including rubber, paint, and plastic technology. The fact being they can be used as an additive or stabilizing agent. In modern days, M(acac) complexes are used as important precursors for the production of metal nanoparticles at a larger scale. Reports like TiO_2 (titanium oxide), ZnO_2 (zinc oxide), γ-Fe_2O_3/Fe_3O_4 (magnetite), V_2O_3 (vanadium trioxide), Ta_2O_5 (tantalum pentoxide), SnO_2 (tin oxide)etc, are some of the metal oxides which will have a broader scope in the upcoming

days[12,14]. Moreover, the M(acac) complexes act as redox agents used for water-splitting mechanisms and electrochemical applications[17,18].

2.2.2.2. Soft-Chemical Sol-Gel synthesis of LDHs

Concurrently, we used the non-aqueous 'soft-chemical' sol-gel route. The method is similar to that of the Sol-Gel method, where the formation of sol to gel-like appearance is obtained[19]. The superiority over other methods is that this method takes the control synthesis of the particle size of LDHs formation, resulting in homogenous LDHs precipitate, and precipitation of LDHs phase was performed at high supersaturation at higher pH (8-9.5). The factors affecting the LDHs nanoparticle size formation mainly depend on pH, reflux time (4.5-7 hrs), and temperature (75-95°C). Moreover, the LDH prepared from this method results in unique structures in terms of diversity in pore morphology (nanopores), which is a special characteristic of the synthesized compounds[15]. Hence, taking into account the benefits and drawbacks, the present investigation focuses on the synthesis, characterization, properties, and applications of LDHs. Moreover, it differs from other reported works in terms of starting precursors and synthetic methodology. The methodology is further modified or enhanced through a non-aqueous benign process. Unlike other precursors or protocols, the current study employs the Sol-Gel route of LDHs synthesis and the mixture of ethanol + acetone as our primary targets. The advantages of the existing studies rely on the green protocol and the use of non-aqueous organic solvents, which prevent the solubilization of carbon dioxide gases responsible for carbonate formation in the LDHs layer[20]. This is because greenhouse gases (CO_2, methane, ethane, CFC) have recently emerged as a major environmental or green chemistry problem. The disadvantages of the other protocols have recently been associated with the use of highly toxic chemicals, low cost-effectiveness, lengthy operating conditions, low precipitation of LDHs particles in solution, low crystallinity, poor surface

or crystal morphology, formation of unhydrolyzed residues, uncontrolled atmospheric contamination of interlayers ions which might cause the interference in LDHs formation, and most importantly the synthesis procedure carried out in aqueous media. Thus, overcoming all of these associated concerns is of significant importance.

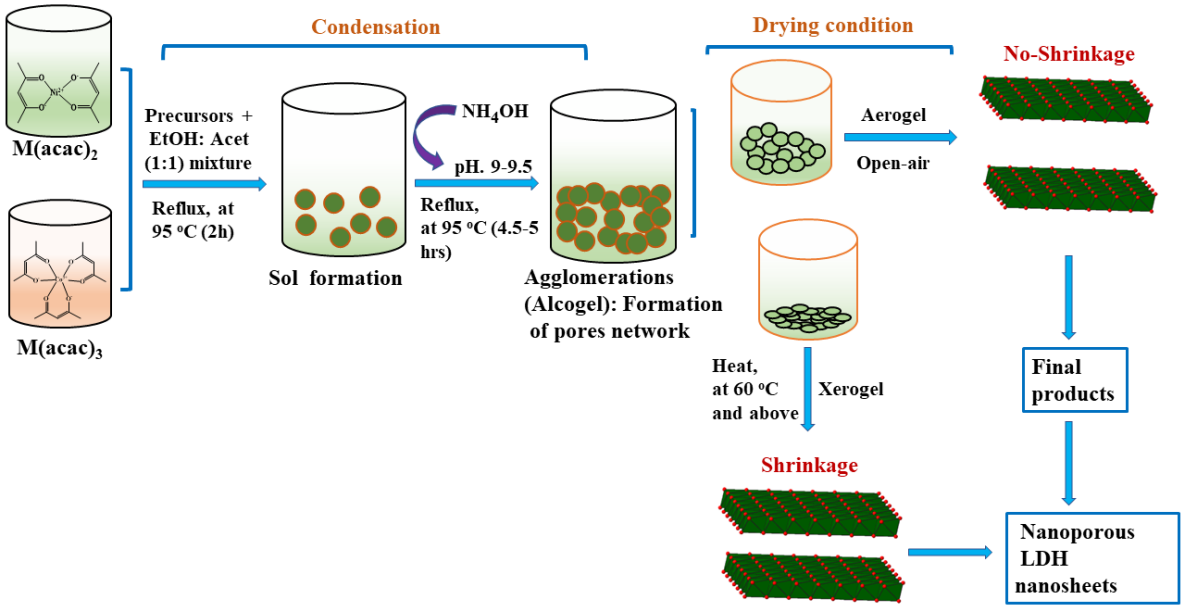

Figure 2.2. Schematic diagram showing the formation of LDHs nanosheet using the non-aqueous 'soft chemical' Sol-Gel route (present protocol)

Figure 2.2. demonstrates the overall synthesis scheme used in this study. In accordance with the current methodology, non-aqueous alcoholysis of acetylacetonate complexes results in unique LDH morphology facilitated by nanopore formation. Additionally, the synthesized LDHs compound yields a highly crystalline product. Thus, the present strategy is concerned with the green synthesis procedure for producing materials with high-quality crystalline products and controllable particle size. Last but not least, the current study method is improved by using less toxic organic solvents to synthesize various LDHs combinations and the use of easily hydrolyzable (typically 70 to 95°C) metal acetylacetonate compounds as our main precursors.

2.3. Characterization techniques used

- Powder X-ray diffraction (PXRD) studies: Used for crystal morphology and formation of LDH phases.
- Fourier-Transform Infrared spectroscopy (FTIR) studies: Used for bonding behavior and determination of functional groups in LDHs.
- Field Emission Scanning Electron Microscopy (FESEM) studies: Used for surface morphologies like pore diversity and stacking of metal hydroxide sheets.
- High Resolution-Transmission Electron Microscopy (HR-TEM) studies: Used for crystal diffraction pattern and type of solid state.
- X-ray Photoelectron Spectroscopy (XPS) studies: Used for chemical oxidation state and determination of molar ratios.
- Thermogravimetric-Differential Thermal Analysis (TGA-DTA) studies: Used for thermal decomposition reactions of LDH.
- Brunauer-Emmett-Teller (BET) studies: Used for pore surface areas and volume.
- Zeta potential studies: Used for surface charge analysis.

References

[1] R. M, M. PG, M. A, V. A, P. R, Layered Double Hydroxides: Tailoring Interlamellar Nanospace for a Vast Field of Applications, Journal of Material Science & Engineering. 06 (2017). https://doi.org/10.4172/2169-0022.1000360.

[2] Layered Double Hydroxide Polymer Nanocomposites, 2020. https://doi.org/10.1016/c2016-0-00811-2.

[3] J. He, M. Wei, B. Li, Y. Kang, D.G. Evans, X. Duan, Preparation of layered double hydroxides, Struct Bond. 119 (2005). https://doi.org/10.1007/430_006.

[4] Q. Wang, S.V.Y. Tang, E. Lester, D. O'Hare, Synthesis of ultrafine layered double hydroxide (LDHs) nanoplates using a continuous-flow hydrothermal reactor, Nanoscale. 5 (2013). https://doi.org/10.1039/c2nr32568c.

[5] D. Basu, A. Das, K.W. Stöckelhuber, U. Wagenknecht, G. Heinrich, Advances in layered double hydroxide (LDH)-based elastomer composites, Prog Polym Sci. 39 (2014). https://doi.org/10.1016/j.progpolymsci.2013.07.011.

[6] R.M. Taylor, The rapid formation of crystalline double hydroxy salts and other compounds by controlled hydrolysis, Clay Miner. 19 (1984). https://doi.org/10.1180/claymin.1984.019.4.06.

[7] V. Rives, Layered Double Hydroxides: Present and Future, 2001.

[8] J.A. Wang, X. Bokhimi, A. Morales, O. Novaro, T. López, R. Gómez, Aluminum local environment and defects in the crystalline structure of sol-gel alumina catalyst, Journal of Physical Chemistry B. 103 (1999). https://doi.org/10.1021/jp983130r.

[9] H. -P Boehm, J. Steinle, C. Vieweger, [Zn2Cr(Oh)6]X·2H2O, New Layer Compounds Capable of Anion Exchange and Intracrystalline Swelling, AngewandteChemie International Edition in English. 16 (1977). https://doi.org/10.1002/anie.197702651.

[10] Q. Wang, D. Ohare, Recent advances in the synthesis and application of layered double hydroxide (LDH) nanosheets, Chem Rev. 112 (2012). https://doi.org/10.1021/cr200434v.

[11] B.M. Choudhary, Process for the Preparation of Metal Acetylacetonates, U.S. Patent 2,004,056,737. (2004).

[12] R.K. Sodhi, S. Paul, An Overview of Metal Acetylacetonates: Developing Areas/Routes to New Materials and Applications in Organic Syntheses, Catalysis Surveys from Asia. 22 (2018). https://doi.org/10.1007/s10563-017-9239-9.

[13] H. Lamprey, Properties and applications of metal acetylacetonates, Ann N Y Acad Sci. 88 (1960). https://doi.org/10.1111/j.1749-6632.1960.tb20049.x.

[14] C. Avci-Camur, J. Perez-Carvajal, I. Imaz, D. Maspoch, Metal Acetylacetonates as a Source of Metals for Aqueous Synthesis of Metal-Organic Frameworks, ACS Sustain Chem Eng. 6 (2018). https://doi.org/10.1021/acssuschemeng.8b03180.

[15] A.R. Sangtam, K. Richa, P. Saikia, N. Longkumer, U.B.Sinha, R. L.Goswamee,Synthesis and characterization of Co(II)–Co(III) LDH and Ac@Co(II)–Co(III) LDH nanohybrid and study of its application as bactericidal agents, J Results in Chemistry. 4 (2022). https://doi.org/10.1016/j.rechem.2022.100671.

[16] A.L. Willis, Z. Chen, J. He, Y. Zhu, N.J. Turro, S. O'Brien, Metal acetylacetonates as general precursors for the synthesis of early transition metal oxide nanomaterials, J Nanomater. 2007 (2007). https://doi.org/10.1155/2007/14858.

[17] K. Chakrapani, G. Bendt, H. Hajiyani, I. Schwarzrock, T. Lunkenbein, S. Salamon, J. Landers, H. Wende, R. Schlögl, R. Pentcheva, M. Behrens, S. Schulz, Role of Composition and Size of Cobalt Ferrite Nanocrystals in the Oxygen Evolution Reaction, ChemCatChem. 9 (2017). https://doi.org/10.1002/cctc.201700376.

[18] R. Chen, R. Hempelmann, Ionic liquid-mediated aqueous redox flow batteries for high voltage applications, ElectrochemCommun. 70 (2016). https://doi.org/10.1016/j.elecom.2016.07.003.

[19] P. Saikia, A. Gautam, R.L. Goswamee, Synthesis of nanohybrid alcogels of SiO2 and Ni-Cr/Mg-Cr-LDH: study of their rheological and dip coating properties, RSC Adv. 6 (2016). https://doi.org/10.1039/c6ra23475e.

[20] A. R.Sangtam, P. Saikia, R. L. Goswamee, D. Sinha, U. B. Sinha, Green synthesis of mesoporous Ni-Co layered double hydroxide and its application for removal of 2,4-dinitrophenol from water: A theoretical study complemented by the first principle density functional theory-Monte-Carlo approach, Environmental chemical engineering. 10 (2022). https://doi.org/10.1016/j.jece.2022.108378.

CHAPTER 3A

Part A: Green synthesis and characterization of mesoporous Ni-Co layered double hydroxide

This chapter describes the synthesis and characterization of a novel mesoporous Ni-Co layered double hydroxide (LDH). A green synthetic method was used involving a non-aqueous 'soft chemical' ethanol: acetone mixture in order to avoid interlayer contamination by CO_2 gas, which is responsible for carbonate formation.

The text of this chapter has been published as:

A.R. Sangtam, P. Saikia, R.L. Goswamee, D. Sinha, U.B. Sinha, **Green synthesis of mesoporous Ni-Co layered double hydroxide and its application for removal of 2,4-dinitrophenol from water: a theoretical study complemented by the first principle density functional theory-Monte-Carlo approach**. *J. Environ. Chem. Eng.* 10 (2022), 108378. https://doi.org/10.1016/j.jece.2022.108378.

3.1. Introduction

Dinitrophenols are recognized as high-risk chemicals because of their carcinogenic and mutagenic effects, among which 2,4-dinitrophenol(2,4-DNP) are nitro derivatives that are highly toxic to aquatic animals and humans in many ways[1]. The US environmental protection agency listed 2,4-DNP as a priority pollutant, limiting its concentration to as low as ten nanograms per liter in freshwater. Some studies have shown that the concentration of 2,4-DNP, even less than 1ppm in water, causes restrictions on the cell growth mechanism[2]. The biggest challenge posed by dinitrophenols is their high solubility and chemical stability, which causes them to be highly resistant to degradation for their treatment[3]. It has long been recognized that 2,4-DNP causes protoplasmic poisoning in biological systems, demobilizing the metabolic "decoupling oxidative phosphorylation" process. Constant DNP exposure accelerates and alters normal living cells, causing weight loss, blood cell damage, hypertension, hyperthermia, vomiting, headaches, and can even cause death[4]. Several recent purification methods have been developed, including membrane filtration[5], ion exchange[6], metal oxide-based catalyst[7], photocatalytic degradation[8], electrochemical oxidation[9], reverse osmosis[10], etc. These methods, however, require high energy consumption and long operational periods. Additionally, the extended degradation duration, reactivity, and oxidizing nature of dinitrophenols limit the efficacy of the abovementioned techniques. Therefore, it is of significant interest to promote the efficacy of such removal through the use of well-functionalized materials. The adsorption method is considered cost-efficient or selective in removing various pollutants during water treatment. The method's advantages over other techniques are its economical usage, procedural simplicity, cost-effectiveness, and low time requirements[11]. Earlier, porous adsorbents such as silica, zeolites, metal-organic framework, activated carbons, metal oxides, alumina, resins, etc., were considered promising adsorbents.

However, despite the efficiency of these materials as good adsorbents, some limitations could be noticed due to the inaccessibility or reduction in the regeneration cycle after adsorption, slow selectivity in the adsorption, and a slower rate of the regeneration cycle[12,13]. Many adsorbents have limited pore size distribution on the adsorbent surface and electrostatic binding affinity towards adsorbates, making them incompatible for adsorption[14]. As a counter to these limitations, transition metals containing layered double hydroxide (LDH) can show excellent adsorption properties like efficient capture of heavy metal ions and high selectivity in adsorption at a faster cycle without requiring any further chemical activation[15,16]. Layered double hydroxides belong to a class of inorganic 2D or 3D layered materials called anionic compounds or hydrotalcite minerals, characterized by the sequence of their layers' stacking pattern. Besides the potential electrochemical, photochemical, catalytic, etc., applications of LDH, their ability for adsorption through ion exchange or intercalation reactions make LDH interesting and promising candidates for eliminating pollutants from aqueous media[17]. Recent studies using LDH composites such as Mn-doped MgAl LDH, mixed oxide LDH, Mg/Al LDH have shown good efficiency in the removal of environmental contaminants like arsenate[18], Mn^{2+}[19], and metronidazole[20] from aqueous solution. LDH-based materials synthesized using hydrothermal, co-precipitation, and mechanochemical methods have also been widely studied for the effective removal of radionuclides[21]. The enhanced adsorption capacity is due to the exchangeable interlayer anions or intercalation of guest molecules between the double metal hydroxide layers. The chemical composition and general formula of LDHs can be expressed as $[M^{2+}_{1-x}\ M^{3+}_{x}\ (OH)_2]^{x+}\ (A^{n-})_{x/n}.\ yH_2O$; where M^{2+} and M^{3+} represent di- and trivalent cations; (A^{n-}) and yH_2O represent the exchangeable interlayer anions (halides, carbonates, polyatomic ions, etc.) and neutral molecules such as

water[22].In addition, the most crucial property of LDH is their ability to undergo reconstruction through a process called the 'memory effect'. This memory effect can be achieved by rehydration or by reactions with solution-containing organic acids, which allow the LDH materials to reorganize or transform into their original structure even after undergoing structural changes during adsorption[23]. In view of the relevance of these materials, the present work aims toward the synthesis of super-fine Ni-Co LDH nanosheets as potential adsorbent material. The synthesis of Ni-Co LDH was considered particularly important because of its high selectivity and efficient removal of several pollutants like dyes, heavy metal ions, etc. Moreover, Ni^{2+} and Co^{3+} bearing double hydroxides have gained attention because of their applications in different areas such as electrochemical applications, an intercalated pillared catalyst for organic reactions, etc[24]. Their applicability in many fields can be attributed to the inherent nanosheets containing tailored or tunable heteroporous structures. The methodology employs a 'Soft-Chemical' sol-gel route using an environmentally benign solvent (ethanol: acetone) mixture to minimize the use of high temperature, electrical energy, and corrosive chemicals during synthesis[25,26]. The greenness of the methodology is enhanced further through the use of acaetylacetonate compounds. The method helps mitigate one of the major drawbacks associated with the usual high pH aqueous phase synthesis of LDH, which is carbonate formation. Most procedures involve the use of Ni and Co salts leading to the creation of an alkaline reaction medium, which easily facilitates the adsorption of atmospheric CO_2 leading to carbonate formation. To circumvent this problem, metal-organic precursors like acetylacetonates of nickel and cobalt were used as active reagents in this methodology. Unlike the other precursors, acetylacetonates containing nickel and cobalt hydroxides can be easily hydrolyzed at moderate

temperature (75-95°C) in the presence of ethanol and acetone mixture[27]. This method of synthesis could be superior to several other preparative methods, including ion exchange, hydrothermal, urea, salt-oxide, etc., since all of these involve high-energy costs and time-consuming processes[28]. In order to establish the Ni-Co LDH as an efficient adsorbent, experiments were conducted, which have been discussed in the ensuing sections. Thereafter, to support the experimental result obtained, theoretical molecular simulation studies were conducted to understand the adsorption mechanisms, such as the nature of interactions, binding energies, and chemical stability of the adsorbate-adsorbent complex[29]. To our knowledge, there are no known reports on the theoretical-based molecular dynamic (MD) simulation for the adsorption studyof2,4-DNP by Ni-Co LDH.

3.2. Materials and methods

3.2.1. Characterization techniques used

All the chemicals were purchased from Merck, Sigma Aldrich, and S. D. Fine Chem. Solvents were distilled before use while the substrates and reagents were used without further purification. The formation of the LDH phase of the synthesized mesoporous Ni-Co LDH was investigated by a powder X-Ray diffractometer operated at 20°C, 20-60 kV (voltage), using Cu-K alpha radiation at the wavelength λ=0.154 nm (Rigaku Japan, model: Ultima IV). The measuring range of 2theta (2θ) and scan rate was maintained at 2-70° with the step size of 0.02^{o}.

The surface morphology of the synthesized compound was examined using Field Emission Scanning Electron Microscopy (FESEM), operated at 20°C, with an acceleration voltage of0.5 to 30 kV (Carl ZEISS Microscopy, Germany, model: ZEISS, SIGMA). Also, the crystal morphology was examined using High-Resolution Transmission Electron Microscopy (HRTEM), operated at 20°C, 200-300 kV (JEOL, Japan, model: JEM-2100

PlusElectronMicroscope). FT-IR analysis was conducted to identify the various functional groups present on the Ni-Co LDH composite, obtained in the IR range 4500-500 cm^{-1}, using KBr pellets (Perkin Elmer, model: Spectrum 100). The chemical composition, oxidation states or molar ratios of the compound were confirmed using X-Ray Photoelectron Spectrometer (XPS) operated at 28°C (RT). The surface of the sample was irradiated using Al Kα (excitation source) in ultrahigh vacuum (UHV) conditions ≤5x10-10mbar (Thermo Fisher Scientific Pvt. Ltd., UK, model: ESCALAB Xi+). The thermal degradation profile of the synthesized compound was studied at the heating rate of 5°C/min, within the degradation range of 50-800°C (M/S TG-DTA Instrument, model: Q-600). BET surface analysis was carried out to understand the specific surface area or pores volume using N_2 gas adsorption at 77 K (Quantachrome USA, model: Autosorb-iQ Station 1). Before analysis, the sample was degassed at 110°C for 1hour. Furthermore, the zeta potential analysis was used to determine the surface charge properties of the synthesized Ni-Co LDH, operated in the range 10-90°C (Malvern Instrument, model: Zetasizer Nano ZS). For adsorption studies, the concentrations for 2,4-DNP were obtained at λ= 360 nm (absorption wavelength), using a UV-Vis spectrophotometer (PerkinElmer, USA, Model: LAMBDA 365).

3.2.2. 'Soft Chemical' Sol-Gel synthesis of mesoporous Ni-Co LDH

1:1 molar ratio of $Ni(acac)_2$ and $Co(acac)_3$ were dissolved in 60 cm^3 of 1:1 ethanol: acetone mixture and refluxed at 95°C for 2 hours. The formation of the metal hydroxides precipitate and maintenance of the pH of the mixture at 9.5 was facilitated by adding a few drops of NH_4OH, and finally the solution was refluxed for ≈5 hours to get Ni-Co LDH. Subsequently, 5 cm^3 of 2M HCl was added to complete the hydrolysis reaction of metals hydroxide sol, followed by stirring at room temperature for 45-50 minutes. The quasi-solid or gel obtained was then filtered off using Whatman no.42 filter paper, washed with approx. 15

cm^3alcohol, and finally dried in a vacuum desiccator containing silica grains [25]. Similarly, the synthesis procedure was iterated for different molar ratios of 1:2, 2:1, and 3:1 respectively.

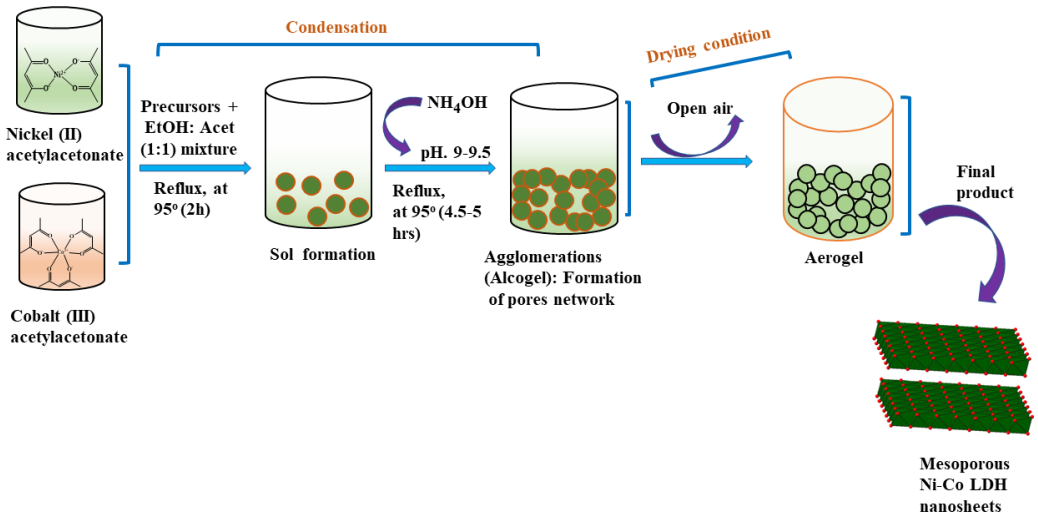

Figure 3.1. Schematic diagram showing the formation of mesoporous Ni-Co LDH nanosheets by non-aqueous 'soft chemical' Sol-Gel route

3.3. Result and discussion

3.3.1. Characterization of mesoporous Ni-Co LDH

3.3.1.1. Powder X-ray diffraction (PXRD) study

The PXRD diffraction pattern of the mesoporous Ni-Co LDH is shown in Figure 3.2. The scan rate was performed at $2\theta.min^{-1}$. The present study illustrates the novel mesoporous Ni-Co LDH by varying the stoichiometric molar ratios of 1:1, 1:2, 2:1, and 3:1 (M(II): M(III)).

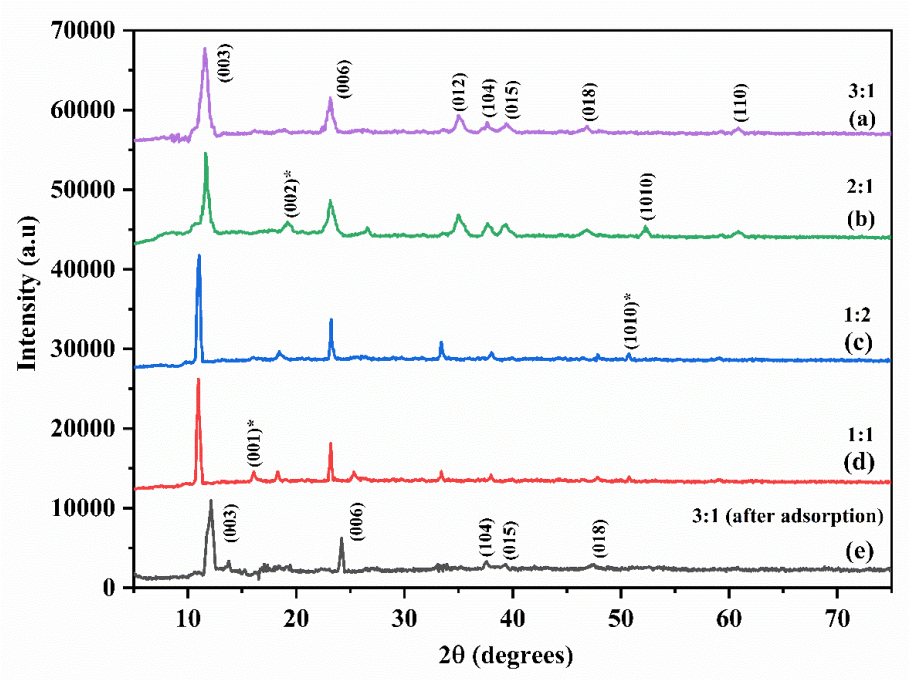

Figure 3.2. PXRD pattern of mesoporous Ni-Co LDH at different molar ratios of: (a) 1:1, (b)1:2, (c) 2:1, (d) 3:1 at 368 K, and (e) after adsorption of 2,4-DNP from aqueous solution

From Figure 3.2, it can be seen that the diffraction patterns of mesoporous Ni-Co LDH (varied molar ratios) exhibited the formation of hydrotalcite-like LDH phases (JCPDS code: 00-040-0216)[30]. It is found that the variation in stoichiometry ratios significantly impacts metal hydroxide phases. In the case of 1:1 and 1:2 Ni:Co ratios, the formation of α-$Co(OH)_3$ phase appears at almost the same diffraction angle at the onset peak of around 11.04° angle. The inclusion of a higher cobalt ratio has no impact on peak position. The variation in Ni ratio, on the other hand, results in a marginal change in peak position at a higher Bragg's angle. It is due to the increase in the Ni radius compared to Co atoms[31]. In general, the synthesized mesoporous Ni-Co LDH appears to be well-hydrolyzed co-existent phases. The planes denoted as (003), (006), (012), (104), (015), (018), (110) represent the various crystallographic planes obtained at every 2θ intervals. The appearance of some minor peaks at (002)*, (1010)*, (001)* planes show the co-existence of Ni and Co hydroxide in minute quantities. From the

obtained result, it can be stated that a decrease in the intensity peaks of Ni-Co LDH towards the higher Bragg's angles confirmed the formation of LDH or hydrotalcite-like compounds. It is clear from Figure 3.2 that the 3:1 Ni-Co LDH molar ratio represents a better LDH phase formation than the other molar ratios. Therefore, further application study has been carried out using a 3:1 ratio.

The PXRD pattern of Ni-Co LDH after the adsorption of 2,4-DNP from an aqueous solution is depicted in Figure 3.2(e). It is observed that the original diffraction pattern is maintained even after adsorption. However, the diffraction planes for (003) and (006) were slightly shifted to higher Bragg's angles obtained at 12.12^{o}, 24.2^{o}, and the intensity peaks became narrower or reduced to some extent, which signifies that despite adsorption, the crystalline structure of the Ni-Co LDH is preserved. Thus 2,4-DNPis well adsorbed on the LDH surface or layers[32]. Moreover, the (012) or (110) planes diminished, which show that some component of the crystal structure of LDH transforms due to adsorption[33].

3.3.1.2. Fourier-transform infrared spectroscopy (FT-IR) analysis

The FT-IR spectrum of the Ni-Co LDH is shown in Figure 3.3. The broadband that emerged at 3426 cm^{-1}can be attributed to the stretching vibration of the hydroxyl (OH) groups. The strong, intense peak recorded at around 1617 cm^{-1}represents the bending mode of interlayer water molecules[34]. In the Figure shown, the presence of the carbonate phase is not observed, which generally ranges from 1500-900 cm^{-1}. This is an important finding as it proves that the deintercalation of the carbonate phase occurs, which could be due to the inhibition of CO_2 gas due to hindrance by non-aqueous solvents during alcoholysis reaction with precursors. The representative peak at 752 cm^{-1} (generally from 800- 450 cm^{-1}) is the M=O stretching (M= Ni, Co; O= oxygen)[35].

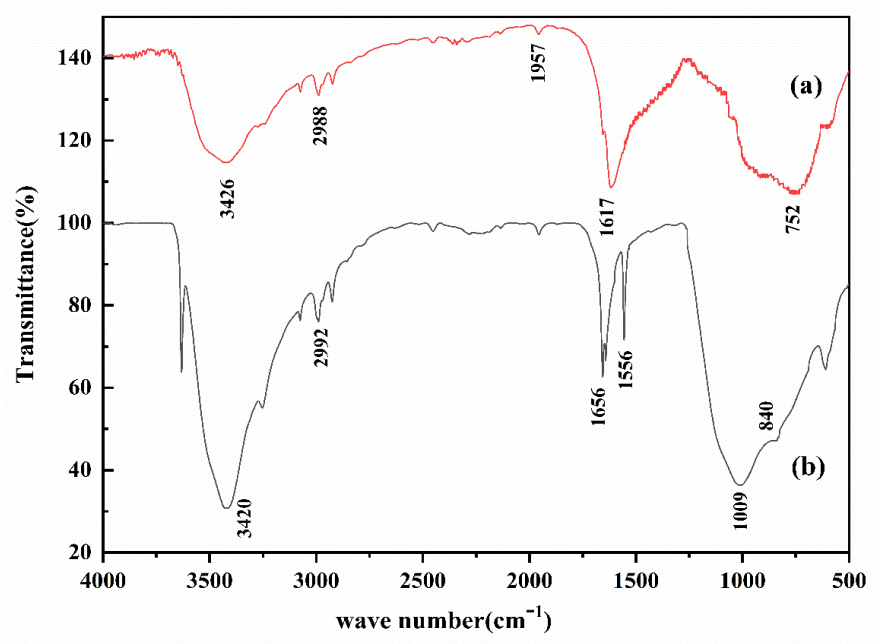

Figure 3.3. FT-IR spectra of mesoporous Ni-Co LDH (3:1) and(a) before adsorption(b) after adsorption of 2,4-DNP from aqueous solution

The FT-IR spectrum of Ni-Co LDH after adsorption of 2,4-DNP from an aqueous solution is shown in Figure 3.3(b). It can be seen that the symmetric stretching vibration of physically absorbed water molecules or OH stretching was recorded at 3420 cm^{-1}, comparable to the original Ni-Co LDH (Figure 3.3(a)). The absorption band at this region becomes slightly extended compared to the parent structure, which may be due to the presence of firmly adsorbed water molecules during the adsorption process[36]. The IR shoulder band at 2992 cm^{-1} (Figure 3.3(b)) or 2988 cm^{-1} (Figure 3.3(a)) represents the asymmetric bridging of OH with water. The medium sharp peak, attributed to interlayer water molecules or lattice water (bending vibration) was obtained at 1656 cm^{-1}, slightly lower than the original structure. In addition, the sharp band assigned at 1556 cm^{-1} can be attributed to the carbonate peak formed during the adsorption process[2]. Furthermore, the broadband obtained at 1009 cm^{-1} ≈ 1000 cm^{-1} or below appear due to metal oxides (MO) stretching or metal hydroxides (MOH) bending vibrations in the Ni-Co LDH layers(original structure).

3.3.1.3. Field emission scanning electron microscopy study (FESEM)

The surface morphology of the mesoporous Ni-Co LDH was characterized using FESEM. From the FESEM images of Figure 3.4 (a), (b), (c), and (d) at different resolutions, it was observed that the obtained mesoporous nanosheets exhibit a dense jelly-like coating layered one on top of the other, containing pores of different sizes which is a special characteristic of the synthesized Ni-Co LDH. The pores are densely packed with mesopores, which vary in size from 33±11 nm as seen in Figure 3.4 (a), (b), (c), (d).

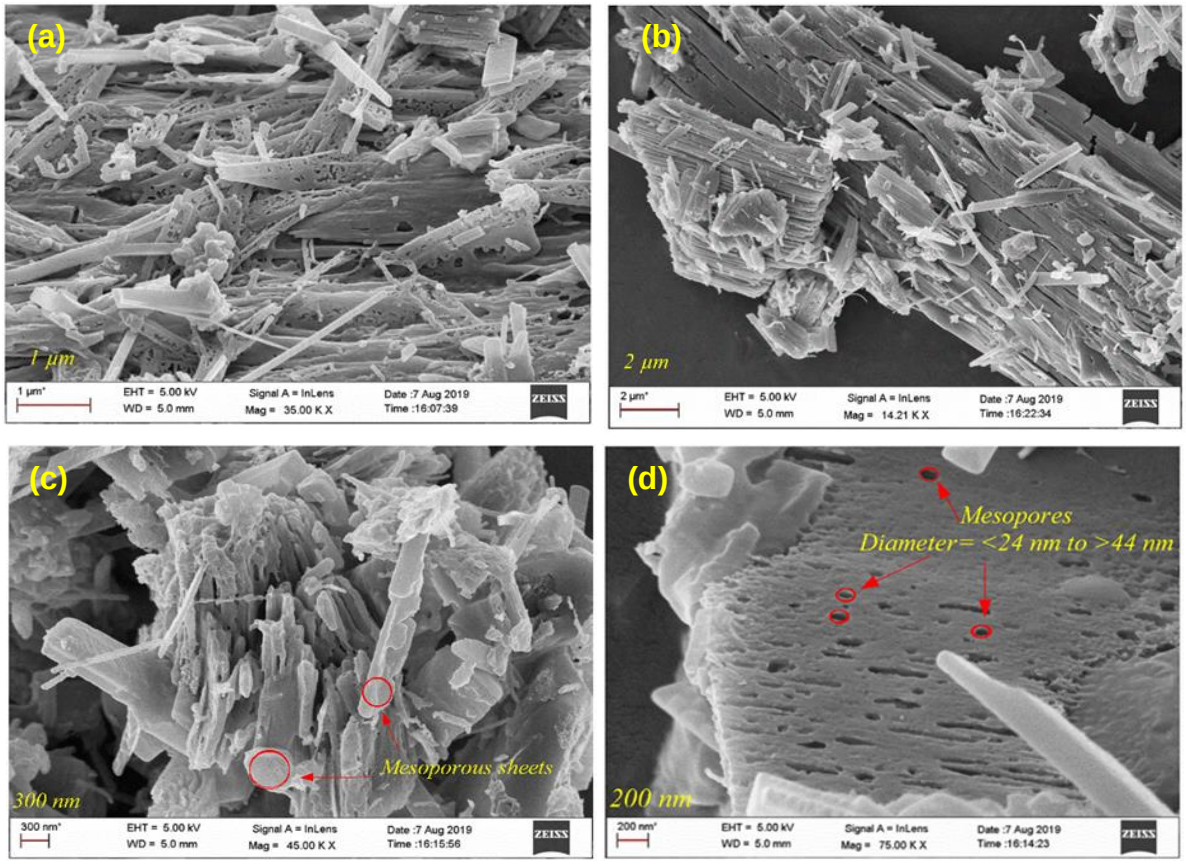

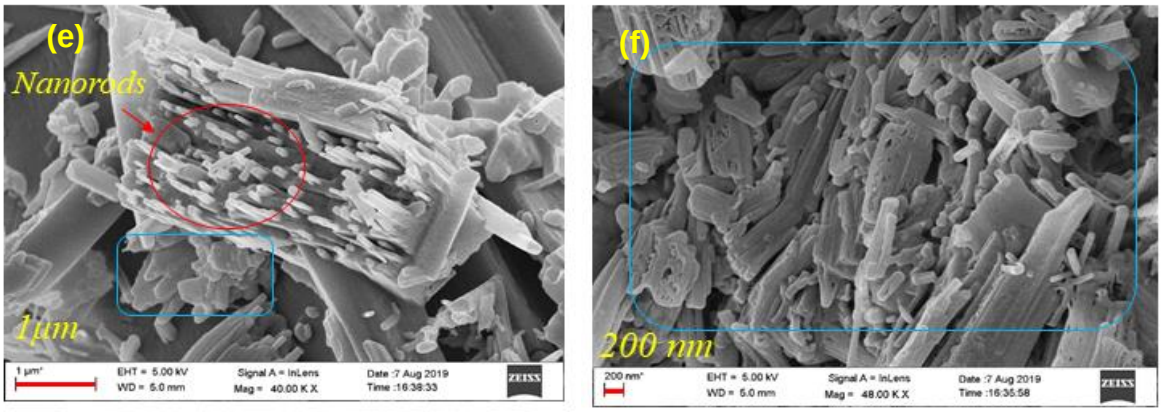

Figure 3.4. Showing mesoporous FESEM microscopy image of 3:1 Ni-Co LDH: Resolution at (a)1µm,(b)2µm, (c) 300 nm, (d) 200 nm, (e) 1µm (after adsorption) and (f) 200 nm (after adsorption)

The characteristic pore formation of mesoporous Ni-Co LDH might be due to the drying process favored by the alcogel property of the material[25]. Figures 3.4(a), (b), (c), and (d) show SEM images of the Ni-Co LDH, dried at 55°C, revealing well-defined pores. However, it has been known that drying conditions cause material shrinkage, particularly in LDH and porous materials in general[37]. Hence, the as-synthesized Ni-Co LDH maintains its pore stability in the material structure. It has been known that LDH complexes filled with nanopores (porosity) can be considered a good choice for different applications like electrochemical, ion exchange, or adsorption[38]. Figure 3.4(e) and (f) depict the surface morphology of mesoporous Ni-Co LDH after 2,4-DNP adsorption. It can be observed that plate-like/rod-like morphologies which were seen in the virgin mesoporous Ni-Co LDH are retained even after adsorption (Figure 3.4 (a), (b), (c)). However, it can be noticed that the morphological organization of the Ni-Co LDH nanosheets collapses into loosely spaced or stacked up forms, distributed in different directions, resulting in a rough surface (2,4-DNP well-adsorbed on the LDH surface) (Figure 3.4 (f)[39]. Importantly, it is apparent from Figure

3.4(f) that the metal hydroxide sheets are filled with mesopores, thereby proving that the Ni-Co LDH retains its pore structure even after undergoing adsorption[40].

3.3.1.4. High-resolution transmission electron microscopy study (HRTEM)

Figures 3.5 (a), (b), (c), and (d) represent the HRTEM images of the mesoporous Ni-Co LDH (3:1). It is evident from Figure 3.5 that the synthesized mesoporous Ni-Co LDH exhibits well-hydrolyzed $Ni(OH)_2$ and $Co(OH)_3$ phases characterized in the form of diffraction planes. The selected area electron diffraction (SAED) Ni-Co LDH diffraction planes showed that diffracted rings tend to be a set of concentric rings. Moreover, according to the study results, lattice planes are scattered in the crystallographic lattice, along with certain dark bands containing pores called nanopores[41]. The orientation of LDH matrices separated by two metal hydroxide layers determines the basal spacing d(00*l*). The (006), (012), (015), and (018) plane refers to the interlayer basal spacing of the synthesized mesoporous Ni-Co LDH. Figure 3.5(c) shows that the diameter of separation between the two layers was 0.259 nm, which corresponds to the (012) plane. The result agrees with the (012) Ni-Co LDH diffraction plane (Figure 3.2). The crystallite size of the synthesized mesoporous Ni-Co LDH was determined using Scherrer's formula and was determined to be 9.5 nm.

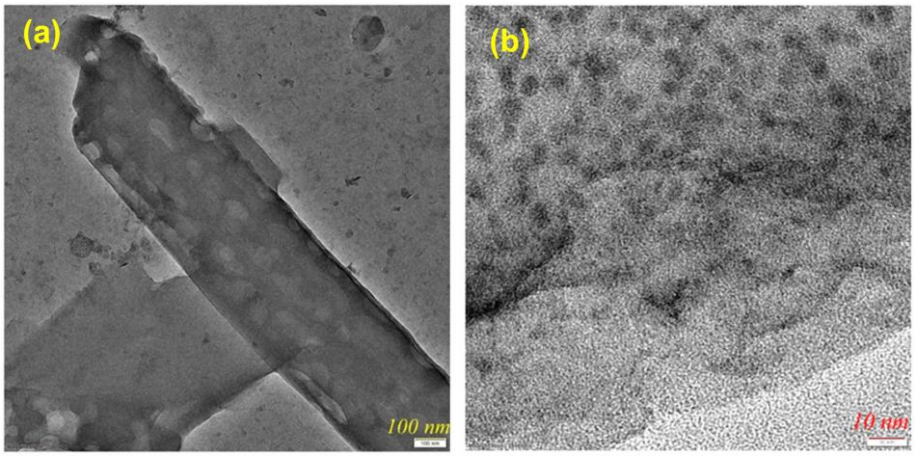

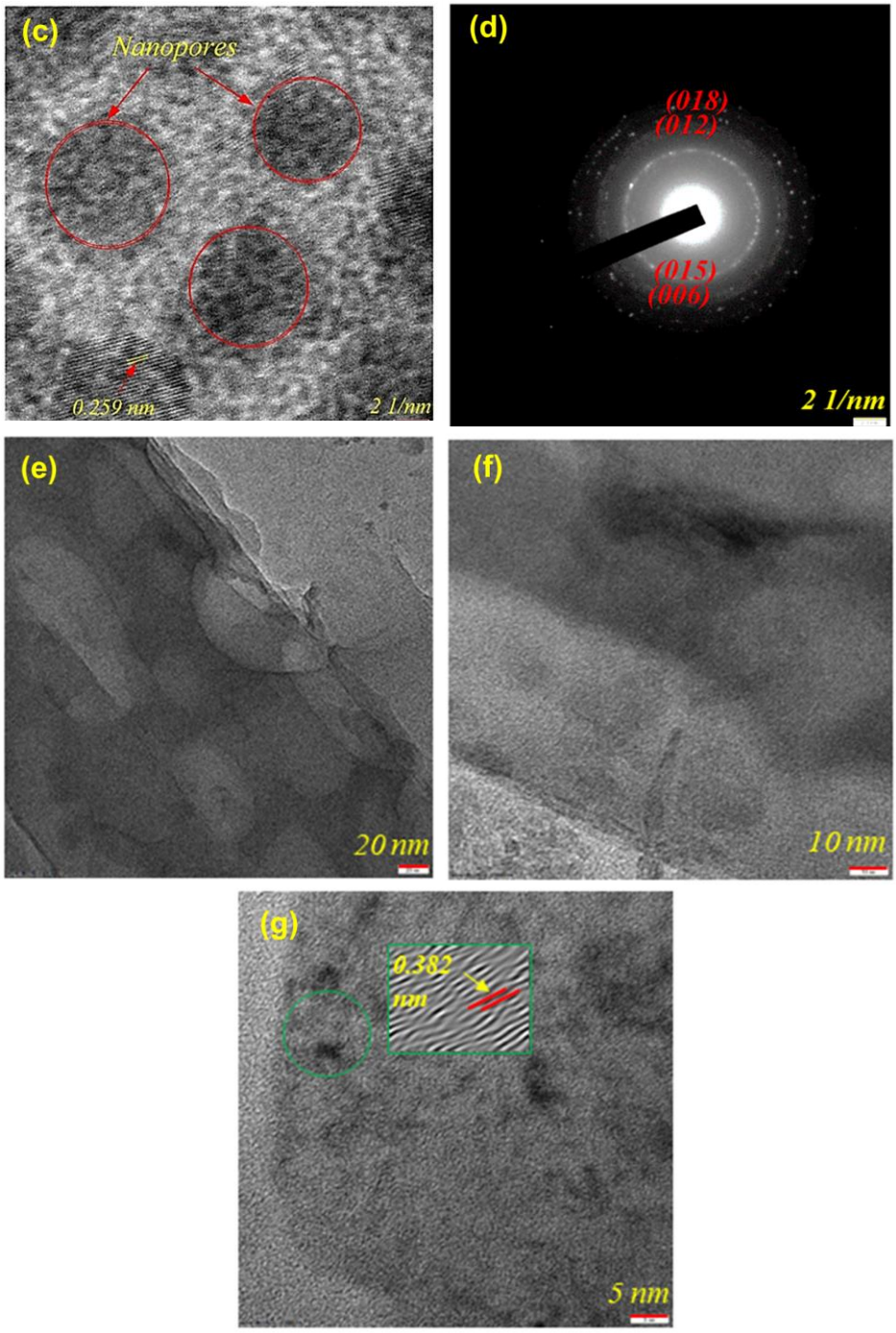

Figure 3.5. HR-TEM microscopy images of Ni-Co LDH (3:1): Resolution at **(a)** 100 nm, **(b)** 10 nm, **(c)** 2 nm, **(d)** SAED at 2nm, **(e)** 20 nm (after adsorption), **(f)** 10 nm (after adsorption) and **(g)** 5 nm (after adsorption)

Figure 3.5(e), (f), and (g) display TEM images of Ni-Co LDH after 2,4-DNP adsorption from an aqueous solution. As seen in Figure 3.5(e), (f), and (g), the lattice fringes or interlayer spacing of the mesoporous Ni-Co LDH decrease or becomes narrow due to 2,4-DNP adsorption, confirming the retention of its crystallinity despite some crystal characters being lost[42].The lattice plane and crystallite size were found to be 0.382 nm which corresponds to the (006) plane, and the size of the crystal increased to 10.3 nm, which is larger than the original Ni-Co LDH. The smaller the crystallite size, the broader will be the diffracted peaks.

3.3.1.5. X-Ray photoelectron spectroscopy (XPS) study

The photoelectron spectroscopy study was carried out to understand the existence of the chemical state of the mesoporous Ni-Co LDH (3:1), and is presented in Figure 3.6. It is seen from Figure 3.6(a) that the Ni 2p binding energy gives two distinct photo-emission lines, Ni 2p3/2 (855.3 eV) and Ni 2p1/2 (872.4 eV), confirming $Ni(OH)_2$ in +2 states. The broadband arose at 861.2 eV due to the paramagnetic effect of Ni in its valence orbital, or so-called 'shake-up satellite'. This phenomenon occurs when the Coulombic potential changes unexpectedly, and as a result, the photo ejected electrons pass through the valence band. Similarly, the presence of Coin trivalent oxidation states is shown by two spectral lines of $Co(OH)_3$, namely Co 2p 1/2 (779.9 eV) and Co 2p 3/2 (796.1 eV). In the case of $Co(OH)_3$, the satellite peak was found on the extreme left at higher binding energy (Figure 3.6(b)[43]. Furthermore, the binding energies of 531.4 eV and 532.3 eV (Figure 3.6 (c)) demonstrate that the core-level spectrum of O 1s contains two oxygen species (O_1 and O_2) intercalated into bimetallic Ni-Co LDH, i.e., metals bonded to oxygen and surface interlayer oxygen as water molecules.

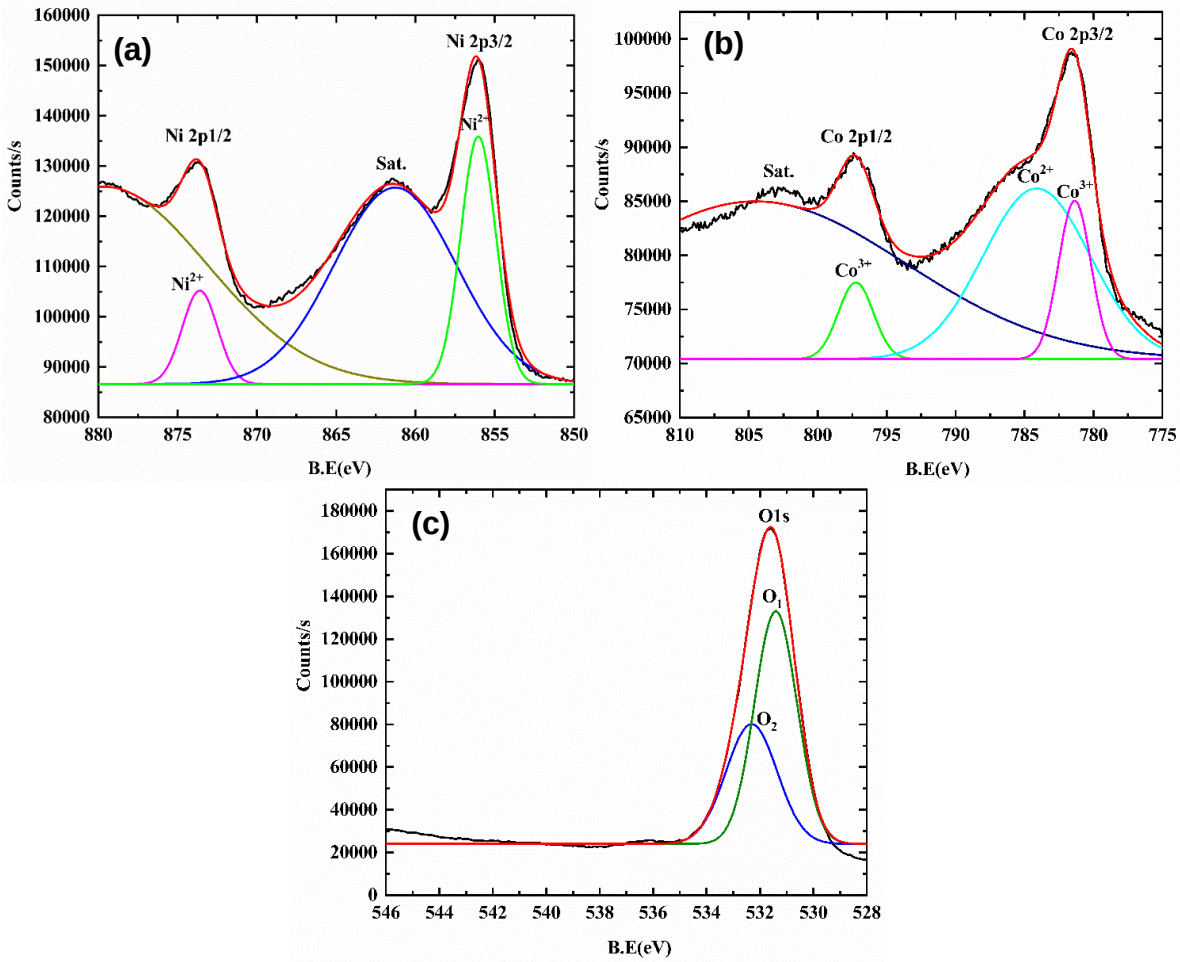

Figure 3.6. XPS spectra of 3:1 mesoporous Ni-Co LDH: **(a)** Ni 2p, **(b)** Co 2p and **(c)** O 1s

3.3.1.6. Thermogravimetric (TGA) analysis

The thermal degradation profile of mesoporous Ni-Co LDH (3:1) is shown in Figure 3.7. The Ni-Co LDH thermogram was obtained at the heating rate ofβ = 5 °C/min. It was observed that the pyrolysis reaction of Ni-Co LDH shows three major mass loss curves without involving the lower temperature range until 170°C. The temperature from 50 to 174°C correlates to the volatilization of moisture content or feebly adsorbed gases from the Ni-Co LDH matrix. The most noticeable difference at the onset temperature (first weight loss) from174 to 273°C (42.35%) implies the complete removal of weakly adsorbed interlayer water molecules. The most important weight loss occurs in the second stage, at around 274 to 405°C

(34.46 % mass loss). The physio-chemical change at this step involves dehydroxylation and complete degradation of interlayer ions bonded in the Ni-Co LDH surface.

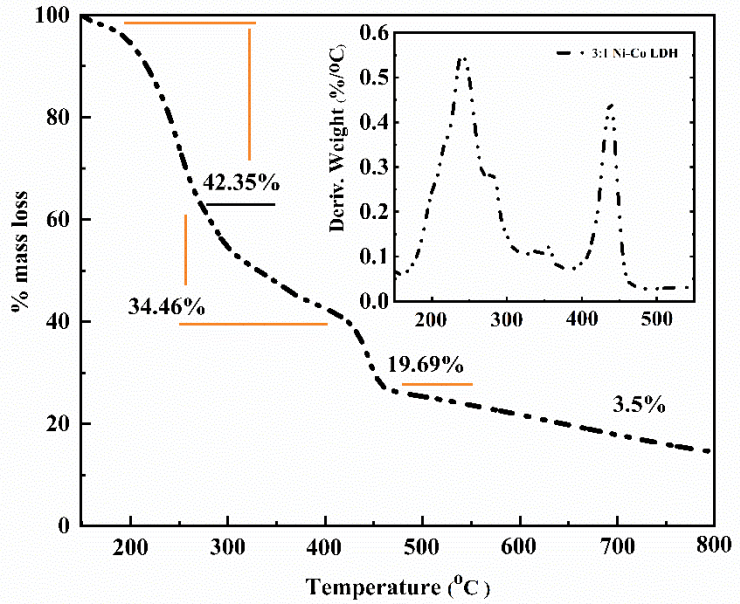

Figure 3.7. TGA degradation profile of the mesoporous Ni-Co LDH (3:1)

Similarly, the temperature at around 405 to 485°C (19.69% mass loss) or above indicates the degradation of the main Ni-Co hydroxide layers[44]. This final step involves the thermal conversion of the chemically bonded heterovalent hydroxide layers into their respective oxide phases. The 3.5% mass loss refers to the amount of residue left during the pyrolysis process.

3.3.1.7. BET surface and Zeta potential analysis of the mesoporous Ni-Co LDH

BET surface and Zeta potential analysis are the two important surface characterization techniques used in porous materials and surface charge analysis. It has been calculated that the synthesized mesoporous Ni-Co LDH having the pore area and pore volume was found to be 109 m^2g^{-1} and 1.63 cm^3g^{-1}. Moreover, the Barrett-Joyner-Halenda (BJH) pore size distribution of the synthesized Ni-Co LDH, which has a pore diameter of 9.5 nm corresponds to a mesoporous structure[45].

According to the Zeta potential (ζ) dissemination analysis, the nature of the surface charge properties of the mesoporous Ni-Co LDH nano sheets is favored by positively charged as +38.21 mV. The surface basicity of Ni-Co LDH nano sheets could be due to the segregation of more OH^- than H^+ ions during hydrolysis reactions of divalent and trivalent Ni/Co $(acac)_x$. In order to understand the electrostatic interaction of LDH with guest ions (electrical charge), the isoelectric value (IEP) was studied. From the calculated result, i.e., IEP=8.7, in which pH equals IEP value, becomes electrically neutral[46]. The utility of this is in studying ion exchange or adsorption phenomena.

3.4. Conclusion

The present study involves the synthesis of mesoporous Ni-Co LDH using an environmentally benign non-aqueous 'Soft Chemical' sol-gel method as an alternative approach. The novelty of the synthetic methodology is that it avoids the generation of CO_2 through the use of mild non-aqueous ethanol: acetone solvent system. The synthesized Ni-Co LDH exhibits typical 'Hydrotalcite' like nanosheets and is highly developed with mesopores of various sizes, as observed from the experimental surface characterization results (FESEM). The crystal morphology analysis by PXRD and HRTEM showed the synthesized compound is a crystalline material and the crystallite size was found to increase from 9.5 nm to 10.3 nm. The FTIR result showed the carbonate phase was absent in Ni-Co LDH, indicating the deintercalation of carbonate ions.

References

[1] A. Azari, M. Yeganeh, M. Gholami, M. Salari, The superior adsorption capacity of 2,4-Dinitrophenol under ultrasound-assisted magnetic adsorption system: Modeling and process optimization by central composite design, Journal of Hazardous Materials. 418 (2021). https://doi.org/10.1016/j.jhazmat.2021.126348.

[2] K. Chandrasekaram, Y. Alias, S.F. Fathullah, V.S. Lee, N. Haron, M. Raoov, N. Zakaria, S. Mohamad, Sporopollenin supported ionic liquids biosorbent for enhanced selective adsorption of 2,4-dinitrophenol from aqueous environment, Materials Today Communications. 28 (2021). https://doi.org/10.1016/j.mtcomm.2021.102587.

[3] V. Hasija, P. Raizada, A. Hosseini-Bandegharaei, P. Singh, V.H. Nguyen, Synthesis and Photocatalytic Activity of Ni–Fe Layered Double Hydroxide Modified Sulphur Doped Graphitic Carbon Nitride (SGCN/Ni–Fe LDH) Photocatalyst for 2,4-Dinitrophenol Degradation, Topics in Catalysis. 63 (2020). https://doi.org/10.1007/s11244-020-01359-z.

[4] J. Grundlingh, P.I. Dargan, M. El-Zanfaly, D.M. Wood, 2,4-Dinitrophenol (DNP): A Weight Loss Agent with Significant Acute Toxicity and Risk of Death, Journal of Medical Toxicology. 7 (2011). https://doi.org/10.1007/s13181-011-0162-6.

[5] A. Urtiaga, Electrochemical technologies combined with membrane filtration, Current Opinion in Electrochemistry. 27 (2021). https://doi.org/10.1016/j.coelec.2021.100691.

[6] M. Rafique, S. Hajra, M.B. Tahir, S.S.A. Gillani, M. Irshad, A review on sources of heavy metals, their toxicity and removal technique using physico-chemical processes from wastewater, Environmental Science and Pollution Research. 29 (2022). https://doi.org/10.1007/s11356-022-18638-9.

[7] T. Velempini, E. Prabakaran, K. Pillay, Recent developments in the use of metal oxides for photocatalytic degradation of pharmaceutical pollutants in water—a review, Materials Today Chemistry. 19 (2021). https://doi.org/10.1016/j.mtchem.2020.100380.

[8] D. Chen, Y. Cheng, N. Zhou, P. Chen, Y. Wang, K. Li, S. Huo, P. Cheng, P. Peng, R. Zhang, L. Wang, H. Liu, Y. Liu, R. Ruan, Photocatalytic degradation of organic pollutants using TiO2-based photocatalysts: A review, Journal of Cleaner Production. 268 (2020). https://doi.org/10.1016/j.jclepro.2020.121725.

[9] R. Rashid, I. Shafiq, P. Akhter, M.J. Iqbal, M. Hussain, A state-of-the-art review on wastewater treatment techniques: the effectiveness of adsorption method, Environmental Science and Pollution Research. 28 (2021). https://doi.org/10.1007/s11356-021-12395-x.

[10] S.F. Anis, R. Hashaikeh, N. Hilal, Reverse osmosis pretreatment technologies and future trends: A comprehensive review, Desalination. 452 (2019). https://doi.org/10.1016/j.desal.2018.11.006.

[11] R. Rashid, I. Shafiq, P. Akhter, M.J. Iqbal, M. Hussain, A state-of-the-art review on wastewater treatment techniques: the effectiveness of adsorption method, Environmental Science and Pollution Research. 28 (2021). https://doi.org/10.1007/s11356-021-12395-x.

[12] J. Yang, B. Hou, J. Wang, B. Tian, J. Bi, N. Wang, X. Li, X. Huang, Nanomaterials for the removal of heavy metals from wastewater, Nanomaterials. 9 (2019). https://doi.org/10.3390/nano9030424.

[13] M. Ahmaruzzaman, Adsorption of phenolic compounds on low-cost adsorbents: A review, Advances in Colloid and Interface Science. 143 (2008). https://doi.org/10.1016/j.cis.2008.07.002.

[14] N.A.A. Qasem, R.H. Mohammed, D.U. Lawal, Removal of heavy metal ions from wastewater: a comprehensive and critical review, Npj Clean Water. 4 (2021). https://doi.org/10.1038/s41545-021-00127-0.

[15] M.H. Zahir, K. Irshad, M.M. Rahman, M.N. Shaikh, M.M. Rahman, Efficient Capture of Heavy Metal Ions and Arsenic with a CaY-Carbonate Layered Double-Hydroxide Nanosheet, ACS Omega. 6 (2021). https://doi.org/10.1021/acsomega.1c03294.

[16] J. Ali, H. Wang, J. Ifthikar, A. Khan, T. Wang, K. Zhan, A. Shahzad, Z. Chen, Z. Chen, Efficient, stable and selective adsorption of heavy metals by thio-functionalized layered double hydroxide in diverse types of water, Chemical Engineering Journal. 332 (2018). https://doi.org/10.1016/j.cej.2017.09.080.

[17] R.M.M. Santos, J. Tronto, V. Briois, C. v. Santilli, Thermal decomposition and recovery properties of ZnAl-CO3 layered double hydroxide for anionic dye adsorption: Insight into the aggregative nucleation and growth mechanism of the LDH memory effect., Journal of Materials Chemistry A. 5 (2017). https://doi.org/10.1039/c7ta00834a.

[18] S. Li, Y. Guo, M. Xiao, T. Zhang, S. Yao, S. Zang, H. Fan, Y. Shen, Z. Zhang, W. Li, Enhanced arsenate removal from aqueous solution by Mn-doped MgAl-layered double hydroxides, Environmental Science and Pollution Research. 26 (2019). https://doi.org/10.1007/s11356-019-04667-4.

[19] C. Modrogan, S. Căprărescu, A.M. Dăncilă, O.D. Orbuleţ, E. Vasile, V. Purcar, Mixed oxide layered double hydroxide materials: Synthesis, characterization and efficient application for Mn2+ removal from synthetic wastewater, Materials. 13 (2020). https://doi.org/10.3390/ma13184089.

[20] M.N. Sepehr, T.J. Al-Musawi, E. Ghahramani, H. Kazemian, M. Zarrabi, Adsorption performance of magnesium/aluminum layered double hydroxide nanoparticles for metronidazole from aqueous solution, Arabian Journal of Chemistry. 10 (2017). https://doi.org/10.1016/j.arabjc.2016.07.003.

[21] P. Gu, S. Zhang, X. Li, X. Wang, T. Wen, R. Jehan, A. Alsaedi, T. Hayat, X. Wang, Recent advances in layered double hydroxide-based nanomaterials for the removal of radionuclides from aqueous solution, Environmental Pollution. 240 (2018).

[22] V. Rives, Layered Double Hydroxides: Present and Future, 2001.

[23] Q. Wang, D. Ohare, Recent advances in the synthesis and application of layered double hydroxide (LDH) nanosheets, Chemical Reviews. 112 (2012). https://doi.org/10.1021/cr200434v.

[24] J. Prince, A. Montoya, G. Ferrat, J.S. Valente, Proposed general sol - Gel method to prepare multimetallic layered double hydroxides: Synthesis, characterization, and envisaged application, Chemistry of Materials. 21 (2009). https://doi.org/10.1021/cm902741c.

[25] V. Purcar, R. Şomoghi, S.G. Niţu, C.A. Nicolae, E. Alexandrescu, I.C. Gîfu, A.R. Gabor, H. Stroescu, R. Ianchiş, S. Căprărescu, L.O. Cinteză, The effect of different coupling agents on nano-zno materials obtained via the sol-gel process, Nanomaterials. 7 (2017). https://doi.org/10.3390/nano7120439.

[26] P. Saikia, A. Gautam, R.L. Goswamee, Synthesis of nanohybrid alcogels of SiO2 and Ni-Cr/Mg-Cr-LDH: study of their rheological and dip coating properties, RSC Advances. 6 (2016). https://doi.org/10.1039/c6ra23475e.

[27] H. Hu, J. Liu, Z. Xu, L. Zhang, B. Cheng, W. Ho, Hierarchical porous Ni/Co-LDH hollow dodecahedron with excellent adsorption property for Congo red and Cr(VI) ions, Applied Surface Science. 478 (2019). https://doi.org/10.1016/j.apsusc.2019.02.008.

[28] J. He, M. Wei, B. Li, Y. Kang, D.G. Evans, X. Duan, Preparation of layered double hydroxides, Structure and Bonding. 119 (2005). https://doi.org/10.1007/430_006.

[29] T. Wang, Y. Sun, S. Wang, X. Li, Y. Yue, Q. Gao, Effective Adsorption of Methyl Orange on Organo-Silica Nanoparticles Functionalized by a Multi-Hydroxyl-Containing Gemini Surfactant: A Joint Experimental and Theoretical Study, ACS Omega. 6 (2021). https://doi.org/10.1021/acsomega.1c01788.

[30] A. Mendiboure, R. Schoellhorn, ChemInform Abstract: Formation and Anion Exchange Reactions of Layered Transition Metal Hydroxides (Ni1-xMx)(OH)2(CO3)x/2(H2O)z (M: Fe, Co)., ChemInform. 18 (1987). https://doi.org/10.1002/chin.198723038.

[31] E.S. Zhitova, S. v. Krivovichev, I. v. Pekov, V.N. Yakovenchuk, Y.A. Pakhomovsky, Correlation between the d-value and the M2 +:M3 + cation ratio in Mg–Al–CO3 layered double hydroxides, Applied Clay Science. 130 (2016). https://doi.org/10.1016/j.clay.2016.01.031.

[32] R.M.M. Santos, J. Tronto, V. Briois, C. v. Santilli, Thermal decomposition and recovery properties of ZnAl-CO3 layered double hydroxide for anionic dye adsorption: Insight into the aggregative nucleation and growth mechanism of the LDH memory effect., Journal of Materials Chemistry A. 5 (2017). https://doi.org/10.1039/c7ta00834a.

[33] X. He, X. Qiu, J. Chen, Preparation of Fe(II)–Al layered double hydroxides: Application to the adsorption/reduction of chromium, Colloids and Surfaces A: Physicochemical and Engineering Aspects. 516 (2017). https://doi.org/10.1016/j.colsurfa.2016.12.053.

[34] J. Zhang, F. Zhang, L. Ren, D.G. Evans, X. Duan, Synthesis of layered double hydroxide anionic clays intercalated by carboxylate anions, Materials Chemistry and Physics. 85 (2004). https://doi.org/10.1016/j.matchemphys.2004.01.020.

[35] X. Wang, P. Wu, Z. Huang, N. Zhu, J. Wu, P. Li, Z. Dang, Solar photocatalytic degradation of methylene blue by mixed metal oxide catalysts derived from ZnAlTi layered double hydroxides, Applied Clay Science. 95 (2014). https://doi.org/10.1016/j.clay.2014.03.016.

[36] S.E. Mousavi, H. Younesi, N. Bahramifar, P. Tamunaidu, H. Karimi-Maleh, A novel route to the synthesis of α-Fe2O3@C@SiO2/TiO2 nanocomposite from the metal-organic framework as a photocatalyst for water treatment, Chemosphere. 297 (2022). https://doi.org/10.1016/j.chemosphere.2022.133992.

[37] V. Prevot, Y. Tokudome, 3D hierarchical and porous layered double hydroxide structures: an overview of synthesis methods and applications, Journal of Materials Science. 52 (2017). https://doi.org/10.1007/s10853-017-1067-9.

[38] K.M. Parida, L. Mohapatra, Carbonate intercalated Zn/Fe layered double hydroxide: A novel photocatalyst for the enhanced photo degradation of azo dyes, Chemical Engineering Journal. 179 (2012). https://doi.org/10.1016/j.cej.2011.10.070.

[39] Y. Yang, X. Yan, X. Hu, R. Feng, M. Zhou, In-situ growth of ZIF-8 on layered double hydroxide: Effect of Zn/Al molar ratios on their structural, morphological and

adsorption properties, Journal of Colloid and Interface Science. 505 (2017). https://doi.org/10.1016/j.jcis.2017.05.100.

[40] C. Dang, W. Yang, J. Zhou, W. Cai, Porous Ni-Ca-Al-O bi-functional catalyst derived from layered double hydroxide intercalated with citrate anion for sorption-enhanced steam reformingof glycerol, Applied Catalysis B: Environmental. 298 (2021). https://doi.org/10.1016/j.apcatb.2021.120547.

[41] T.L.P. Galvão, C.S. Neves, A.P.F. Caetano, F. Maia, D. Mata, E. Malheiro, M.J. Ferreira, A.C. Bastos, A.N. Salak, J.R.B. Gomes, J. Tedim, M.G.S. Ferreira, Control of crystallite and particle size in the synthesis of layered double hydroxides: Macromolecular insights and a complementary modeling tool, Journal of Colloid and Interface Science. 468 (2016). https://doi.org/10.1016/j.jcis.2016.01.038.

[42] K. Gupta, J.B. Huo, J.C.E. Yang, M.L. Fu, B. Yuan, Z. Chen, (MoS4)2− intercalated CAMoS4·LDH material for the efficient and facile sequestration of antibiotics from aqueous solution, Chemical Engineering Journal. 355 (2019). https://doi.org/10.1016/j.cej.2018.08.200.

[43] L. Zhang, H. Xia, S. Liu, Y. Zhou, Y. Zhao, W. Xie, Nickel–Cobalt Hydroxides with Tunable Thin-Layer Nanosheets for High-Performance Supercapacitor Electrode, Nanoscale Research Letters. 16 (2021). https://doi.org/10.1186/s11671-021-03543-w.

[44] J.S. Valente, G. Rodriguez-Gattorno, M. Valle-Orta, E. Torres-Garcia, Thermal decomposition kinetics of MgAl layered double hydroxides, Materials Chemistry and Physics. 133 (2012). https://doi.org/10.1016/j.matchemphys.2012.01.026.

[45] S.Y. Jung, H.M. Kim, S. Hwang, D.G. Jeung, K.J. Rhee, J.M. Oh, Physicochemical properties and hematocompatibility of layered double hydroxide-based anticancer drug

methotrexate delivery system, Pharmaceutics. 12 (2020). https://doi.org/10.3390/pharmaceutics12121210.

[46] J.Y. Lee, G.H. Gwak, H.M. Kim, T. il Kim, G.J. Lee, J.M. Oh, Synthesis of hydrotalcite type layered double hydroxide with various Mg/Al ratio and surface charge under controlled reaction condition, Applied Clay Science. 134 (2016). https://doi.org/10.1016/j.clay.2016.03.029.

CHAPTER 3B

Part B: Applications of adsorption study on 2,4-DNP removal from aqueous solution: A theoretical study complemented by first principle DFT Monte-Carlo approach

This chapter explains the removal of 2,4-dinitrophenol (2,4-DNP) from aqueous solution by Ni-Co LDH. Various adsorption models involving equilibrium, kinetic and thermodynamic parameters as well as theoretical molecular dynamic simulation (MD) studies were used to describe the adsorption process.

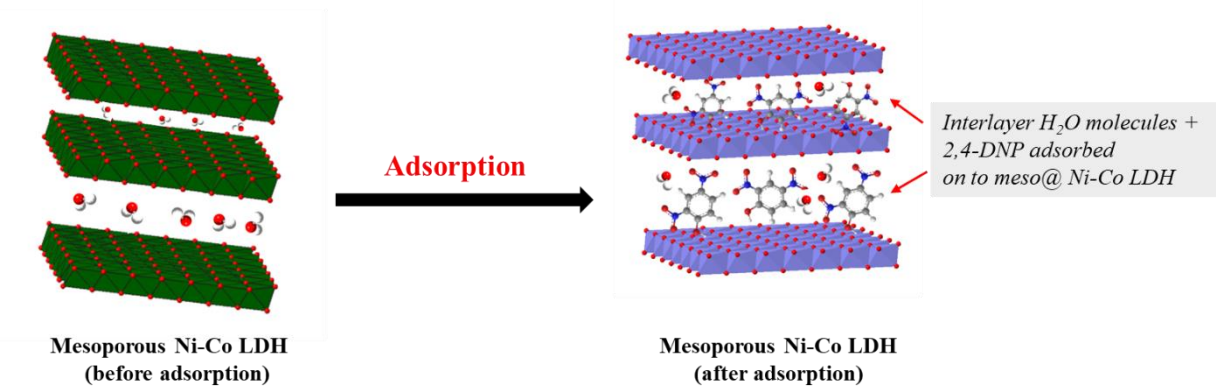

The text of this chapter has been published as:

A.R. Sangtam, P. Saikia, R.L. Goswamee, D. Sinha, U.B. Sinha, **Green synthesis of mesoporous Ni-Co layered double hydroxide and its application for removal of 2,4-dinitrophenol from water: a theoretical study complemented by the first principle density functional theory-Monte-Carlo approach**. *J. Environ. Chem. Eng.* 10 (2022), 108378. https://doi.org/10.1016/j.jece.2022.108378.

3.6. Experimental Section

3.6.1. Adsorption studies

The present study underlines the adsorptive removal of 2,4-dinitrophenol from the aqueous solution using a mesoporous Ni-Co LDH (3:1). The batch adsorption parameters such as pH, contact time, dosage, concentration, and temperature were determined to optimize the overall adsorption mechanism. Briefly, a 500 ppm stock solution was prepared by dissolving 500 mg of 2,4-DNP in double distilled water. Accordingly, solutions of different ppm varying from 10, 30, 60, 90 $mg.L^{-1}$ (50 ± 40) were prepared. The other batch parameters such as adsorbent dose of 0.01, 0.035, 0.055, 0.085, 0.1 g (0.055 ± 0.045), contact time of 30, 60, 90, 120, 150, 180, 210, 240, 280 (155 ± 125 mins), pH of 2, 4, 6, 8, 10, 12 (7 ± 5) maintained by 0.2 M NaOH or 0.1 M HCl, and temperature of 30, 40, 50°C (40 ± 10) were also varied. Before the adsorption studies were conducted, the mesoporous Ni-Co LDH was dried in an air oven at 65 ^{o}C for 1h to ensure the removal of any moisture or gases adsorbed on the LDH surface. The batch adsorption experiment was done in triplicate, and the mean value of the findings was used. The experiments were performed in a fume hood to minimize contamination.

After optimizing the batch adsorption parameters, the optimal 2,4-DNP concentration of 30 $mg.L^{-1}$ and equilibrium dose of 26.45 $mg.g^{-1}$ (0.055 g adsorbent) were chosen as the standard for the present study. The adsorbate concentrations before and after were quantified using a photo spectrometer at the UV_{max} absorption wavelength of λ=360 nm. The removal efficiency (%) of the adsorbate was calculated as:

$$\% \text{ of } 2,4-\text{DNP removal} = \frac{(C_o - C_e)}{C_o} \times 100 \qquad (1)$$

Where, C_o and C_e represent the initial and the equilibrium concentration of adsorbate $(mg.L^{-1})$. The amount of 2,4-DNP adsorbed at equilibrium time $q_e(mg.g^{-1})$ can be expressed as:

$$q_e = \frac{(C_o - C_e) \times V}{m} \qquad (2)$$

Where, q_e is the equilibrium adsorption capacity, m and V represent the mass of adsorbent (g) and volume of solution in liters (cm^3)[1].

For evaluation of equilibrium parameters, Langmuir, Freundlich, and Dubinin−Radushkevich isotherm models were applied. The linearized form of the Langmuir equation can be expressed as:

$$\frac{C_e}{q_e} = \frac{1}{q_m K_L} + \frac{1}{q_m C_e} \qquad (3)$$

The parameters $q_m(mg.g^{-1})$ *and* $K_L(L.mg^{-1})$ representing the Langmuir adsorption constants, refers to the maximum adsorption capacity in terms of monolayer coverage and free energy of adsorption related to an interaction affinity between adsorbate and adsorbents. The plot of $\frac{C_e}{q_e}$ vs q_e yields a straight line. The feasibility of Langmuir adsorption isotherm can be described by the R_L (separation factor) value and can be calculated as:

$$R_L = \frac{1}{(1 + K_L \times C_o)} \qquad (4)$$

The value of $R_L$describes the nature of the adsorption process. If $R_L > 1$ (unfavorable),$R_L = 0$ (irreversible), $R_L = 1$ (linear), $0 < R_L < 1$ (favourable)

Freundlich adsorption isotherm is an empirical model based on multilayer adsorption on a heterogeneous surface. The linearized form of the equation can be represented as:

$$log\ q_e = logK_F + \frac{1}{n}\ log\ C_e \qquad (5)$$

The parameters $K_F(L.mg^{-1})$ and $n\ (mg.g^{-1})$ are Frendulich adsorption constants and correspond to adsorption capacity and intensity. The plot of $log\ q_e$ vs $log\ C_e$ yields a straight line[2]. Dubinin-Radushkevich (D-R) isotherm model assumes physical adsorption of adsorbate (usually organic molecules) on microporous adsorbents. It is also based on multilayer adsorption and explains the Van der Waals interaction of adsorbate-substrate molecule, giving rise to a maximum monolayer adsorption capacity. The linearized equation of the D-R model can be expressed as:

$$lnq_e = lnq_m - (\beta\varepsilon^2) \qquad (6)$$

Plot of $q_e\ Vs\ \varepsilon^2$ yields a straight line. The adsorption potential $\varepsilon = RT\ \ln\left(1 + \frac{1}{C_e}\right)$.The parameters $q_e(mg.g^{-1})$ and $\beta(mol/g)^2$ correspond to the maximum amount of adsorbate adsorbed on the adsorbent surface and the activity coefficient used for obtaining the mean sorption energy[3]. The mean sorption energy can be calculated as:

$$E_m = \frac{1}{\sqrt{2\beta}} \qquad (7)$$

Evaluation of kinetic parameters was determined using pseudo-first and pseudo-second-order based on the Lagergen model. Similarly, the intra-particle kinetic model is based on Weber-Morris's theory. The linearized form of the pseudo-first and second-order can be independently represented as:

$$\log\,[q_e/(q_e - q_t)] = k_1 t \qquad (8)$$

$$\frac{t}{q_t} = \frac{1}{k_2 q_e^2} + \frac{t}{q_e} \qquad (9)$$

The quantities $k_1(min^{-1})$, $k_2(min^{-1})$and $q_e(mg.g^{-1})$ represent the pseudo-first and second-order constants. q_e and q_t represent the amount of adsorbate adsorbed at equilibrium and

equilibrium time $'t'$. The plot of log $(q_e - q_t)$ vs $'t'$ and $\frac{t}{q_t}$ vs $'t'$ would yield a straight line. The linearized form of the intra-particle diffusion model (Weber-Morris) can be described as:

$$q_t = k_{id} t^{0.5} + C \qquad (10)$$

The variables $k_{id}(mg.g^{-1}min^{0.5})$ and $C(mg.g^{-1})$ represent the intra-particle rate constant and boundary layer thickness. Plot of $q_t(mg.g^{-1})\ Vs\ t^{0.5}$gives a linear plot[4].The thermodynamic of adsorption of 2,4-DNP by the mesoporous Ni-Co LDH involves the calculation of activation energy $E_a(KJ.mol^{-1})$, standard Gibbs free energy $\Delta G^o(KJ.mol^{-1})$, enthalpy $\Delta H^o(KJ.mol^{-1})$, and entropy $\Delta S^o(JK^{-1}.mol^{-1})$. Considering the following expression:

$$lnK_D = \left(\frac{\Delta S^o}{R}\right) - \left(\frac{\Delta H^o}{RT}\right) \qquad (11)$$

$$\Delta G^o = -RT\ lnK_b \qquad (12)$$

$$\ln k_a = lnA - \left(\frac{E_a}{R}\right)\frac{1}{T} \qquad (13)$$

Equation (11) can be used to calculate the standard entropy and enthalpy from the Van't Hoff plot of $ln\ K_D$ vs reciprocal $\left(\frac{1}{T}\right)$. Similarly, standard Gibbs energy of adsorption can be evaluated using the equation (12). The Arrhenius parameters $E_a(KJ.mol^{-1})$ and $lnA(min^{-1})$ can be obtained from the linear plot of $\ln k_a$ vs reciprocal temperature[5].

3.6.2. Theoretical molecular simulation of 2,4-DNP adsorbed on mesoporous Ni-Co LDH surface

The MD simulation study of dinitrophenol adsorbed on Ni-Co LDH surface was investigated using BIOVIA material studio modules such as adsorption locator (Monte-Carlo approach) and DFT-based DMoL^3 calculation[6]. DFT-Based DMoL^3 Monte-Carlo simulation

was employed in the present study to understand physio-chemical adsorption parameters such as binding energy, energy minimization, nature of adsorbate-adsorbent interaction, orbital energy, chemical stability, or reactivity in terms of energy gaps, etc.[7]. The energy minimization or Molecular Dynamic (MD) calculation was performed using the adsorbate-substrate complex's periodic and non-periodic crystal systems. The comparison of both systems was made in terms of the same or different energy minimization functionals. Briefly, before energy simulations, the supercells containing (2a×2b×2c), (3a×3b×2a) P1 cell symmetry with the (006) and (003) mesoporous Ni-Co LDH planes was constructed using the 3D atomistic window located in the Material Studio. The main focus of building 2,4-DNP adsorption at various LDH planes was to establish the most stable receptors on the hydroxide layers, i.e., contact points at different hydroxyl terminals. The intermolecular interactions between 2,4-DNP and would arise due to the charge densities of LDH atoms on the configurational or lattice space in a solid-liquid media[8]. The cells containing both the crystal systems were then minimized (adsorbate and substrate, individually) using DMoL^3 *meta* GGA energy exchange functional. Later, the cells containing optimized adsorbate and adsorbent structures were introduced in the adsorption locator to find out the low energy configuration and determine the active binding site of the adsorbate. Moreover, the subsequent procedure for the cells containing the optimized adsorbate-adsorbent complex was used for orbital energy calculations[9].

3.6.3. Adsorption-desorption regeneration study

In the present study, the usefulness of Ni-Co LDH as an adsorbent was assessed for its efficacy as well as cost-effectiveness. Therefore, besides the adsorption modeling in terms of economic importance and cost-efficiency, a study was conducted to determine the regeneration adsorption cycles. Briefly, the optimal amount of Ni-Co LDH containing 0.05 g was saturated with the adsorbate concentration (2,4-DNP) containing 30 mg/L (50 cm^3) and was equilibrated

for 5 hours. After the adsorption equilibrium was established, the Ni-Co LDH residues were collected by centrifugation and washed several times with deionized water (to ensure removal of excess 2,4-DNP), and dried in an air oven at 65ºC. Subsequently, the desorption procedure was carried out using the adsorbent (reused) dispersed in such as NaOH and NH_3 solutions containing different concentrations. After the desorption run was completed, the resulting mixture containing the Ni-Co LDH and desorbent residues was separated by centrifugation, washed with deionized water, and the release of 2,4-DNP was analyzed. The regeneration procedure was repeated until the fifth cycle. The amount of adsorption/desorption concentrations were measured using a spectrophotometer. Referring eq.1, the desorption removal % of 2,4-DNP release can be expressed as:

$$R_{desorption}\ \% = 100 \times \frac{Q_{des}}{Q_{ads}} \qquad (14)$$

Where, Q_{ads} and Q_{des} represent the amount of 2,4-DNP adsorbed and released on the Ni-Co LDH surface at equilibrium[10].

3.7. Result and discussion

3.7.1. Adsorption isotherm

The various equilibrium modeling parameters for 2,4-DNP adsorption by a mesoporous Ni-Co LDH at 303 K, 313 K and 323 K, respectively is shown in Table 3.1. From the Langmuir and D-R adsorption parameters shown in Table 3.1. and Figure 3.8. (a), (c), the value of K_L(Langmuir) and q_e (D-R) increases with an increase in temperature (K). Also, the mean adsorption energies E_m for D-R lie between 0.337- 0.415 J mol^{-1}.

Table 3.1. Evaluation of equilibrium parameters

Langmuir	$Q_{max}(mg.g^{-1})$	$K_L(L.mg^{-1})$	R_L	R^2
303 K	36.95	1.49	0.06 ($10mg.L^{-1}$), 0.02 ($30\ mg.L^{-1}$), 0.01 ($60mg.L^{-1}$), 0.007 ($90mg.L^{-1}$)	0.9588
313 K	51.17	1.56	0.041 ($10mg.L^{-1}$), 0.014 ($30mg.L^{-1}$), 0.0071 ($60mg.L^{-1}$), 0.0047 ($90mg.L^{-1}$),	0.9662
323 K	53.67	2.31	0.062 ($10\ mg.L^{-1}$), 0.021 ($30\ mg.L^{-1}$), 0.011 ($60\ mg.L^{-1}$), 0.0074 ($90mg.L^{-1}$),	0.9558
Freundlich	n	$1/n$	K_f	R^2
303 K	1.808	2.412	2.522	0.9995
313 K	2.125	3.025	2.675	0.9997
323 K	2.164	3.071	2.681	0.9998
D-R model	$\beta(mol/g)^2 \times 10^{-3}$	$q_e(mg.g^{-1})$	$E_m(Jmol^{-1})$	R^2
303 K	3.04	63.04	0.337	0.9474
313 K	3.32	64.38	0.387	0.9485
323 K	4.38	67.36	0.415	0.9558

It was observed that the correlation factor (R^2) in the case of Langmuir and D-R were found to be less compared to Freundlich isotherm. Apparently, from the calculated parameters and Figure 3.8. (b), the Freundlich represents the best fitting model. It was found that the value of K_f (2.522-2.681) and n (1.808-2.164) increases slightly with the rise in temperature. It indicates that the interaction of adsorbate-adsorbent follows multilayer adsorption on the heterogeneous surface. The active binding site becomes stronger with the temperature rise, and the adsorption becomes endothermic[11]. The correlation coefficient (R^2) lies between 0.9995-0.9999.

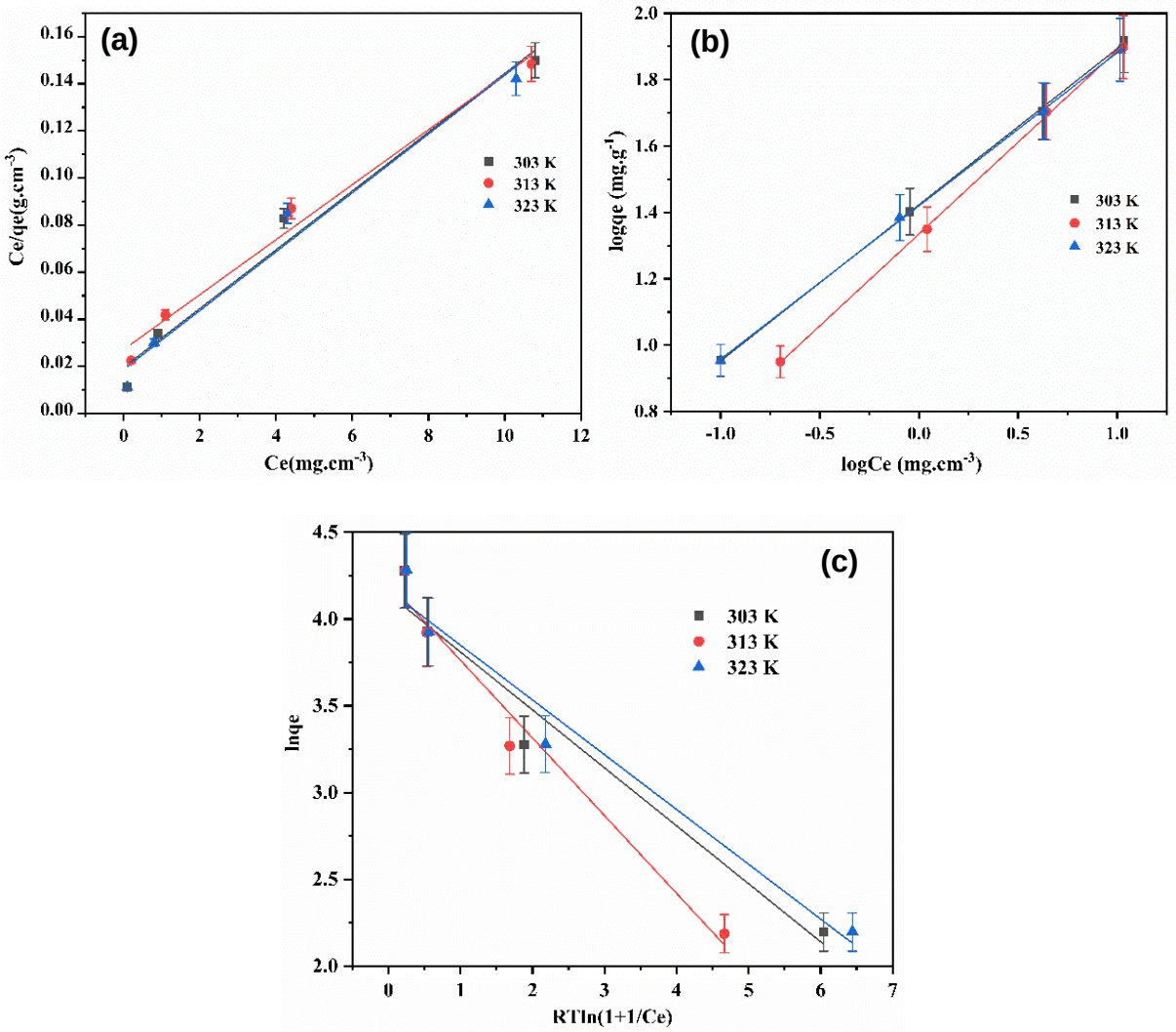

Figure 3.8. Isotherm modeling: (a) Langmuir, (b) Frendulich, and (c) Dubinin–Radushkevich at different temperatures (K)

3.7.2. Adsorption kinetics

The adsorption kinetic models are shown in the Table 3.2. From the calculated results, the pseudo-second order was the best fitting model with $R^2 = 0.9997$. This model assumes that the adsorption rate is proportional to the square of the vacant adsorption sites. Hence, the 2,4-DNP molecule adsorbed on the adsorbent surface dramatically influences the reaction rate. Moreover, from the calculated q_e values, the pseudo-second order model gives closer experimental values than those of the pseudo-first-order kinetic with the rate determining step

assumed to be chemisorptions[12]. The intra-particle diffusion model shows three stages: boundary layer diffusion, intra-particle, and equilibrium, as shown in Figure 3.9.(c).

Table 3.2. Calculation of kinetic parameters

Lagergren Pseudo-first order	$k_1(min^{-1})$	$q_e(mg.g^{-1})$	R^2
303 K	-1.6×10^{-2}	0.993	0.9725
313 K	-1.63×10^{-2}	1.052	0.9758
323 K	-1.57×10^{-2}	1.036	0.9772
Langergren Pseudo-second order	$k_2(min^{-1})$	$q_e(mg.g^{-1})$	R^2
303 K	0.99×10^{-3}	29.66	0.9995
313 K	1.02×10^{-3}	29.79	0.9992
323 K	1.04×10^{-3}	29.72	0.9998
Intraparticle diffusion model	$k_{id}(mg.g^{-1}min^{-0.5}$	$C(mg.g^{-1})$	R^2
303 K	1.38 1.4 1.43	10.03 10.12 11.05	$0.9884(k_1)$ $0.9882(k_2)$ $0.9885(k_3)$
313 K	1.54 1.56 1.57	15.82 15.91 16.14	$0.9872(k_1)$ $0.9985(k_2)$ $0.9988(k_3)$
323 K	1.68 1.73 1.77	17.57 17.69 17.7	$0.9983(k_1)$ $0.9987(k_2)$ $0.9989(k_3)$

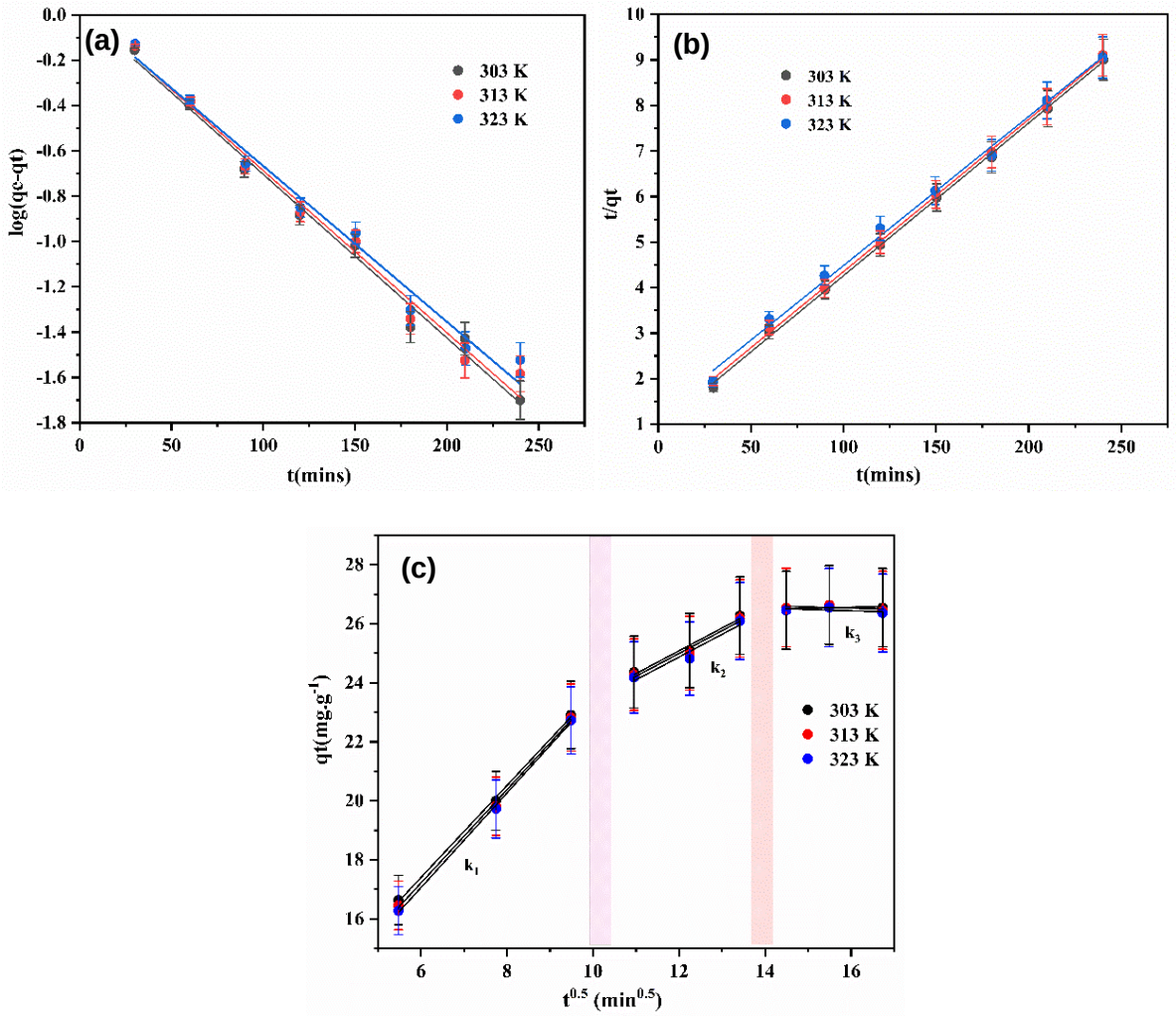

Figure 3.9. Kinetic modelling: (a) pseudo-first order, (b) pseudo-second order, and (c)Weber-Morris hypothesis at different temperatures (K)

From plot 3.9(c), the lines of the slopes represent the rates of adsorption. The values of diffusion constants k_1 and k_2 are much higher than k_3. The higher the slope, the faster will be the adsorption.

Therefore, it can be concluded that the rate of adsorption of adsorbate-adsorbent interactions is governed by a boundary layer diffusion (dominating step)[13].

3.7.3. Adsorption thermodynamics

Thermodynamic parameters determine the processes occurring in the adsorption process. The change in thermodynamic quantities such as free energy, enthalpy, and entropy determine the reaction feasibility and mechanism of the adsorption process. From Figure 3.10.(a) and Table 3.3., the Arrhenius activation energy and pre-exponential factor of the 2,4-DNP adsorption were found to be $E_a = 66.74(kJ\ mol^{-1})$ and $lnA(min^{-1}) = 1.43 \times 10^2$ in the temperature range 295-323 K. Moreover, from the calculated Table 3.3. and Figure 3.10., it can be seen that the positive value of Gibbs energies and enthalpy change indicates that the adsorption process is non-spontaneous and endothermic. It further confirms the adsorption process accompanied by chemisorption[14]. Moreover, the positive values of ΔG^o and ΔH^o suggest that the adsorption occurs better at low thermodynamic temperatures. The positive value of ΔS^o also indicates that an increase in temperature increases disorderness of the adsorption system.

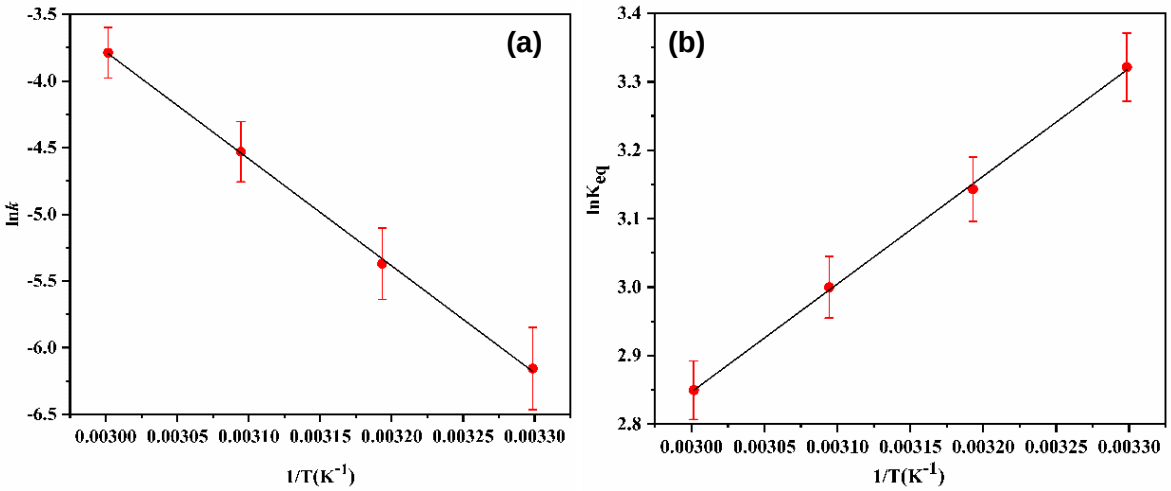

Figure 3.10. Thermodynamic parameters: (a) Arrhenius activation energy plot and (b) Van Hoff plot of enthalpy and entropy

Table 3.3. Evaluation of thermodynamic and Arrhenius parameters

LDH-2,4-DNP complex	
$\Delta H (kJ\ mol^{-1})$	0.65
$\Delta S (JK^{-1}\ mol^{-1})$	0.0225
$\Delta G (kJ\ mol^{-1})$	0.62 (295 K) 0.60 (303 K) 0.56 (313 K) 0.49 (323 K)
Activation Energy $E_a (kJ\ mol^{-1})$	66.73
Pre-exponential factor $\ln A\ (min^{-1})$	1.43×10^2

Table 3.4. Comparison of adsorption parameters of the present study with reported literature

Adsorbent	**Adsorbate**	**Experimental conditions**					**Ref.**
		Adsorbent dosage (g)	Equilibrium time (mins/hrs)	Conc. (mg/L)	Adsorpti-on Capacity (mg/g)	pH	
Molecular imprinted polymers (MIP)	2,4-DNP	0.05	-	10	3.50	6	[15]
βCD-TDI	2,4-DNP	2	120	10	3.895	4	[16]
βCD-HDI	2,4-DNP	2	120	10	3.438	4	[16]
Dried sludge	2,4-DNP	0.5	60	50	4.35	7	[17]
Modified sludge	2,4-DNP	0.5	60	50	4.75	7	[17]
Microwave -d sludge	2,4-DNP	0.5	60	50	5.49	7	[17]
$SilprSP_3NI$ mB	2,4-DNP	0.025	180	50	51.81	4	[18]
CA-MIP	2,4-DNP	-	60	10	≈4	7	[19]
PS-MIP	2,4-DNP	-	120	10	≈3.5	5	[19]
Char ash	2,4-DNP	1	-	40	7.55	9	[20]
MgAl-mixed oxide	PhOH	0.10	20–25h	100	25.5	5, 10	[21]
Ni-Co LDH	**2,4-DNP**	**0.05**	**150-180**	**30**	**53.67**	**2,4,6**	**Prese -nt study**

Table 3.4. represents a comparative study of adsorption parameters of the present study with some earlier reported literature. Contact time, adsorbent dose, and adsorption capacity are essential parameters to measure the efficiency of an adsorbent. From Table 3.4., it can be observed that the present synthesized adsorbent i.e., Ni-Co LDH has a higher adsorption capacity of 53.67 mg/g at a dosage of 0.05 g.

3.7.4. Adsorption locator

In this study, we used the Compass II force field with ultra-fine grid resolution to study 2,4-DNP preferential adsorption on Ni-Co LDH. The simulation resulted in varied energy values of adsorbate deposited on (003) Ni-Co LDH supercells. Adsorption energies can be calculated as:

$$E_{ads} = E_{LDH+2,4\,DNP} - \left(E_{LDH} + E_{2,4\,DNP}\right) \qquad (14)$$

Where, $E_{LDH+2,4\,DNP}$ represents the energy of adsorbate plus substrate and $E_{LDH} + E_{2,4\,DNP}$ represents individual energies of adsorbate and substrate[22]. The maximum adsorption distance of the adsorbate-substrate was precisely set at 9.00 Å[8].

3.7.5. Prediction of adsorbate-substrate binding site interactions and calculation of adsorption energy parameters

The intramolecular adsorption of 2,4-DNP on the (003) Ni-Co LDH surface as indicated by the number of dots by field values is shown in Figure 3.11 (c). In this figure, the green dots indicate the most probable binding sites on the adsorbent surface in contrast to the red ones. The blue dots represent the accumulation of unreacted water molecules. According to recent literature, the adsorption locator module calculates the adsorbate-adsorbent interaction behavior and predicts the actual binding sites of molecules based on the nature of the interaction[9]. From the results generated, the sorption processes were found to occur through OH-terminal facing

upward and downward towards adsorbate molecules. According to Table 3.5. and simulated results (Figure 3.11.), the LDH molecules may react with 2,4-DNP molecules in several ways. These might occur due to an interchange of interlayer ions or molecules between the dual hydroxide layers or as a consequence of OH^- terminals representing the upper/ lower layers[23].

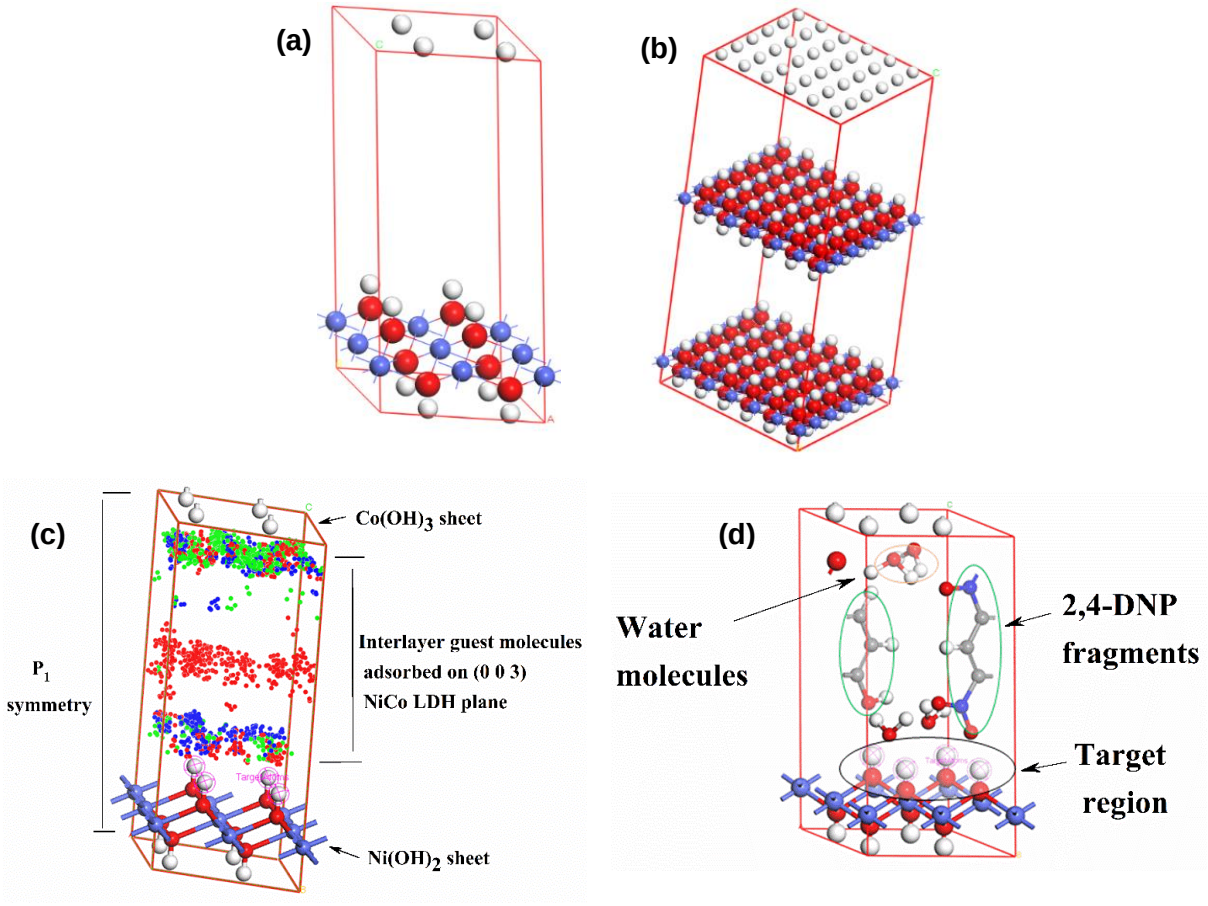

Figure 3.11. Optimized structures of Ni-Co LDH **(a)** (2a×2b×2c) and **(b)** (3a×3b×2c) supercells, **(c)** 2,4-DNP molecule adsorbed on (2a×2b×2c) (003) Ni-Co LDH plane and **(d)** visualized structure of **(c)**

Table 3.5. Calculated energy parameters obtained by Monte-Carlo Simulation Method (MCSM)

Ni-Co LDH	2,4-DNP	Total energy	Adsorption energy	Rigid adsorption energy	Interaction distance (A°)	Substrate binding sites	Total interactions	Nature of interaction
2-layer	1-mol	-92.7 (kcal/mol)	-137.83 (kcal/mol)	-144.81 (kcal/mol)	1.45(NO_{2ads}-OH_{subs}) 1.62 (OH_{ads}-OH_{subs}) 1.59 (NO_{ads}-OH_{subs})	OH_{ter}-(lower) OH_{ter}-(both) OH_{ter}-(upper)	3	Hydrophobic
3-layer	1-mol	-177 (kcal/mol)	-373 (kcal/mol)	-212 (kcal/mol)	1.16 (NO_{2ads}-OH_{subs}) 1.27 (NO_{ads}-OH_{subs}) 1.39 (OH_{ads}-OH_{subs}) 2.05(CH_{ads}-OH_{subs}) 1.46 (CO_{ads}-OH_{subs})	OH_{ter}-(Both) OH_{ter}-(Both) OH_{ter}-(Both) OH_{ter}-(upper) OH_{ter}-(lower)	5	Hydrophobic

Consequently, the interaction binding sites were determined through OH-terminals lying on the top, middle, or margins. These connect the adsorbate molecules through hydrophobic affinity. The solvent or non-polar molecules (water) do not influence hydrophilic adsorbate molecules. As a result, the interaction may be said to be hydrophobic interaction. From Figure 3.11(d), it can be seen that the molecule of adsorbate dissociates into different fragments. These fragments are created in the system and typically react with the solvent molecules[24]. Due to the high intermolecular force exerted on the substrate layer, adsorbate fragments containing NO_2 or OH^- radicals tend to draw towards the adsorbent (LDH) surface. Table 3.5. depicts the computation of bond distances between adsorbate and substrate. It was found that the length of the interaction of 2,4-DNP-LDH increases in the order OH_{subs}-CH_{ads}>OH_{subs}-CO_{ads}>OH_{subs}-OH_{ads}>OH_{subs}-NO_{ads}>OH_{subs}-NO_{2ads}. The shorter the bond distance, the greater would be the

adsorption affinity[25]. From Table 3.5. it can be observed that an increase in the Ni-Co LDH molecule increases the order of 2,4-DNP adsorbed on Ni-Co LDH layers. On the other hand, through simulated annealing, the 2,4-DNP molecule dissociates into small components and form fragments on the LDH complex interface which is referred to as adsorption by fragments. However, when the Ni-Co LDH surface increases and conversely decreases the adsorbate species, the periodic system of the 2,4-DNP has enough space to interact with the host molecules without undergoing the fragment's adsorption. As a result, the adsorption energies yield negative energy values.

3.7.6. Molecular orbital energy calculation

A computation analysis of frontier orbital energy provides information about the energy excitation from the ground state to the excited state of atoms. The energy difference (E) is the most influential property that governs the orbital energies of the different complexes. The energy difference of frontier orbitals can be calculated as follows:

$$\Delta E_{ind/grp} = HOMO_{ind/grp} - LUMO_{\frac{ind}{grp}} \qquad (15)$$

Where $HOMO_{ind/grp}$ and $LUMO_{ind/grp}$ represent the energy state for the individual/group of Ni-Co LDH- 2,4-DNP complex. The mGGA energy correlation functional was employed to understand the complex system's orbital. The electronic ground orbital was treated using all-electron relativistic with the DNP basis set[26]. The result of the molecular orbital energy calculations is shown in Table 6., and Figure 3.12. shows the energy minimization of Ni-Co LDH and 2,4-DNP interactions using the DmoL^3 DFT-method.

Table 3.6. Calculation for the frontier molecular orbital energies of adsorbate-substrate complex and energy gaps from the DMoL[3] *meta*GGA-TPSS energy functional

Complex	HOMO	LUMO	HOMO-LUMO
(2a×2b×2c) Ni-Co LDH supercell	-53.68 eV	-39.37 eV	14.31 eV
(3a×3b×3c) Ni-Co LDH supercell	-99.13 eV	-59.18 eV	39.95 eV
2,4-DNP molecule	-25.82 eV	-23.18 eV	2.64 eV
(2a×2b×2c) Ni-Co LDH-2,4-DNP	-146.31 eV	-89.22 eV	57.09 eV
(3a×3b×2c) Ni-Co LDH-2,4-DNP	-170.12 eV	-107.10 eV	63.02 eV

Table 3.6. demonstrates that the frontier HOMO molecular orbitals of Ni-Co LDH (substrate) or 2,4-DNP (adsorbate) molecules produce a more significant negative value than the LUMO energy state. The bonding orbital, which is more stable than the anti-bonding orbital, has a higher energy level. However, if the ground state orbitals yield an energy value larger than zero, it correlates to less stability and, as a consequence, weakens the chemical bonds. According to the simulated results, the Ni-Co LDH energy gap produces large values with the increases in surface layer as compared to 2,4-DNP, which gives small energy gap values. The crucial distinction between a small and big energy gap implies chemical stability or reactivity.

As a consequence, the substrate (Ni-Co LDH) is chemically more stable than the adsorbate (2,4-DNP). On the other hand, 2,4-DNP molecules are more reactive than Ni-Co LDH molecules. When 2,4-DNP and Ni-Co LDH molecules interact, the chemical stability of the composite adsorbate/substrate is greater than that of the individual adsorbate/substrate as the energy gaps expand linearly.

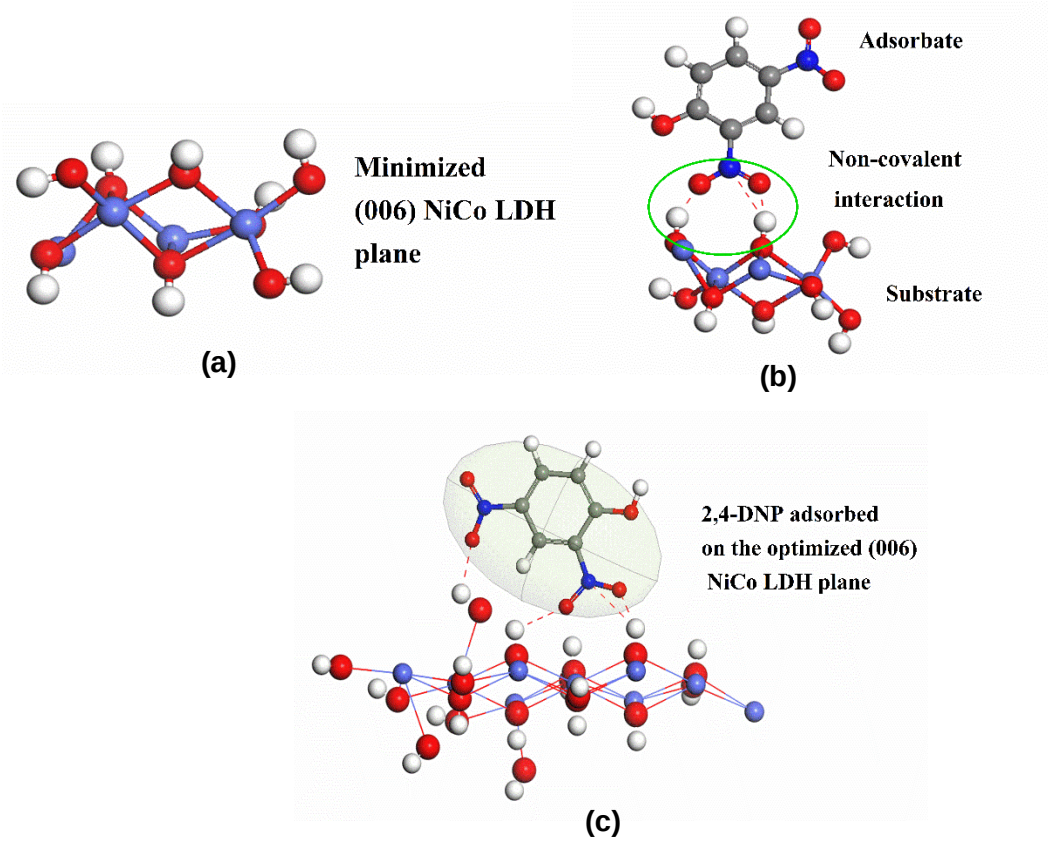

Figure 3.12. Showing: **(a)** Minimized (2a×2b×2c) Ni-Co LDH supercell, **(b)** Electrostatic interactions of Ni-Co $LDH_{(006)\ plane}$-2,4-$DNP_{(1\text{-molecule})}$ complex**, (c)** 2,4-DNP adsorbed on the surface containing (3a×3b×2c) Ni-Co LDH supercell

3.7.7. Adsorption-desorption and regeneration study

The adsorption-desorption process of the adsorbate 2,4-DNP molecule was studied on the Ni-Co LDH surface in order to assess its regeneration capacity. The LDHs, in general, is composed of a variety of interlayer ions, and the ease of LDHs interlayer ions exchange happens due to the presence of weak hydrogen bonds between the two metal hydroxide layers, due to electrostatic interaction between the adsorbent and adsorbate which may be established resulting in desorption of 2,4-DNP. When NaOH was used for desorption, it was observed that due to its strong affinity towards Ni-Co LDH layers, the NaOH acts as a good desorbent as the regeneration cycle progresses, as shown in Figure 3.13. In the case of ammonia, the binding

affinity of NH_4^+ ions towards the Ni-Co LDH layer is relatively lower, hence, it doesn't have sufficient energy to release the 2,4-DNP at a faster rate. This could be due to irreversible chemical adsorption (according to kinetic and equilibrium modeling) that may be established in the host Ni-Co LDH layer. Thereafter it was found that the adsorption property of Ni-Co LDH shows an excellent removal capacity of 2,4-DNP as the cycle increases from LDH-1 to LDH-4, which is about 80-96% removal in 180 minutes (differ by only 8 to 9%). Further increase in the number of cycles does not have much impact on 2,4-DNP adsorption. This could be due to the contribution of pores, which become less accessible or become more saturated at the end of adsorption.

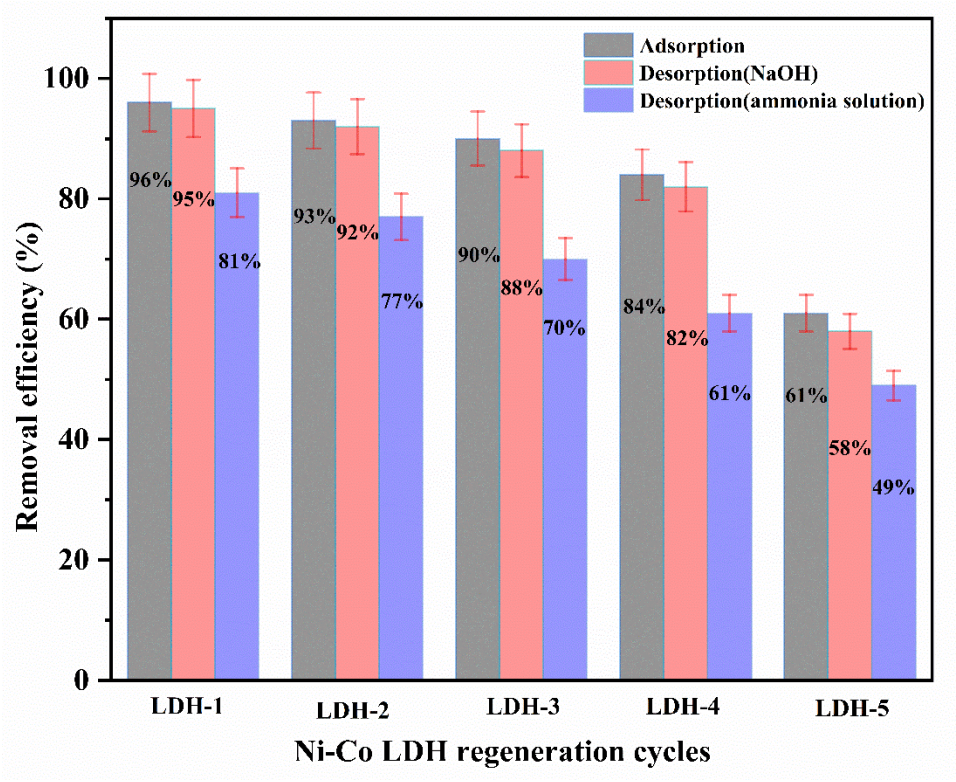

Figure 3.13. Ni-Co LDH regeneration cycles from 1-5 steps. Parameters (pH-9.5, conc-30mg/L, temperature 30℃, and contact time180 minutes) were fixed

3.8. Conclusion

As confirmed by the results of the adsorption analysis (experimental), the synthesized mesoporous Ni-Co LDH acts as an excellent adsorbent for removing 2,4-dinitrophenol from the aqueous solution, making it a suitable absorbent with the potential for environmental remediation. The maximum adsorption capacity was found to be 53.67 mg/g at 323K. The adsorption process was found to be heterogeneous (Freundlich adsorption isotherm), favorable, non-spontaneous, and endothermic (thermodynamic modeling) and the adsorption mechanism is favored by the chemisorption process (pseudo second order).

The most promising and excellent adsorption property of Ni-Co LDH is that the adsorption capacity increases with the subsequent increase in the adsorbent dosage, and the equilibrium adsorption can be attained within 150-180 minutes. The regeneration study showed that the mesoporous Ni-Co LDH has excellent removal affinity towards 2,4-DNP, having regeneration from cycles 1 to 4 within 150-180 minutes. Furthermore, theoretical molecular dynamic simulation (MD) revealed that the nature of adsorbate-substrate (2,4-DNP- Ni-Co LDH) interactions were hydrophobic interactions. DFT-based DMoL^3 approach showed that the adsorbate-substrate energy gap (eV) increases with the increase in the interfacial region, explaining the high chemical stability after the adhesion of adsorbate molecules.

In conclusion, the unique properties shown by the synthesized mesoporous Ni-Co LDH suggest that the synthesized compound would have importance in different applications such as efficient adsorbent in environmental remediation, intercalation (exchangeable property), electrochemical (pore diversity), antimicrobial (biocidal property), etc. To our knowledge, the 2,4-DNP adsorption from an aqueous medium by the mesoporous Ni-Co LDH represents the first investigation in the present study.

References

[1] S. Raghav, D. Kumar, Adsorption Equilibrium, Kinetics, and Thermodynamic Studies of Fluoride Adsorbed by Tetrametallic Oxide Adsorbent, Journal of Chemical and Engineering Data. 63 (2018). https://doi.org/10.1021/acs.jced.8b00024.

[2] M. Maruthapandi, V.B. Kumar, J.H.T. Luong, A. Gedanken, Kinetics, Isotherm, and Thermodynamic Studies of Methylene Blue Adsorption on Polyaniline and Polypyrrole Macro-Nanoparticles Synthesized by C-Dot-Initiated Polymerization, ACS Omega. 3 (2018). https://doi.org/10.1021/acsomega.8b00478.

[3] M.E. Mahmoud, M.F. Amira, S.M. Seleim, A.K. Mohamed, Adsorption Isotherm Models, Kinetics Study, and Thermodynamic Parameters of Ni(II) and Zn(II) Removal from Water using the LbL Technique, Journal of Chemical and Engineering Data. 62 (2017). https://doi.org/10.1021/acs.jced.6b00865.

[4] B. Oladipo, E. Govender-Opitz, T. v. Ojumu, Kinetics, Thermodynamics, and Mechanism of Cu(II) Ion Sorption by Biogenic Iron Precipitate: Using the Lens of Wastewater Treatment to Diagnose a Typical Biohydrometallurgical Problem, ACS Omega. 6 (2021). https://doi.org/10.1021/acsomega.1c03855.

[5] A.S. Ghatbandhe, H.G. Jahagirdar, M.K.N. Yenkie, S.D. Deosarkar, Evaluation of thermodynamic parameters of 2, 4-dichlorophenoxyacetic acid (2, 4-D) adsorption, Journal of Chemistry. (2013). https://doi.org/10.1155/2013/519304.

[6] Y. Zhang, Y. Wu, J. Zhuo, Q. Yao, Investigation of the Adsorption Behavior of Organic Sulfur in Coal via Density Functional Theory (DFT) Calculation and Molecular Simulation, Journal of Physical Chemistry A. 125 (2021). https://doi.org/10.1021/acs.jpca.1c02299.

[7] M.A.M. Abdalla, H. Peng, D. Wu, L. Abusin, T.J. Mbah, Prediction of Hydrophobic Reagent for Flotation Process Using Molecular Modeling, ACS Omega. 3 (2018). https://doi.org/10.1021/acsomega.8b00413.

[8] K.W. Jung, S.Y. Lee, J.W. Choi, M.J. Hwang, W.G. Shim, Synthesis of Mg–Al layered double hydroxides-functionalized hydrochar composite via an in situ one-pot hydrothermal method for arsenate and phosphate removal: Structural characterization and adsorption performance, Chemical Engineering Journal. 420 (2021). https://doi.org/10.1016/j.cej.2021.129775.

[9] M.J. Harrison, D.P. Woodruff, J. Robinson, Density functional theory investigation of the structure of SO2 and SO3 on Cu(1 1 1) and Ni(1 1 1), Surface Science. 600 (2006). https://doi.org/10.1016/j.susc.2006.02.020.

[10] S.M. Ashekuzzaman, J.Q. Jiang, Study on the sorption-desorption-regeneration performance of Ca-, Mg- and CaMg-based layered double hydroxides for removing phosphate from water, Chemical Engineering Journal. 246 (2014). https://doi.org/10.1016/j.cej.2014.02.061.

[11] G. Rathee, S. Kohli, A. Awasthi, N. Singh, R. Chandra, MoS42-intercalated NiFeTi LDH as an efficient and selective adsorbent for elimination of heavy metals, RSC Advances. 10 (2020). https://doi.org/10.1039/d0ra02766a.

[12] S. Das, S.K. Dash, K.M. Parida, Kinetics, Isotherm, and Thermodynamic Study for Ultrafast Adsorption of Azo Dye by an Efficient Sorbent: Ternary Mg/(Al + Fe) Layered Double Hydroxides, ACS Omega. 3 (2018). https://doi.org/10.1021/acsomega.7b01807.

[13] S.R. Khairkar, S. v. Pansare, A.A. Shedge, S. Chhatre, D.K. Kulal, V.R. Patil, A. v. Pansare, Biological macromolecule chitosan grafted co-polymeric composite: bio-

adsorption probe on cationic dyes, Polymer Bulletin. (2021). https://doi.org/10.1007/s00289-021-03954-w.

[14] M. Khnifira, A. Mahsoune, M.E. Belghiti, L. Khamar, M. Sadiq, M. Abdennouri, N. Barka, Combined DFT and MD simulation approach for the study of SO2 and CO2 adsorption on graphite (111) surface in aqueous medium, Current Research in Green and Sustainable Chemistry. 4 (2021). https://doi.org/10.1016/j.crgsc.2021.100085.

[15] M.F. Hsieh, J.Y. Cheng, J.C. Yang, D.S. Lin, K. Morgenstern, W.W. Pai, Determination of dissociative fragment-adsorbate interaction energy during chemisorption of the diatomic molecule HCI on Si(100), Physical Review B - Condensed Matter and Materials Physics. 81 (2010). https://doi.org/10.1103/PhysRevB.81.045324.

[16] G.Y. Abo El-Reesh, A.A. Farghali, M. Taha, R.K. Mahmoud, Novel synthesis of Ni/Fe layered double hydroxides using urea and glycerol and their enhanced adsorption behavior for Cr(VI) removal, Scientific Reports. 10 (2020). https://doi.org/10.1038/s41598-020-57519-4.

[17] C. Liu, F. Min, L. Liu, J. Chen, Density Functional Theory Study of Water Molecule Adsorption on the α-Quartz (001) Surface with and without the Presence of Na+, Mg2+, and Ca2+, ACS Omega. 4 (2019). https://doi.org/10.1021/acsomega.9b01570.

[18] T. Alp Tokat, B. Türkmenoğlu, Y. Güzel, D.Ş. Kızılcan, Investigation of 3D pharmacophore of N-benzyl benzamide molecules of melanogenesis inhibitors using a new descriptor Klopman index: uncertainties in model, Journal of Molecular Modeling. 25 (2019). https://doi.org/10.1007/s00894-019-4120-6.

[19] B. Bai, Y. Wu, R.B. Grigg, Adsorption and desorption kinetics and equilibrium of calcium lignosulfonate on dolomite porous media, Journal of Physical Chemistry C. 113 (2009). https://doi.org/10.1021/jp9028326.

[20] Y.M. Magdy, H. Altaher, E. ElQada, Removal of three nitrophenols from aqueous solutions by adsorption onto char ash: equilibrium and kinetic modeling, Applied Water Science. 8 (2018). https://doi.org/10.1007/s13201-018-0666-1.

[21] N.D. Zakaria, N.A. Yusof, J. Haron, A.H. Abdullah, Synthesis and evaluation of a molecularly imprinted polymer for 2,4-Dinitrophenol, International Journal of Molecular Sciences. 10 (2009). https://doi.org/10.3390/ijms10010354.

[22] J.M. Anne, Y.H. Boon, B. Saad, M. Miskam, M.M. Yusoff, M.S. Shahriman, N.N.M. Zain, V. Lim, M. Raoov, b-Cyclodextrin conjugated bifunctional isocyanate linker polymer for enhanced removal of 2,4-dinitrophenol from environmental waters, Royal Society Open Science. 5 (2018). https://doi.org/10.1098/rsos.180942.

[23] H. Niknejad, A. Esrafili, M. Kermani, V. Oskoei, M. Farzadkia, Comparing the efficiency of unmodified dried sludge adsorbents and those modified via chemical and microwave methods in removing 2,4-dinitrophenol from aqueous solutions, Journal of Environmental Health Science and Engineering. 18 (2020). https://doi.org/10.1007/s40201-020-00568-8.

[24] Z. Wang, C. Ye, H. Wang, Preparation of amino functionalized imidazolium-modified silicas by different coupling agents for removal of 2,4-dinitrophenol from aqueous solutions, International Journal of Environmental Science and Technology. 13 (2016). https://doi.org/10.1007/s13762-015-0827-9.

[25] N.A. Yusof, N.D. Zakaria, N.A.M. Maamor, A.H. Abdullah, M.J. Haron, Synthesis and characterization of molecularly imprinted polymer membrane for the removal of 2,4-dinitrophenol, International Journal of Molecular Sciences. 14 (2013). https://doi.org/10.3390/ijms14023993.

[26] S. Chen, Z.P. Xu, Q. Zhang, G.Q.M. Lu, Z.P. Hao, S. Liu, Studies on adsorption of phenol and 4-nitrophenol on MgAl-mixed oxide derived from MgAl-layered double hydroxide, Separation and Purification Technology. 67 (2009). https://doi.org/10.1016/j.seppur.2009.03.016.

CHAPTER 4A

Part A: synthesis and characterization of a Co(II)-Co(III) LDH and Ac@Co(II)-Co(III) LDH nanohybrid

This chapter describes the detail synthesis and characterization of a highly mesoporous Co(II)-Co(III) LDH and its nanohybrid through a sol-gel route with non-aqueous ethanol: acetone mixture as greener reagents. The compounds were characterized using PXRD, FESEM, HRTEM, FTIR, XPS, TGA-DTA, etc.

The text of this chapter has been published as:

A.R. Sangtam, K. Richa, P. Saikia, N. Longkumer, U.B. Sinha, R.L. Goswamee **Synthesis and characterization of Co(II)–Co(III) LDH and Ac@Co(II)–Co(III) LDH nanohybrid and study of its application as bactericidal agents.** *Results in Chemistry* 4 (2022), 100671. https://doi.org/10.1016/j.rechem.2022.100671.

4.1. Introduction

Layered double hydroxides (LDHs) are well-known nanosized or nanostructured inorganic compounds containing metal hydroxide in the main layers characterized by the stacking of double hydroxide sheets, separated by the space containing ions called interlayer anions[1,2]. The chemical composition and formula of layered double hydroxides (LDHs) can be represented as follows: $[M^{2+}_{1-x} M^{3+}_{x} (OH)_2]^{x+} (A^{n-})_{x/n} \times yH_2O$, wherein the M^{2+} (Mg, Ca, Ni, Fe, Co, etc.) and M^{3+} (Al, Co, Fe, Cr, etc.) denote divalent and trivalent metal ions, and A^{n-} and yH_2O represent the interlamellar ions and water molecules[3]. LDHs exhibit excellent properties, including ion exchange, intercalation, memory effect, catalytic, etc. Besides the properties shown by LDHs, the material can be used as important precursors in many applications such as electrochemical, adsorption, thermal, photocatalytic, and biological applications such as drug carriers, antimicrobial agents, etc. The fact about LDHs, which makes it more interesting, is that they are built up with highly positively charged metal hydroxide sheets, high surface area, and high ion exchange capacity. These diverse properties make the LDHs potential candidates for various applications[4,5]. The present study emphasizes a green synthesis of Co(II)-Co(III) LDH or Ac@Co(II)-Co(III) LDH nanohybrid using the non-aqueous Sol-Gel route. The greenness of the present methodology is that it uses non-corrosive metal acetylacetonates as the main precursors. Unlike other methods of synthesis of LDH where metal salts are taken as precursors and are subjected to hydrolysis in a highly alkaline medium resulting in the formation of soluble alkaline metal salts like NaCl, Na_2SO_4 as by-products, thereby requiring subsequent elaborate purification methods. However, in the present method, there is the formation of acetylacetonate as a by-product which can be easily separated from the products by filtration and low-temperature distillation, thereby rendering the procedure green.

The acetylacetonate complexes can be easily hydrolyzed at moderate temperature, with the use of ethanol: acetone mixture as 'mild organic solvents'. The present methodology further emphasizes the controlled co-precipitation of individual cobalt hydroxide phases stabilized in a non-aqueous acetone and ethanol mixture. This di- and tri-valent molar ratio in a given range, basically x= 0.2-0.5 ratio[6], has so far been a difficult objective to achieve because cobalt-containing divalent and trivalent LDHs combinations were rare to obtain as purely hydrolyzed separate phases earlier. This might have been due to an unstable trivalent Co^{3+} state in the aqueous medium, easily oxidized to a divalent Co^{2+} state, or in the presence of complexing reagents, Co^{2+} becomes unstable in LDH complex[7]. Therefore, the present study reports the unusual combination of divalent and trivalent cobalt hydroxide, which would result in a unique cobalt LDH, and in view of the ease of synthesis and greenness, the present methodology can be considered superior to various other methods such as hydrothermal, ion-exchange, salt-oxide, co-precipitation, etc[6,8]. Subsequently, the synthesized cobalt LDH and its nanohybrid were characterized using FESEM and HRTEM for morphological, PXRD and HRTEM for crystallographic information, FTIR, XPS, TGA-DTA, BET, and Zeta potential for bonding complex, chemical oxidation state and molar ratios, thermal degradation properties, pore areas and pore volumes, and zeta for surface charge analysis of the synthesized compounds. The antibacterial properties of Co(II)-Co(III) LDH or Ac@Co(II)-Co(III) LDH nanohybrid were thereafter assessed in order to study the applications of these compounds as antimicrobial agents. The advantages of cobalt LDH in the present study is that, unlike other LDHs, it is comparatively less toxic, cost-effective, and shows a diverse morphology. In other words, LDH containing cobalt precursor is considered unique because it is rarely reported in LDHs research. From the study's point of view, the applicability of cobalt LDH is not restricted to the specific

target in the study. On the other hand, it can also be applied to different fields of study due to its flexibility and versatility. In addition, LDH containing cobalt oxides (nanocomposite) exhibits high catalytic, oxidizing, electrochemical and acts as biocidal agents[9]. Also, they are particularly important in the current study in terms of microbial applications due to their reported biological activities[10,11]. So far, different LDHs combinations include Mg-Al LDH, Co-Al LDH, Zn-Ti LDH, Cu-Al LDH, Ni-Al LDH, Mn-Al LDH, and silver nanoparticles intercalated LDH nanocomposite or lysozymes@LDH or antibiotics@LDHs, etc. had been used in antibacterial studies[12-15]. The general mechanism of how the LDHs function as important antimicrobial precursors is affected by important factors like the nature of metallic ions, high basicity and positively charged metal hydroxide sheets, nature of guest ions/molecules hosted into LDH composite, di- and trivalent metallic LDH ratios, high ion exchange capacity, high surface area, and nature of interlayer charged ions etc[12,13,16]. In recent times, acetylacetone inhibition property towards microbes has been tested as an excellent antimicrobial agent, and reports revealed that hydrazide Schiff@ metal acetylacetonates had been used as a targeted drug against bacterial strains[17]. It is believed that metal nanoparticles containing antibacterial metallic or transition elements such as Ag, Zn, Cu, Co, Mn etc. are superior to most antibiotics as the particle size falls in the nanosize range, and they have biocidal properties, high permeability or penetrability against the bacterial cell membrane[18-20]. However, drawbacks still arise due to long operating procedures or a lack of greener approaches. Another drawback for most antibacterial agents is the lack of strong inhibition properties against any bacterial strains. Hence, transition metal-containing an effective combination of Co(II)-Co(III) LDH or Ac@Co(II)-Co(III) LDH nanohybrid would produce some practical outputs for the study of

antibacterial activity. To our knowledge, no known reports for the organic acetylacetone@ Co(II)-Co(III) LDH have been used as an antibacterial agent or other LDH in particular.

4.2. Materials and methods

4.2.1. Chemicals and reagents

All chemicals and reagents in the study were of analytical grade. Co(II) and Co(III) acetylacetonates, acetylacetone, ammonia hydroxide solution, phosphate-buffered saline(PBS), dimethyl sulfoxide solution (DMSO), MTT indicator, hydrochloric acid, ethanol, acetone, silica gel (230-400 mesh particle size) were purchased from Sigma Aldrich, Merck. Ethanol and acetone were further distilled in the presence of magnesium turning and iodine.

4.2.2. Non-aqueous sol-gel synthesis of Co(II)-Co(III) LDH and Ac@Co(II)-Co(III) LDH

0.021 M of $Co(C_5H_7O_2)_2$ and 0.007 M of $Co(C_5H_7O_2)_3$ were dissolved in 80 cm^3 of 1:1 ethanol-acetone mixture and refluxed at 95°C for 2 hours. The precipitation of metal hydroxide sol was obtained at a pH of 10.5 by adding a few drops of ammonium hydroxide solution and refluxed for 5 hours to get Co(II)-Co(III) LDH. To complete the hydrolysis reactions of di- and trivalent metal hydroxides, 5 cm^3 of 2M HCl was added and left stirring at room temperature for 45 minutes[21]. The gel obtained was filtered out using the Whatman no.42 filter paper and dried in a vacuum desiccator containing silica gel. Subsequently, the pre-synthesized Co(II)-Co(III) LDH was further intercalated with 2,4-pentandione (acetylacetone). Briefly, 1:3 LDH to Pent-2,4-dione molar ratio was treated and refluxed at 70°C for 7 hours [22]. A gel-like compound was obtained, filtered out, washed several times with distilled alcohol, and dried in a vacuum desiccator containing silica.

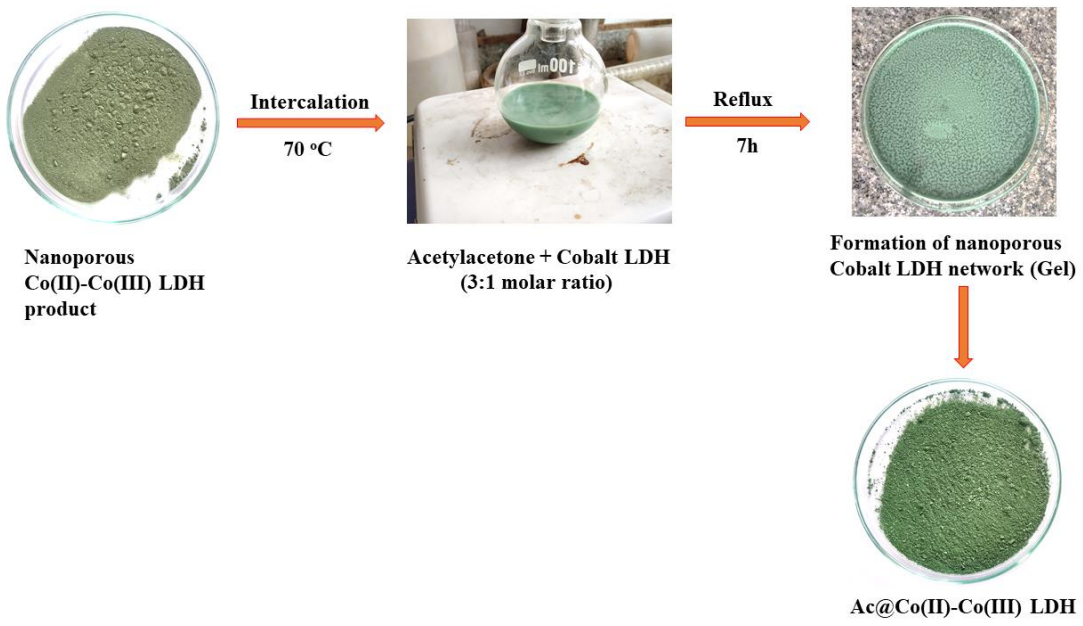

Figure 4.1. Schematic diagram showing the intercalation reaction of the synthesized cobalt LDH with acetylacetone (1:3 molar ratio)

4.2.3. Characterization techniques

The powder diffractogram profile of the synthesized compounds was characterized using a Rigaku powder Diffractometer with the Cu-K alpha radiation (λ=0.154 nm, Rigaku Japan, model: Ultima IV). The surface morphologies of the synthesized products were investigated using Carl ZEISS-Field Emission Scanning Electron Microscopy (Germany, model: ZEISS, SIGMA) and High Resolution-Transmission Electron Microscopy (Japan, model: JEM-2100 Plus Electron Microscope). The presence of various functional groups in the samples was examined using FTIR spectroscopy (Perkin Elmer, model: Spectrum 100). The measurement of molar ratio and oxidation states of the co-existing di- and trivalent cobalt hydroxide phases were confirmed using X-Ray Photoelectron Spectroscopy (Thermo Fisher Scientific Pvt. Ltd., UK, model: ESCALAB Xi+). The surface area and pore volume of the samples were characterized using BET N_2 adsorption at 77K (Quantachrome USA, model: Autosorb-iQ Station 1).

Moreover, Zeta potential study was carried out to understand the surface charge properties of the synthesized products (Malvern Instrument, model: Zetasizer Nano ZS), and the thermal decomposition profile of the synthesized samples was obtained using TGA-DTA at the heating rate of 5°C/min (M/S TG-DTA Instrument, model: Q-600).

4.3. Results and discussion

4.3.1. Intercalation reactions of Co(II)-Co(III) LDH with acetylacetone

In the present study, the intercalation reactions of the synthesized cobalt LDH with acetylacetone were carried out at the reflux temperature of 70°C. Figure 4.1 is a schematic representation of the reactions. It is seen in the PXRD (Figure 4.2 (b)) that the nanohybrid cobalt LDH produces an effect or slight shift in the diffraction pattern at higher Bragg's angles and also causes a reduction in peak intensity or peaks become broader. Also, the FESEM and FTIR studies confirmed that the interactions of the cobalt LDH with acetylacetone produce a significant change in the morphology into highly transformed nanopores and also cause a significant shift in the OH functional group at the higher infrared region. The effect of such a shift is due to the strong hydrogen bonding interaction of the acetylacetone molecule with the host LDH complex[23].

4.3.2. Powder diffractogram profile of Co(II)-Co(III) LDH and Ac@Co(II)-Co(III) LDH nanohybrid

The powder diffractogram profiles of the Co(II)-Co(III) LDH and intercalated Ac@Co(II)-Co(III) LDH nanohybrid are shown in Figure 4.2(a) & (b) respectively. It can be observed from Figure 4.2(a) that the Co(II)-Co(III) LDH diffraction pattern is analogous to that of the Mg-Al LDH material, which is characterized by the uniform stacking sequence of layers after every peak interval PDF: 00-014-0191[24,25]. It can be observed in the case of the currently synthesized Co(II)-Co(III) LDH that the PXRD pattern consists of high-intensity *00l*

type reflection peaks such as (003), (006), (009) etc. at periodic intervals of d-spacings with gradual proportionate reduction of intensities at higher Bragg's angles, and also the ionic radii which is similar to the trend seen in Mg-Al type LDH[6,26]. The presence of a highly noticeable peak followed by other peaks occurs at low Bragg's position, indicating a high crystallinity at higher pH[27,28]. Moreover, it was observed that the synthesized products show very distinct hydrolyzed peaks of Co(II)/Co(III) phases. The most intense peak was obtained at the 2θ of 8.42 Å followed by other peaks of the Bragg's angles obtained at 16.26°, 25.4°, 30.46°, 37.64°, 44.2°, and 52.34° (A) respectively.

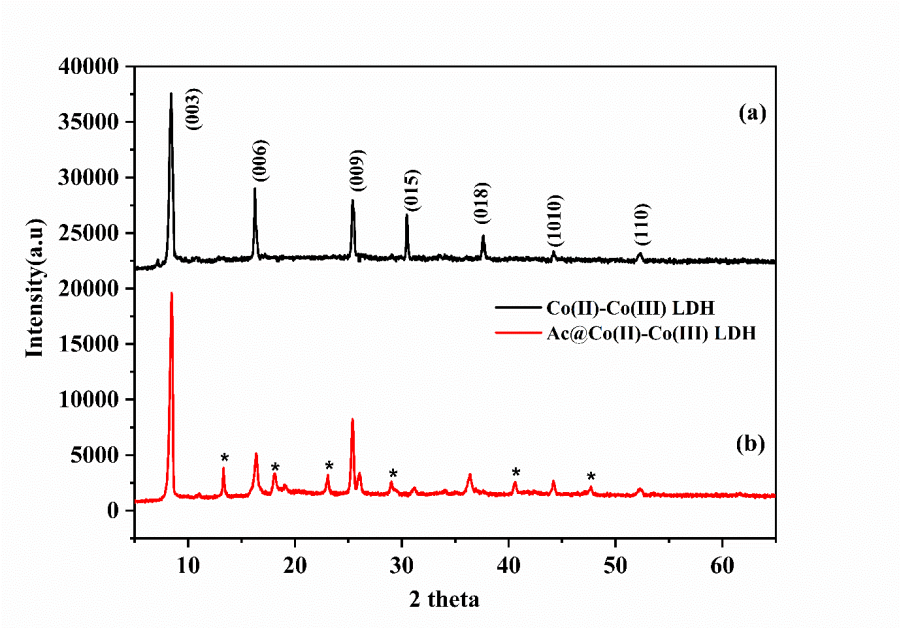

Figure 4.2. Powder diffractogram profile of **(a)** Co(II)-Co(III) LDH and **(b)** intercalated Ac@Co(II)-Co(III) LDH nanohybrid (*= acac)

From the powder XRD profile (Figure 4.2(b)), it can be observed that the organic acetylacetone intercalated Co(II)-Co(III) LDH nanohybrid shows a slight change in basal spacing (d_{00l}) of the parent Co(II)-Co(III) LDH peaks position, confirming the intercalation of acetylacetone molecule in the LDH composite[29]. Though the effect of the intercalated acetylacetone molecule does not produce a remarkable change in the parent cobalt LDH pattern,

it causes a reduction in the intensity of peaks and becomes broader i.e., the compound becomes less crystalline[30,31]. Consequently, the peaks with the asterisks mark obtained at 13.32°, 18.08°, 23.1°, 31.24°, 40.62° and 47.7° denote acetylacetone intercalated into the LDH nanocomposite. The Debye–Scherrer formula i.e. $D = \frac{K\lambda}{\beta cos\theta}$ was used to calculate the crystallite size of the synthesized compounds. The crystallite size was calculated corresponding fortwo peaks viz. (003) and (110) diffraction planes and were found to be 11.38 nm (cobalt LDH) and 10.7 nm (intercalated cobalt LDH)[32]. As a result of intercalation, the size decreases slightly, leading to the broadening of the diffracted peaks. Furthermore, Table 4.1 and 4.2 show the calculations of d-spacing (interplanar spacing).

Table 4.1. Comparison of observed and calculated d-spacing values of Co(II)-Co(III) LDH

Peak index	2θ (observed)	2θ (calculated)	2θ(obs-cal	d-values (observed)	d-values (calculated)	d-values(obs-cal)	100.*I/Imax	a,b	c	Cell angles
1	8.42	8.4183	0.0017	10.507	10.49468	0.01232	100	8.066	15.26	α=β=90, γ=120
2	16.263	16.2596	0.0004	5.458	5.44689	0.01111	39.5			
3	25.442	25.4012	0.0388	3.527	3.503555	0.023445	34.06			
4	30.484	30.4615	0.0185	2.935	2.932086	0.002914	26.72			
5	37.628	37.6173	0.0027	2.395	2.38914	0.00586	14.43			
6	44.235	44.2012	0.0288	2.064	2.047344	0.016656	5.78			
7	52.344	52.3375	0.0025	1.757	1.746601	0.010399	5.47			

Values obtained for both Co(II)-Co(III) LDH and intercalated Ac@ Co(II)-Co(III) LDH, respectively. The calculation of interplanar spacing for a hexagonal crystal system can be expressed as:

$$\frac{1}{d^2} = \frac{4}{3}\left(\frac{h^2 + hk + k^2}{a^2}\right) + \frac{l^2}{c^2} = \frac{4\,sin^2\theta}{\lambda^2} \qquad (1)$$

The variables a and c are the hexagonal lattice constants, and (h, k, l) represent the diffraction planes. λ = wavelength and $sin\theta$ is Bragg's angle[33].

Table 4.2. Comparison of observed and calculated d-spacing values Ac@Co(II)-Co(III) LDH

Peak index	2θ (observed)	2θ (calculated)	2θ(obs-cal	d-values (observed)	d-values (calculated)	d-values(obs-cal)	100.*I/Imax	a,b	c	Cell angles
1	8.46	8.4596	0.0004	10.44346	10.436	0.00746	100	9.38	19.05	α=β=90, γ=120
2	13.32	13.3198	0.0002	6.641749	6.64	0.001749	14.24			
3	16.36	16.3612	-0.0012	5.413291	5.4066	0.006691	18.88			
4	18.08	18.081	-0.001	4.902107	4.9048	-0.00269	10.3			
5	19	19.0026	-0.0026	4.666378	4.6625	0.003878	3.78			
6	23.1	23.0978	0.0022	3.847464	3.8371	0.010364	9.47			
7	25.38	25.3804	-0.0004	3.506378	3.5015	0.004878	36.71			
8	26.04	26.04	0	3.419041	3.422	-0.00296	9.36			
9	29.04	29.0405	-0.0005	3.072245	3.062	0.010245	6.04			
10	31.18	31.1782	0.0018	2.866304	2.8658	0.000504	4.18			
11	34.06	34.04	0.02	2.631584	2.6382	-0.00662	2.6			
12	36.4	36.3941	0.0059	2.466588	2.4537	0.012888	9.21			
13	40.62	40.6184	0.0016	2.219278	2.2246	-0.00532	6.29			
14	44.18	44.1813	-0.0013	2.048221	2.0266	0.021621	7.3			
15	47.7	47.6982	0.0018	1.905079	1.910	-0.00492	4.26			
16	52.32	52.3181	0.0019	1.747202	1.7329	0.014302	4.12			

From the calculated values presented in Tables 4.1 and 4.2, it can be observed that the change in the lattice parameters in the case of intercalated Ac@Co(II)-Co(III) LDH becomes large. The large lattice constant can be attributed to the change in the atomic radius of the intercalated acetylacetone molecule in the cobalt LDH complex[22]. Moreover, it is seen that the d-spacing values of cobalt LDH did not show a significant change. These constant d-spacing values of LDH may be attributed to the fact that the intercalation of acetylacetone molecules into LDH does not affect the interlayer spacing of the parent LDH. On the other hand, acetylacetone molecules get intercalated into the LDH surface but not between the two hydroxide layers and are connected by hydrogen bonding.

4.3.3. FT-IR analysis

The FT-IR spectra of the Co(II)-Co(III) LDH and intercalated Co(II)-Co(III) LDH nanohybrid are shown in Figure 4.3. It is seen in Figure 4.3 (a) that the broad spectrum at 3420 cm^{-1} corresponds to the stretching vibrations of polar OH groups in cobalt LDH composite. The IR shoulder peak at 2992 cm^{-1} could be due to the asymmetric bridging of C-H groups, resulting from during alcoholysis reaction of ethanol and acetone mixture. The band at 1620 cm^{-1} represents the bending mode of interlayer water molecules. The band at 1405-1521 cm^{-1} may be attributed to interlayer anions, mostly carbonate stretching. The IR range from 400-1021 cm^{-1} is due to the metal oxides stretching[34].

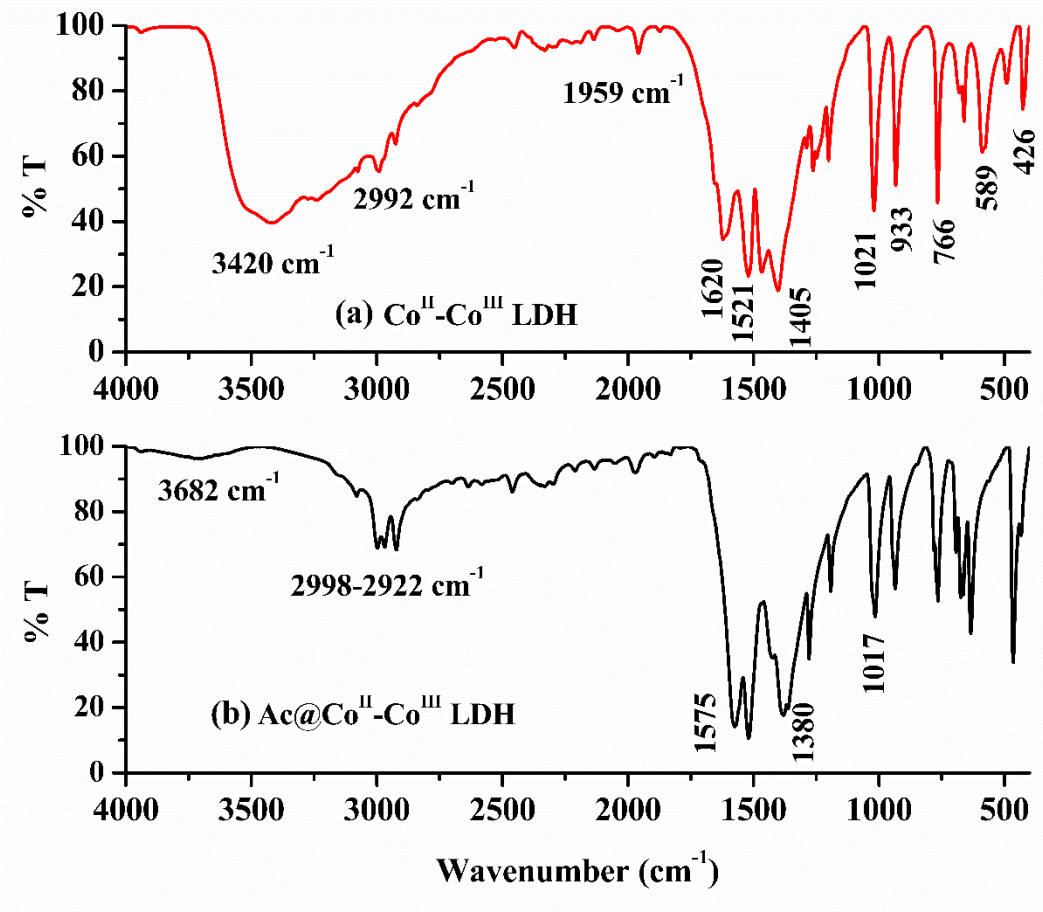

Figure 4.3. FTIR spectra of: (a) Co(II)-Co(III) LDH & (b) Ac@ Co(II)-Co(III) LDH

From the spectra, it can be observed that the OH stretching in the case of Ac@Co(II)-Co(III) LDH is shifted to 3682 cm^{-1}, and a medium broad peak at 2998-2922 cm^{-1} can be observed. This medium broad peak could be due to the asymmetric C-H stretching vibration originating from the acetylacetone bonded in LDH composite (Figure 4.3(b)). The large shift in OH peak position in the intercalated LDH is due to the acetylacetone molecule bonded in the LDH composite, which is responsible for stabilizing the LDH structure[35]. The medium broadband at 1575 cm^{-1} and 1380 cm^{-1} is due to the deformation mode of interlayer water molecules and the asymmetric stretching vibration of C=O (carbonate) groups in the intercalated

LDH complex. Furthermore, the IR range at 900 to 500 cm^{-1} corresponds to M=O (metal oxides) vibrations in the LDH composite[36].

4.3.4. FE-SEM study of the Co(II)-Co(III) LDH and nanohybrid

The field emission scanning electron microscopy (FESEM) images of Co(II)-Co(III) LDH and intercalated LDH nanohybrid are shown in Figure 4.4 (a),(b),(c) & (d). Figure 4.4 (a) & (b) of the Co(II)-Co(III) LDH revealed that the synthesized cobalt LDH exhibits flakes of nanosheets highly composed of mesopores. The occurrence of such pore diversity is obviously due to the process being favored by the alcogel property, which involves the evaporation of the physiosorbed interlayer water molecules during drying[37].

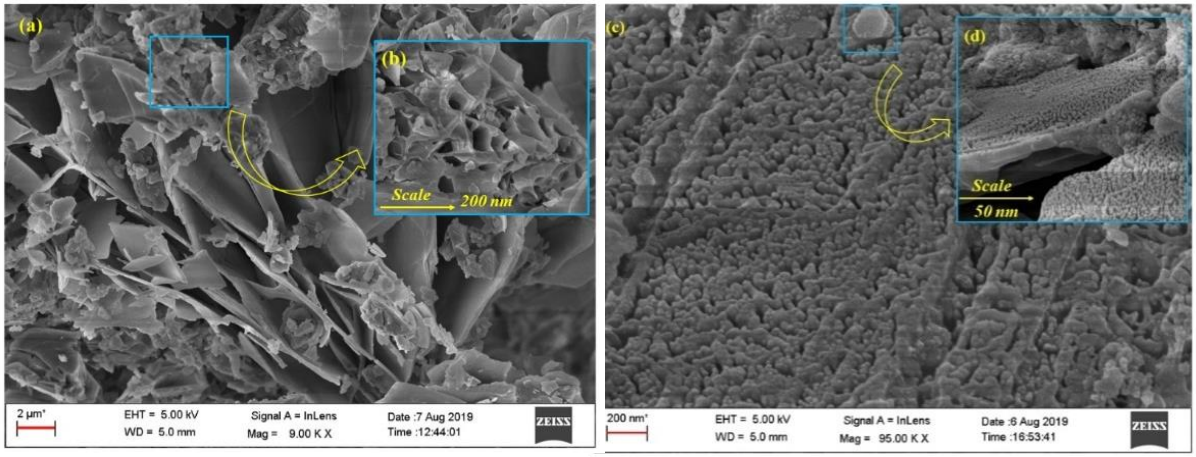

Figure 4.4. Showing the high-resolution FESEM images of: (a) Typical Co(II)-Co(III) LDH nanosheets at 2µm, (b) Mesopores at 200 nm, (c) Intercalation effects of acetylacetone with Co(II)-Co(III) LDH, and (d) Formation of micropores at 50 nm

Similarly, Figure 4.4 (c) & (d) show the development of highly transformed meso to micropores characteristic after the intercalation reaction of acetylacetone reacted at 70°C. Qualitatively, the nanocomposite has pores filled with a number of spherical micropores, which gives unique characteristics to the synthesized material[3,38]. Similar reported work has shown that this highly transformed meso to microporous cobalt LDH is due to the fact that

acetylacetone molecules, through keto-enol tautomeric effect, can undergo a transformation in surface morphology favored by the oxidation process [23].

4.3.5. HR-TEM study

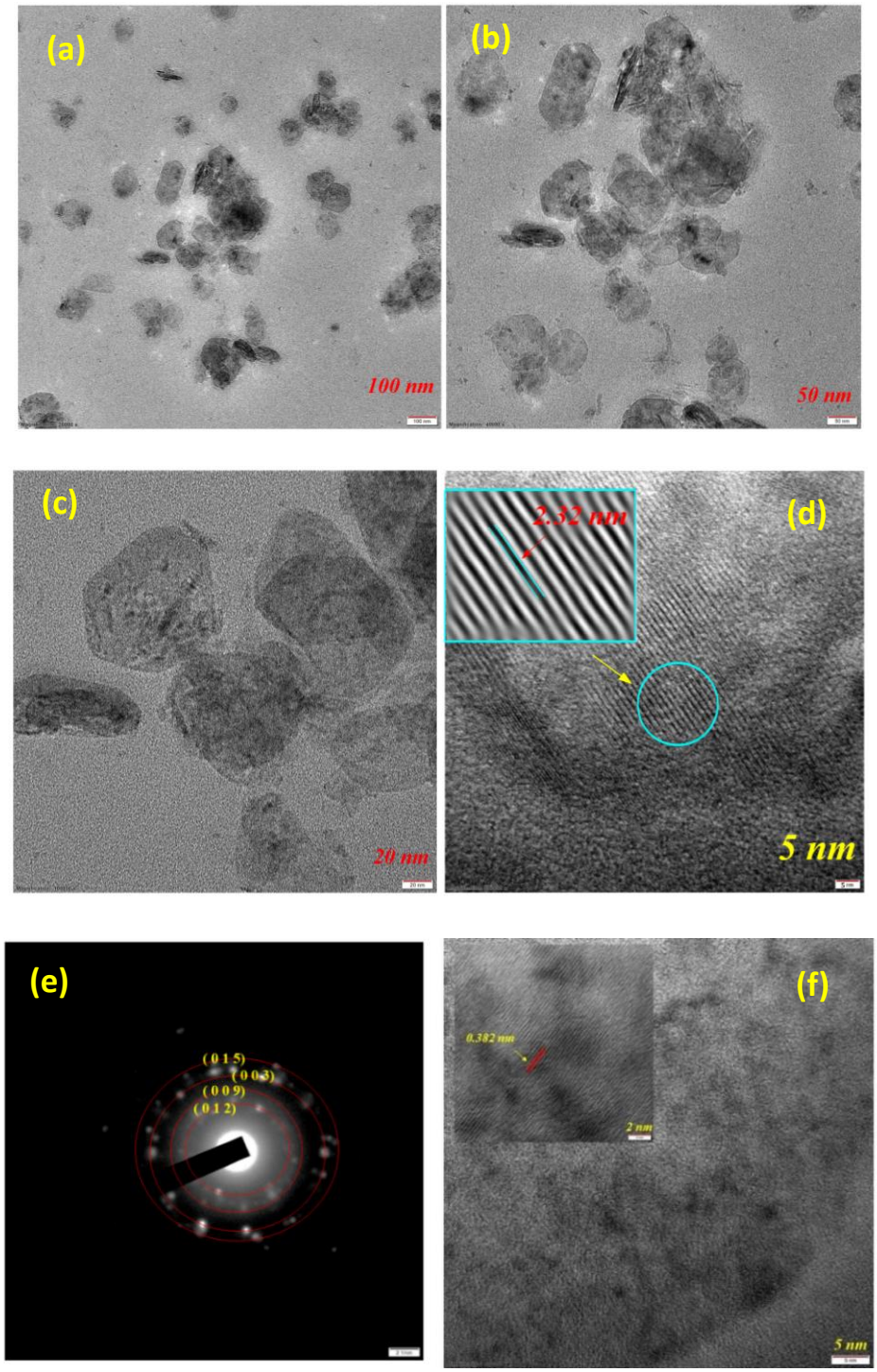

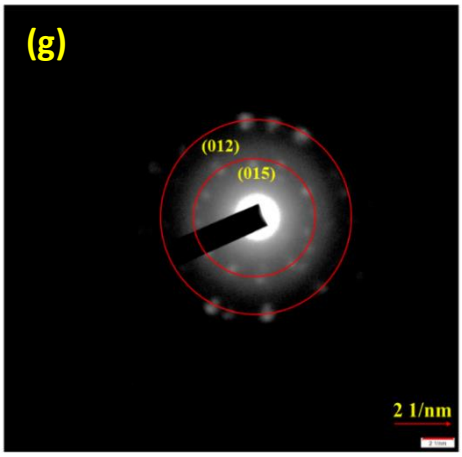

Figure 4.5. HRTEM images of Co(II)-Co(III) LDH: Resolution at (a) 100 nm, (b) 50 nm, (c) 20 nm, (d) 5 nm & (e) Selected area electron diffraction (SAED),(f) nanohybrid at 2nm, and (g) SAED

High resolution-transmission electron microscopy (HR-TEM) of Co(II)-Co(III) LDH and nanohybrid images at different resolution is shown in Figure 4..5 (a), (b), (c), (d), (e), (f) & (g). Figure 4.5 (a), (b) & (c) represent the formation of hexagons cobalt LDH platelets of different sizes. From the figures, it can be observed that the synthesized cobalt LDH and its nanohybrid are highly crystalline[39,40]. From Figure 4.5 (d) & (f), it is seen that the lattice strips have a value of 0.382 nm & 2.32 nm, which represents the d-spacing of LDH crystal at (012) & (015) planes. Moreover, from Figure 4.5 (e) & (g), it is observed that the selected area electron diffraction (SAED) represents various lattice planes *viz.* (003), (009), (012) & (015) for Co(II)-Co(III) LDH and (012) & (015) for nanohybrid, respectively, which are in agreement with the diffractogram result (Figure 4.2). The SAED diffraction pattern of Co(II)-Co(III) LDH and nanohybrid show that the diffracted planes tend to be a set of concentric rings indicated by various planes.

4.3.6. X-ray Photoelectron spectroscopy studies

XPS analysis was conducted to understand the chemical composition and existence of the chemical oxidation state of mesoporous Co(II)-Co(III) LDH and its nanohybrid. The broad scan XPS spectra of Co(II)-Co(III) LDH and intercalated cobalt nanohybrid are shown in Figure 4.6 (a). It is observed that a slight change in cobalt Co2S and Co2P position before and after intercalation reactions could be noticed i.e., at 782 eV (parent cobalt LDH) and 780 eV (intercalated). This indicates an isomorphous substitution of di- and trivalent cobalt atoms within the LDH layers, which might result in new chemical bond formation[41]. Literally, the cobalt atoms are octahedrally coordinated to hydroxyl groups in their octahedral configuration. However, the binding energy of carbon did not show any shift in XPS spectra at 284 eV (in both parent and intercalated). This could be attributed to the fact that the carbon is chemically bonded to an oxygen atom in the form of C=O as an interlayer anion between the LDH layer without forming new bonds. Moreover, it is evident from the full XPS survey that there is a co-existence of Co 2s, Co 2P3/2, O 1s, and C 1s elements present in the sample. In order to visualize more clearly, the 2p cobalt peaks of the Co(II)-Co(III) LDH and intercalated nanohybrid are shown in Figure 4.6 (b) & (c), respectively. The binding energy that emerged at 782 eV and 784 eV corresponds to the co-existence of divalent and trivalent cobalt hydroxide phases[42]. The Co 2p1/2 spectra at around 797 eV in both Co(II)-Co(III) LDH and intercalated showed the lack of a Co^{2+} state. On the other hand, the Co^{3+} state appears more significant in both cases.

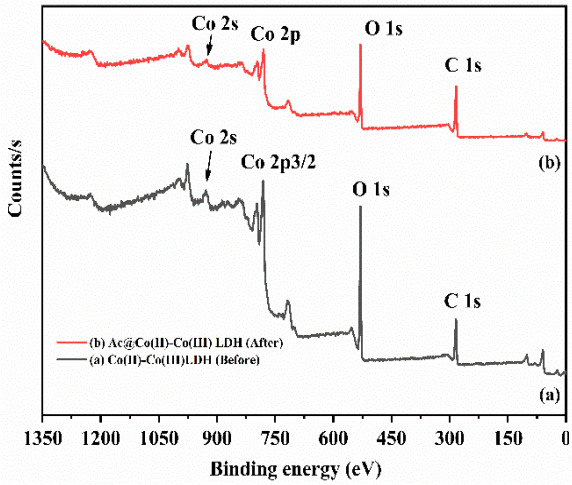
Co 2s
Co 2p
O 1s
C 1s
Co 2s
Co 2p3/2
O 1s
C 1s
(b)
(a)
(b) Ac@Co(II)-Co(III) LDH (After)
(a) Co(II)-Co(III)LDH (Before)
Counts/s
Binding energy (eV)

(a)

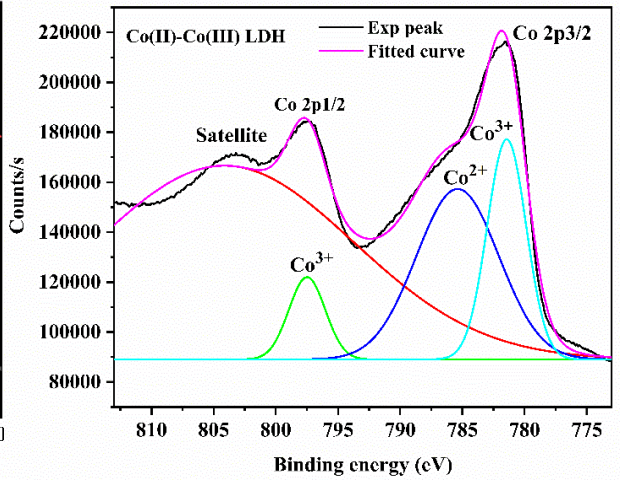
Co(II)-Co(III) LDH
Exp peak
Fitted curve
Co 2p3/2
Co 2p1/2
Satellite
Co3+
Co2+
Co3+
Counts/s
Binding energy (eV)

(b)

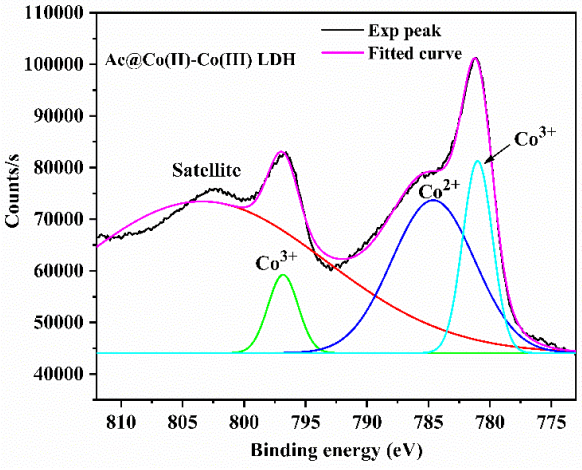
Ac@Co(II)-Co(III) LDH
Exp peak
Fitted curve
Satellite
Co3+
Co2+
Co3+
Counts/s
Binding energy (eV)

(c)

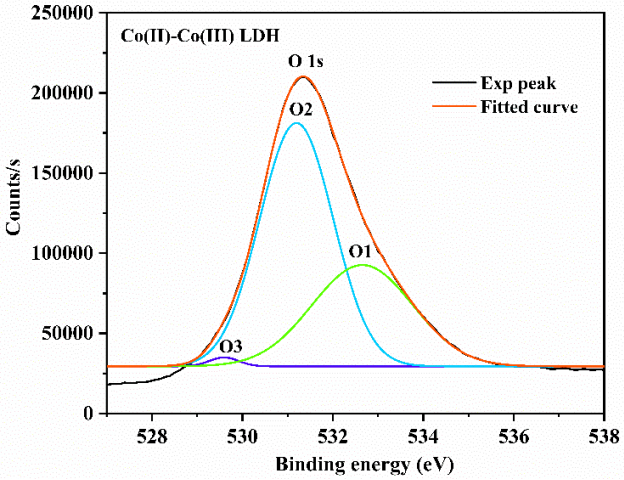
Co(II)-Co(III) LDH
O 1s
O2
O1
O3
Exp peak
Fitted curve
Counts/s
Binding energy (eV)

(d)

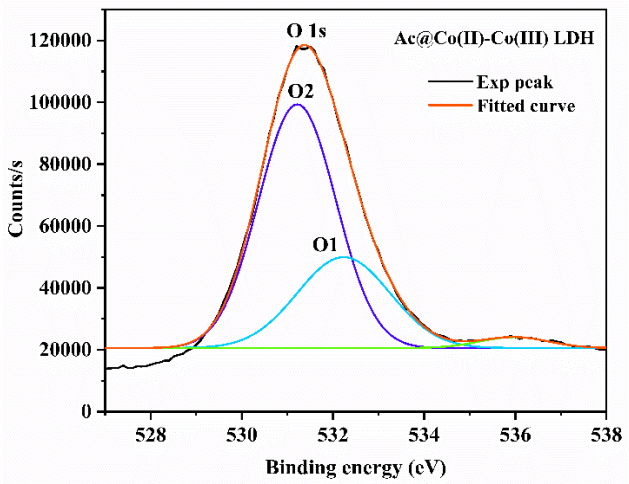

(e)

Figure 4.6. (a) Full XPS survey of Co(II)-Co(III) LDH and Ac@Co(II)-Co(III) LDH, (b) Co 2p peaks of Co(II)-Co(III) LDH, (c) Co 2p peaks of Ac@Co(II)-Co(III) LDH, (d) O1s peaks of Co(II)-Co(III) LDH and (d) O1s peaks of Ac@Co(II)-Co(III) LDH

These observations prove that the mesoporous cobalt-layered double hydroxide and its nanohybrid are strongly dominated by the formation of trivalent cobalt cations rather than divalent cations[43]. This unique feature might be due to the fact that during the formation of Co(II)-Co(III) layered structure, Co(III) ions take positions in isomorphous sites. Further, mechanistically it can be suggested that the Co^{2+} ion, which is more stable in an aqueous solution, becomes easily oxidized to a trivalent state due to the presence of acetylacetone, which even though it acts as a complexing agent, possesses inherent oxidizing properties. As a consequence, some of the divalent Co^{2+} ions are oxidized to trivalent states due to the intercalation effect[44]. Moreover, the results proved that the formation of mesoporous cobalt LDH sheets occurs due to the reduction of Co^{2+} ions during the synthesis. The binding energy at around 803-804 eV indicates the satellite peak formation. The satellite peak occurs when the Coulombic potential changes unexpectedly, and as a result, the photo-ejected electrons pass

through the valence band[45]. Furthermore, the binding energies of Co(II)-Co(III) LDH recorded at 533 eV, 531 eV, and 529 eV indicate that the core-level spectrum of O 1s produces three elemental oxygens (O_1, O_2, and O_3) bonded into bimetallic Co(II)-Co(III) LDH, i.e. O-M, O-H, and surface interlayer oxygen as water molecules (Figure 4.6(d)). Similarly, the intercalated Ac@cobalt LDH bears two elemental oxygens (O1 & O2). The absence of one oxygen-deficient was seen in the intercalated Co LDH, which might be due to the loss of interlayer oxygen atom (Figure 4.6(e)[46].

4.3.7. Thermogravimetric (TGA) analysis

Thermal pyrolysis reactions give knowledge about the thermal degradation behavior of the material. The present study investigates the thermal decomposition properties of the newly synthesized Co(II)-Co(III) LDH and its intercalated complex or nanohybrid. The Heating curves were obtained at the heating rate of $\beta = 5^{o}C.min^{-1}$. Figure 4.7 depicts the thermal decomposition profile of the synthesized compounds. It can be seen that the TGA curves of both compounds exhibit characteristics analogous to the family of LDHs. All LDHs show a degradation pattern of three significant steps[47]. The temperature recorded at 150-245°C, which is the first step, corresponds to the 13.5% mass loss of the weakly bonded water molecules. The temperature below 50-150°C was excluded from the study. It represents the volatilization of loosely adsorbed gases or moistures from the parent LDH[23]. The second weight loss from 246 to 460°C represents a huge weight transition. The second weight loss at 47.29 % indicates the dehydroxylation or anions (H_2O or OH molecules) bonded in the Co(II)-Co(III) LDH matrix.

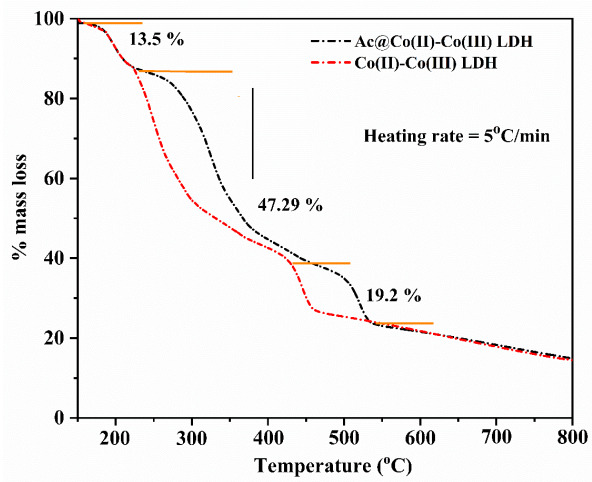

Figure 4.7. TGA profile of Co(II)-Co(III) LDH and of Ac@Co(II)-Co(III) LDH

Similarly, the temperature from 462 to 542°C (19.2% mass loss) and above represent the collapse of the main hydroxide layers, resulting in the formation of divalent and trivalent cobalt oxide phases. Furthermore, it was observed that the degradation curve of Ac@ Co(II)-Co(III) LDH shows decomposition at a higher temperature than that of the parent LDH. This could be due to various gases or moisture adsorbed in the nanohybrid LDH and, most importantly, acetylacetone substrate bonded in the LDH composite, which had a stabilizing effect on the LDH structure.

4.3.8. BET and Zeta potential surface analysis

The measurement of surface areas or pore volume can be accomplished using a surface BET analysis. The BET N_2 adsorption was carried out at 77 K. Figure 4.8 (a), (b) show the BET and BJH pore size distribution. The surface area and pores volume of the Co(II)-Co(III) LDH were found to be 88 $m^2.g^{-1}$ and 1.37 cm^3g^{-1}, respectively, and for the intercalated nanohybrid, it was 169 $m^2.g^{-1}$ and 1.26 cm^3g^{-1}. The formation of a large surface area could be due to the acetylacetone which was intercalated into the parent LDH, causing the nanocomposite to undergo a redox process and release physisorbed interlayer water molecules[23,44].

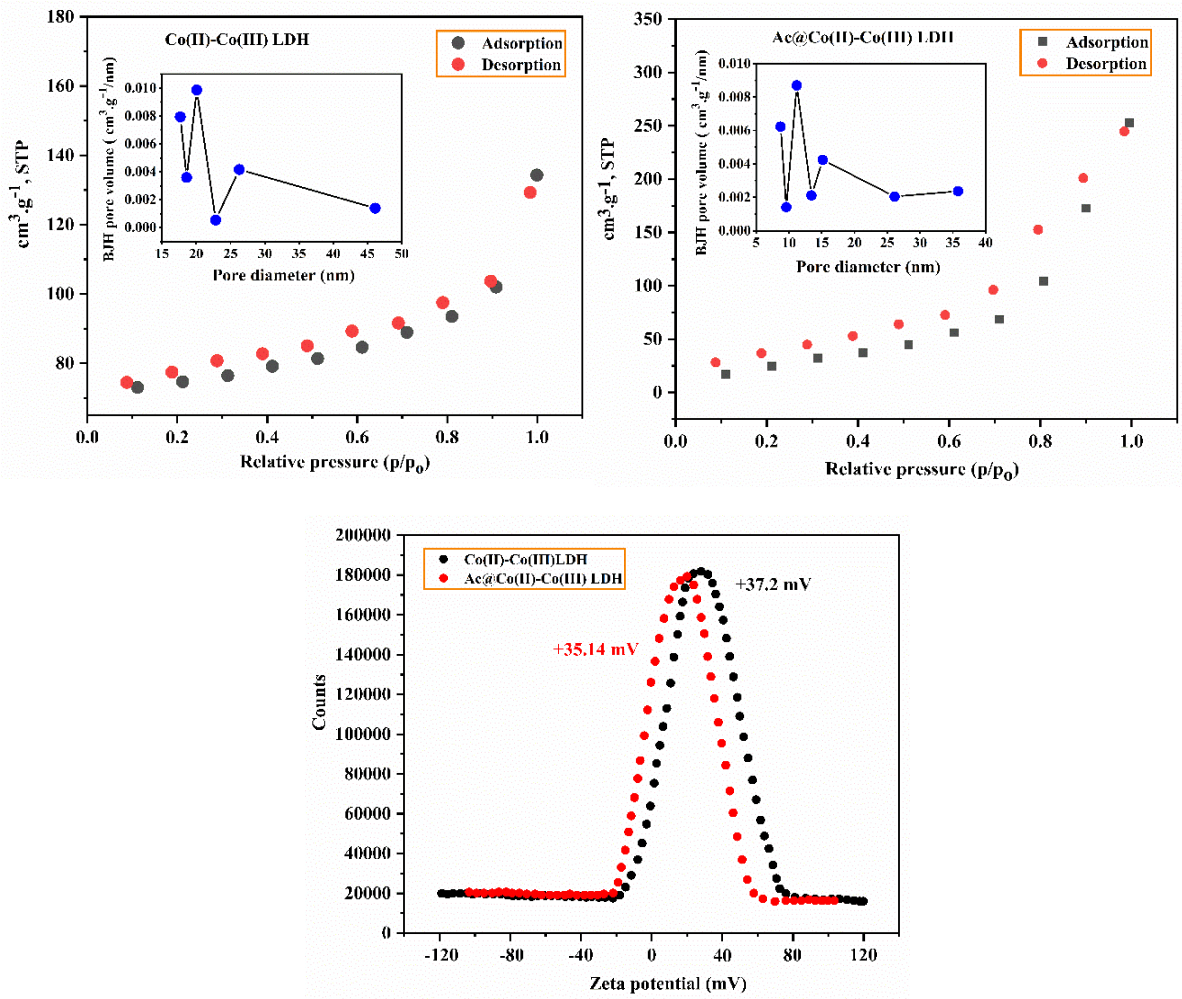

Figure 4.8. BET, BJH pore size distribution, and Zeta potential analysis of Co(II)-Co(III) LDH and Ac@ Co(II)-Co(III) LDH

The BJH pore size distribution further confirmed that the synthesized cobalt LDH and its nanohybrid correspond to a mesoporous material with pore diameters <50 nm. The Zeta potential (ζ) measurement helps to understand particles' charge properties as a function of pH. The results of the study showed that the synthesized Co(II)-Co(III) LDH and Ac@ Co(II)-Co(III) LDH were found to be inherently built up with positively charged particles, which were +35.14 mV and +37.2 mV for intercalated and Co(II)-Co(III) LDH, respectively. Hence, it can have an affinity toward negatively charged anionic species. The surface basicity of the synthesized compounds could be due to the organization of more OH^- ions during the

alcoholysis reactions of di- and trivalent cobalt acetylacetonate precursors. Furthermore, the isoelectric point recorded at IEP=7.4 and 8.2, in which pH equals IEP values, becomes globally neutral[32].

4.3.9. Formation of active LDH cobalt nanoparticles and particle size effect on antibacterial activity

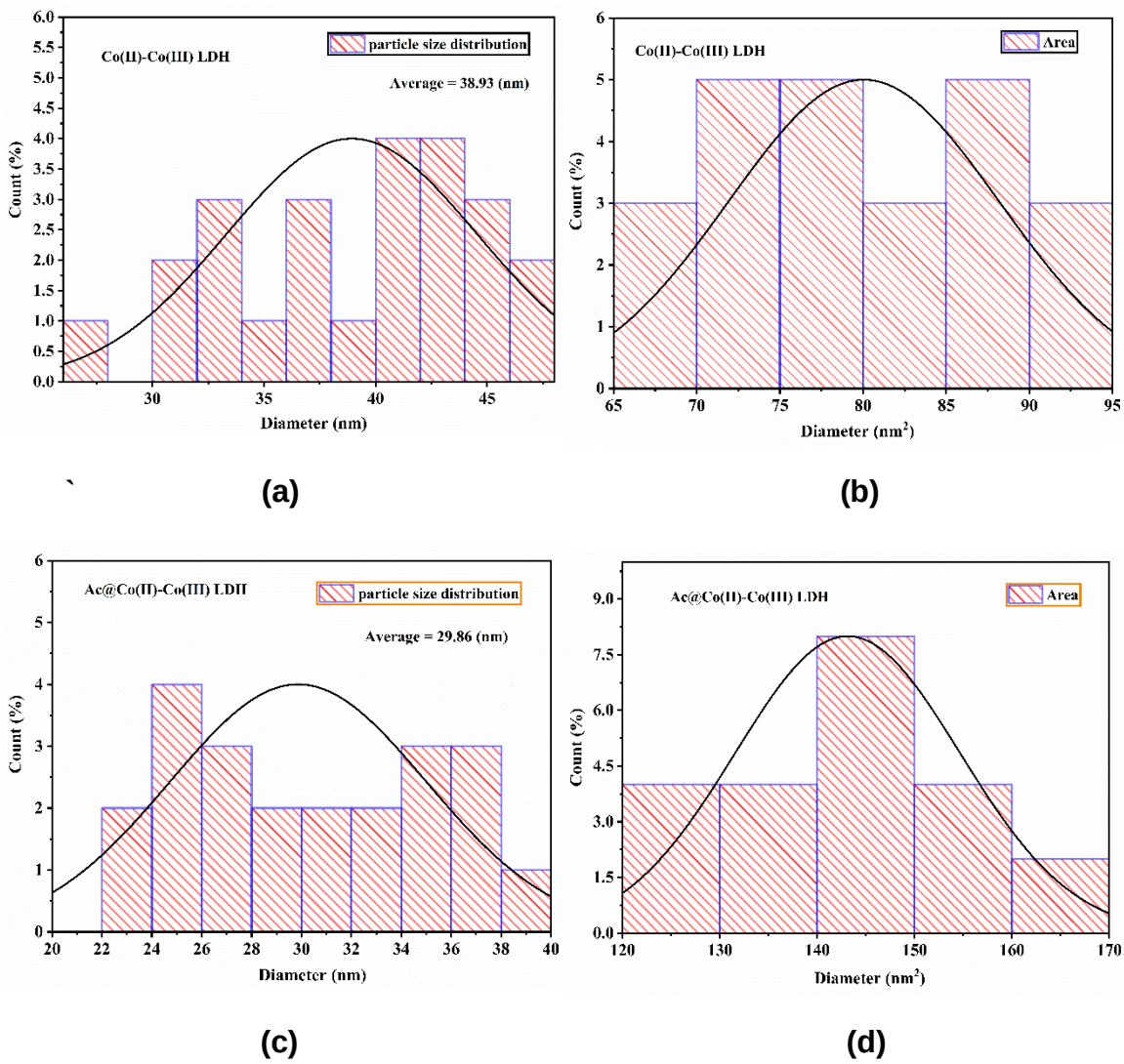

Figure 4.9. Particle size and pores area analysis of: (a), (b) Co(II)-Co(III) LDH, and (c), (d) Ac@Co(II)-Co(III) LDH

In the present study, the relation of particle size of active cobalt LDH nanoparticles and its nanohybrid to its inhibition potential on bacterial strains is explored. Mechanistically it can be explained that the partial substitution of di- or trivalent metals within the LDHs structure results in positive charge metal hydroxide sheets. Likewise, in the defined reaction media, the synthesized cobalt LDH and its nanohybrid produce electrostatic interaction due to the strong binding affinity of active cobalt LDH nanoparticles toward the host cells. In other words, the formation of active cobalt LDH nanoparticles is the inherent property of LDHs which arise from the positively charged LDH nanosheets. Figure 4.9 (a), (b), (c), and (d) show the particle size and pores area analysis of the synthesized Co(II)-Co(III) LDH and its nanohybrid. It can be noticed from Figure 4.9 (c), (d) that the effect of intercalation of acetylacetone molecules into cobalt LDH decreases the particle size from 38.93 to 29.86 nm (average). Moreover, the diameter of the area of the pores increases in the case of intercalated cobalt LDH. Fundamentally, the decrease in particle size and increase in pore areas have a significant effect on antibacterial activity. This is because the smaller the particle size or larger the pores area, the greater would be the antibacterial activity against bacterial cells.

4.4. Conclusion

The present study reports the green synthesis of a highly mesoporous Co(II)-Co(III) LDH and Ac@ Co(II)-Co(III) LDH nanohybrid through the Sol-Gel method and the use of non-aqueous ethanol: acetone solvent as an alternative greener approach. Results revealed that the synthesized compounds exhibit a typical LDH structure analogous to Mg-Al hydrotalcite as confirmed by PXRD, FESEM, HRTEM, XPS, TGA-DTA etc. From the study, it can be concluded that cobalt LDH nanoparticles synthesized in the non-aqueous Sol-Gel method provide a promising alternative greener approach for obtaining materials with greater pore diversity.

References

[1] V. Rives, Layered Double Hydroxides: Present and Future, Nova Publishers,2001.

[2] X. Bi, H. Zhang, L. Dou, Layered double hydroxide based nanocarriers for drug delivery, Pharmaceutics(2014). https://doi.org/10.3390/pharmaceutics6020298.

[3] Q. Wang, D. Ohare, Recent advances in the synthesis and application of layered double hydroxide (LDH) nanosheets, Chem. Rev. (2012).https://doi.org/10.1021/cr200434v.

[4] S. Daniel, S. Thomas. 2020. Layered double hydroxides: fundamentals to applications, in: Layered Double Hydroxide Polymer Nanocomposites.10.1016/b978-0-08-101903-0.00001-5.

[5] R. Sharma, G.G.C. Arizaga, A.K. Saini, P. Shandilya, Layered double hydroxide as multifunctional materials for environmental remediation: from chemical pollutants to microorganisms, Sustainable Mater. Technol. (2021).https://doi.org/10.1016/j.susmat.2021.e00319.

[6] F. Cavani, F. Trifirò, A. Vaccari, Hydrotalcite-type anionic clays: Preparation, properties and applications, Catal.Today11(1991).https://doi.org/10.1016/0920-5861(91)80068-K.

[7] M. Herrero, P. Benito, F.M. Labajos, V. Rives, Stabilization of Cȯ2 in layered double hydroxides(LDHs) by microwave-assisted ageing, J. Solid State Chem.180(2007).https://doi.org/10.1016/j.jssc.2006.12.011.

[8] J. He, M. Wei, B. Li, Y. Kang, D.G. Evans, X. Duan, Preparation of layered double hydroxides, Struct. Bond. 119

(2005).https://doi.org/10.1007/430_006.

[9] A. Badruzzaman, A. Yuda, A. Ashok, A. Kumar, Recent advances in cobalt based heterogeneous catalysts for oxygen evolution reaction, Inorganica Chim Acta(2020).https://doi.org/10.1016/j.ica.2020.119854.

[10] A.A. Abass, W.A.M. Abdulridha, W.K. Alaarage, N.H. Abdulrudha, J. Haider, Evaluating the antibacterial effect of cobalt nanoparticles against multidrug resistant pathogens, J. Med. Life 14(2021).https://doi.org/10.25122/jml-2021-0270.

[11] M. Hafeez, R. Shaheen, B. Akram, Zain-Ul Abdin, S. Haq, S. Mahsud, S. Ali, R.T. Khan, Green synthesis of cobalt oxide nanoparticles for potential biological applications, Mater. Res. Express 7(2020).https://doi.org/10.1088/2053-1591/ab70dd.

[12] M. Li, L. Li, S. Lin, Efficient antimicrobial properties of layered double hydroxide assembled with transition metals via a facile preparation method, Chin. Chem. Lett.31(2020).https://doi.org/10.1016/j.cclet.2019.09.047.

[13] Q.Z. Yang, Y.Y. Chang, H.Z. Zhao, Preparation and antibacterial activity of lysozyme and layered double hydroxide nanocomposites, Water Res.47(2013).https://doi.org/10.1016/j.watres.2013.09.002.

[14] G. Mishra, B. Dash, S. Pandey, P.P. Mohanty, Antibacterial actions of silver nanoparticles incorporated Zn-Al layered double hydroxide and its spinel. J. Environ. Chem. Eng.1(2013).https://doi.org/10.1016/j.jece.2013.08.031.

[15] S.J. Ryu, H. Jung, J.M. Oh, J.K. Lee, J.H. Choy, Layered double hydroxide as novel antibacterial drug delivery system, J. Phys. Chem. Solids

71(2010).https://doi.org/10.1016/j.jpcs.2009.12.066.

[16] Y. Wang, D. Zhang, Q. Bao, J. Wu, Y. Wan, Controlled drug release characteristics and enhanced antibacterial effect of graphene oxide drug intercalated layered double hydroxide hybrid films, J. Mater. Chem.22(2012). https://doi.org/10.1039/c2jm35144g.

[17] C.W. Dikio, I.P. Ejidike, F.M. Mtunzi, M.J. Klink, E.D. Dikio, 2017. Hydrazide schiff bases of acetylacetonate metal complexes: synthesis, spectroscopic and biological studies. Int. J. Pharm.Pharm.Sci.9.10.22159/ijpps.2017v9i12.22225.

[18] A. Brandelli, A.C. Ritter, F.F. Veras, 2017. Antimicrobial activities of metal nanoparticles, in: Metal Nanoparticles in Pharma.10.1007/978-3-319-63790-7_15.

[19] A.A. Yaqoob, H. Ahmad, T. Parveen, A. Ahmad, M. Oves, I.M.I. Ismail, H.A. Qari, K. Umar, M.N. Mohamad Ibrahim, Recent advances in metal decorated nanomaterials and their various biological applications: a review, Front. Chem.(2020).https://doi.org/10.3389/fchem.2020.00341.

[20] I.S. Okeke, K.K. Agwu, A.A. Ubachukwu, F.I. Ezema, Influence of transition metal doping on physiochemical and antibacterial properties of ZnO[sbnd] Nanoparticles: a review, Appl. Surface Sci. Adv.(2022).https://doi.org/10.1016/j.apsadv.2022.100227.

[21] P. Saikia, A. Gautam, R.L. Goswamee, Synthesis of nanohybrid alcogels of SiO_2 and Ni-Cr/Mg-Cr-LDH: study of their rheological and dipcoating properties, RSC Adv.6(2016).https://doi.org/10.1039/c6ra23475e.

[22] P. Saikia, J. Saikia, S. Sąrmah, N.B. Allou, R.L. Goswamee, Mesoporous oxidic holey nanosheets from Zn-Cr LDH synthesized by soft chemical etching of Cr3 and its application as CO_2 hydrogenation catalyst. J. CO_2 Util.21(2017). https://doi.org/10.1016/j.jcou.2017.06.017.

[23] V.R.R. Cunha, P.A.D. Petersen, M.B. Gonçalves, H.M. Petrilli, C. Taviot-Gueho, F. Leroux, M.L.A. Temperini, V.R.L. Constantino, Structural, spectroscopic (NMR,IR, and Raman), and DFT investigation of the self-assembled nanostructure of pravastatin LDH (layered double hydroxides) systems. Chem. Mater.24 (2012),https://doi.org/10.1021/cm202953y.

[24] D. Sokol, D.E.L. Vieira, A. Zarkov, M.G.S. Ferreira, A. Beganskiene, V.V. Rubanik, A.D. Shilin, A. Kareiva, A.N. Salak, Sonication accelerated formation of Mg-Al-phosphate layered double hydroxide via sol-gel prepared mixed metal oxides, Sci. Rep.9 (2019).https://doi.org/10.1038/s41598-019-46910-5.

[25] F. Prinetto, G. Ghiotti, P. Graffin, D. Tichit, Synthesis and characterization of sol-gel Mg/Al and Ni/Al layered double hydroxides and comparison with co-precipitated samples, Microporous Mesoporous Mater. 39 (2000).https://doi.org/10.1016/S1387-1811(00)00197-9.

[26] Y. Wang, L. Yang, X. Peng, Z. Jin, High catalytic activity over novel Mg-Fe/Ti layered double hydroxides (LDHs) for polycarbonate diols(PCDLs): Synthesis, mechanism and application, RSC Adv. 7(2017).https://doi.org/10.1039/c7ra05892f.

[27] G. Nyongombe, G.L. Kabongo, L.L. Noto, M.S. Dhlamini, Investigating the Impact of the Washing Steps of Layered Double Hydroxides (LDH) on the

Electrochemical Performance. Nanomaterials 12(2022),https://doi.org/10.3390/nano12030578.

[28] M.A. Thyveetil, P.V. Coveney, H.C. Greenwell, J.L. Suter, Role of host layer flexibility in DNA guest intercalation revealed by computer simulation of layered nanomaterials, J. Am. Chem.Soc.130(2008).https://doi.org/10.1021/ja8037068.

[29] M.P. Figueiredo, V.R.R. Cunha, F. Leroux, C. Taviot Gueho, M.N. Nakamae, Y.R. Kang, R.B. Souza, A.M.C.R.P.F. Martins, I.H.J. Koh, V.R.L. Constantino, Iron-based layered double hydroxide implants: potential drug delivery carriers with tissue biointegration promotion and blood microcirculation preservation, ACS Omega 3(2018).https://doi.org/10.1021/acsomega.8b02532.

[30] K.M. Dietmann, T. Linke, M.D.N. Sánchez, J.L.P. Pavón, V. Rives, Layered double hydroxides with intercalated permanganate and peroxydisulphate anions for oxidative removal of chlorinated organic solvents contaminated water, Minerals 10(2020).https://doi.org/10.3390/min10050462.

[31] Y. Tokudome, T. Morimoto, N. Tarutani, P.D. Vaz, C.D. Nunes, V. Prevot, G.B.G. Stenning, M. Takahashi, Layered double hydroxide nanoclusters: aqueous, concentrated, stable, and catalytically active colloids toward green chemistry, ACS Nano 10(2016).https://doi.org/10.1021/acsnano.6b02110.

[32] C. Suryanarayana, M.G. Norton(Eds.), Xray Diffraction: A Practical Approach, Plenum Press, New york, London, 1998, Pp.1–267.

[33] P.X. Zhi, Q.L. Guo, Hydrothermal synthesis of layered double hydroxides

(LDHs) from mixed MgO and Al_2O_3: LDH formation mechanism, Chem. Mater. 17(2005).https://doi.org/10.1021/cm048085g.

[34] K. Nejati, A.R. Akbari, S. Davari, K. Asadpour-Zeynali, Z. Rezvani, Zn-Fe-layered double hydroxide intercalated with vanadate and molybdate anions for electrocatalytic water oxidation, New J. Chem. 42(2018).https://doi.org/10.1039/c7nj04469k.

[35] Y. Du, L. Liu, Y. Feng, B. Yang, X. Wu, Enhancement of NH3-SCR performance of LDH-based MMnAl (MCu,Ni,Co) oxide catalyst: Influence of dopant M, RSC Adv. 9(2019).https://doi.org/10.1039/c9ra08391j.

[36] A.R. Sangtam, P. Saikia, R.L. Goswamee, D. Sinha, U.B. Sinha, Green synthesis of mesoporous Ni-Co layered double hydroxide and its application for removal of 2,4-dinitrophenol from water: A theoretical study complemented by the first principle density functional theory-Monte-Carlo approach. J. Environ. Chem. Eng. 10(2022),108378.https://doi.org/10.1016/j.jece.2022.108378.

[37] L. Jin, Q.J. Huang, H.Y. Zeng, J.Z. Du, S. Xu, C.R. Chen, Hydrotalcite-gated hollow mesoporous silica delivery system for controlled drug release, Microporous Mesoporous Mater. 274(2019).https://doi.org/10.1016/j.micromeso.2018.09.001.

[38] G. Mishra, B. Dash, D. Sethi, S. Pandey, B.K. Mishra, Orientation of organic anions in Zn-Al layered double hydroxides with enhanced antibacterial property, Environ. Eng. Sci. 34(2017).https://doi.org/10.1089/ees.2016.0531.

[39] S. Mandal, S. Kalaivanan, A.B. Mandal, Polyethylene glycol-modified layered double hydroxides: synthesis, characterization, and study on adsorption

characteristics for removal of acid orange II from aqueous solution, ACS Omega 4(2019).https://doi.org/10.1021/acsomega.8b02743.

[40] D. Zhang, J. Cao, X. Zhang, N. Insin, R. Liu, J. Qin, NiMn layered double hydroxide nanosheets in-situ anchored on Ti3C2MXene via chemical bonds for superior supercapacitors, ACS Appl Energy Mater 3(2020).https://doi.org/10.1021/acsaem.0c00863.

[41] J. Li, Z. Li, F. Ning, L. Zhou, R. Zhang, M. Shao, M. Wei, Ultrathin Mesoporous Co_3O_4 nanosheet arrays for high-performance lithium-ion batteries, ACS Omega 3(2018).https://doi.org/10.1021/acsomega.7b01832.

[42] S.V. Sadavar, N.S. Padalkar, R.B. Shinde, A.S. Patil, U.M. Patil, V.V. Magdum, Y.M. Chitare, S.P. Kulkarni, R.N. Bulakhe, V.G. Parale, J.L. Gunjakar, Graphene oxide as an efficient hybridization matrix for exploring electrochemical activity of two-dimensional cobalt-chromium-layered double hydroxide-based nanohybrids, ACS Appl. Energy Mater. 5(2022).https://doi.org/10.1021/acsaem.1c03619.

[43] A.I. Khan, D. O'Hare, Intercalation chemistry of layered double hydroxides: Recent developments and applications, J. Mater. Chem. (2002).https://doi.org/10.1039/b204076j.

[44] R. Ma, J. Liang, X. Liu, T. Sasaki, General insights into structural evolution of layered double hydroxide: underlying aspects in topochemical transformation from brucite to layered double hydroxide, J. Am. Chem. Soc. 134 (2012). https://doi.org/10.1021/ja310246r.

[45] S.Y. Kim, A. Yu, Y. Lee, H.Y. Kim, Y.J. Kim, N.S. Lee, C. Lee, Y. Lee,

M.H. Kim, Single phase of spinel Co_2RhO_4 nanotubes with remarkably enhanced catalytic performance for the oxygen evolution reaction. Nanoscale 11(2019),https://doi.org/10.1039/c9nr02197c.

[46] X. Dai, Y. Dai, J. Lu, L. Pu, W. Wang, J. Jin, F. Ma, N. Tie, Cobalt oxide nanocomposites modified by NiCo-layered double hydroxide nanosheets as advanced Electrodes for supercapacitors, Ionics (Kiel) 26(2020).https://doi.org/10.1007/s11581-019-03333-6.

[47] Y. Kim, W. Yang, P.K.T. Liu, M. Sahimi, T.T. Tsotsis, Thermal evolution of the structure of a Mg-Al-CO_3 layered double hydroxide: sorption reversibility aspects, Ind. Eng. Chem. Res. 43(2004).https://doi.org/10.1021/ie0308036.

CHAPTER 4B

Part B: Study of Co(II)-Co(III) LDH and Ac@Co(II)-Co(III) LDH nanohybrid as antibacterial agents

In this chapter, antibacterial evaluation studies using a well-diffusion method, broth serial dilution method (MIC/MBC), and time-kill efficacy test were carried out to study the inhibition effect of synthesized compounds against the two bacterial strains viz S. aureus(gram-positive) and E. coli (gram-negative).

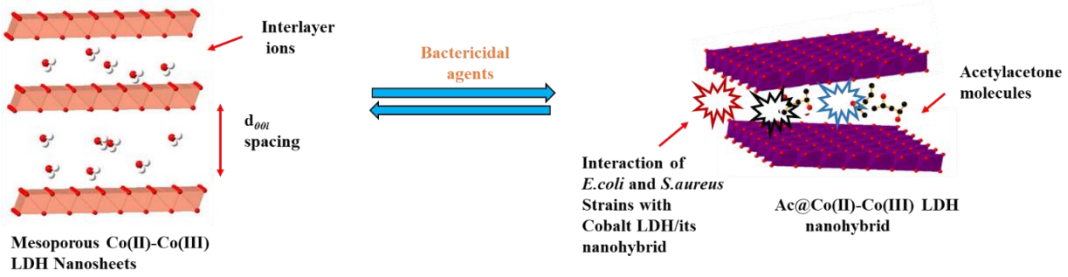

The text of this chapter has been published as:

A.R. Sangtam, K. Richa, P. Saikia, N. Longkumer, U.B. Sinha, R.L. Goswamee **Synthesis and characterization of Co(II)–Co(III) LDH and Ac@Co(II)–Co(III) LDH nanohybrid and study of its application as bactericidal agents.** *Results in Chemistry* 4 (2022), 100671. https://doi.org/10.1016/j.rechem.2022.100671.

4.6. Materials and method

4.6.1. Determination of antibacterial activity of the Co(II)-Co(III) LDH and Ac@Co(II)-Co(III) LDH

The *in vitro* antibacterial study of the synthesized compounds was done against *Escherichia coli* and *Staphylococcus aureus.* The preliminary antibacterial activity of the compounds was determined by studying the zone of inhibition using the agar well diffusion method[1]. Subsequently, the minimum inhibition concentrations (MIC) of the compounds were determined by the two-fold broth dilution method. Nutrient agar and nutrient broth were used for the experiments[2]. The compounds were dissolved in dimethyl sulphoxide (DMSO) to obtain a 10 mg/ml stock solution. The target strains used in the investigation were Gram-negative bacteria *Escherichia coli* (TLTE11), and Gram-positive bacteria *Staphylococcus aureus* (TLTE03) acquired from the Microbiology Laboratory (Department of Botany, Nagaland University, Lumami, India). All the strains were grown in nutrient broth and incubated at 37°C overnight. The antibiotic streptomycin was used as the reference drug.

4.6.2. Time rate kill assay

Time rate kill bacterial experiment was carried out similar to the contact time study [3], and the studies were performed at 30 minutes intervals. Bacterial cells (0.5 MacFarland, ~10^8 CFU/ml) in phosphate buffer saline (PBS) were prepared from a fresh bacterial broth culture. Then, the LDHs at their respective MICs were added to the solution and incubated at 37°C in a shaker incubator. Following each 30 minutes interval, i.e., at 0, 30, 60, 90,120, 150, 180, and 210 minutes, 100µL of the solution medium was pipetted out and spread over the nutrient agar plates. The plates were then incubated overnight at 37°C. Subsequently, the number of visible bacterial colonies was counted as colony-forming units (CFU) to determine the time rate of the kill.

4.7. Results and discussion

4.7.1. Antibacterial activity of the Co(II)-Co(III) LDH and Ac@Co(II)-Co(III) LDH

The results of the antibacterial tests performed against *E. coli* and *S. aureus* are shown in Tables 4.3 and 4.4. The antibacterial evaluation of the synthesized cobalt LDHs showed that they possessed good bactericidal properties. There are reports available to suggest that compounds containing cobalt ions with other transition metals show an effective bactericidal property [4], and this has been proved through our studies also. However, this work further assesses the bactericidal property of intercalated Co(II)-Co(III) LDH. The result obtained showed active inhibition towards the bacterial strain understudy, revealing that Ac@Co(II)-Co(III) LDH nanohybrid has potential as an antibacterial agent.

Table 4.3. Zone of inhibition (mm) of the synthesized compounds

Compound (10 mg/ml)	Gram-positive	Gram-negative
	S. aureus	***E. coli***
Ac@Co(II)-Co(III) LDH	22 mm	25 mm
Co(II)-Co(III) LDH	17 mm	19 mm
Streptomycin	30 mm	31 mm

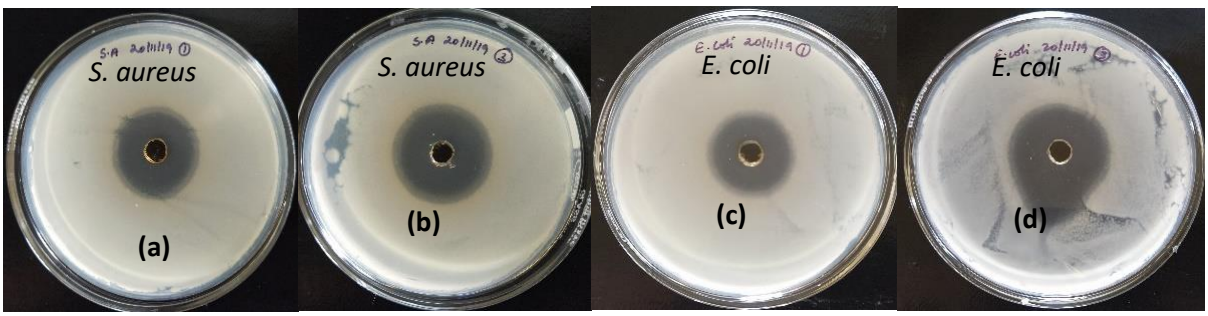

Figure 4.10. Zones of inhibition of *S.aureus* growth by **(a)** Co(II)-Co(III) LDH **(b)** Ac@Co(II)-Co(III) LDH; against *E.coli* by **(c)** Co(II)-Co(III) LDH (d) Ac@Co(II)-Co(III) LDH

The inhibitory action of cobalt LDH and its nanohybrid might be due to the small LDH nanoparticles attributed to the increase in surface area of the bimetallic cobalt oxides/hydroxides[5]. Therefore, the smaller the size of the nanoparticles, the greater would be the bactericidal effect. Additionally, intercalated acetylacetone onto host molecules may boost inhibitory efficacy since acetylacetone molecules have been reported to be antimicrobial in a recent study[6]. The antibactericidal impact of intercalation of the nanohybrid is depicted in Figure 4.10.

Table 4.4. Minimum inhibitory concentration (MIC) of the compounds

Compound	*S. aureus*	*E. coli*
Ac@Co(II)-Co(III) LDH	39 µg/ml	18.5 µg/ml
Co(II)-Co(III) LDH	78 µg/ml	39 µg/ml
Streptomycin	9.7 µg/ml	9.7 µg/ml

The MIC study was conducted to optimize the minimal effect of sample concentration. It is observed that the MIC was found to be more significant in the case of cobalt LDH nanohybrid than that of the parent Co(II)-Co(III) LDH as shown in Tab.4.4. The more substantial impact of a such compound against bacterial strains can be attributed to the effective combination of divalent and trivalent cobalt ions or acetylacetone intercalated into the host LDH molecule.

4.7.2. Time-kill bacterial assay

Time kill bacterial or antibacterial efficacy test is considered the most appropriate and effective method of determining the bactericidal effect[1]. In the present study, the synergistic effect of organic acetylacetone@Co(II)-Co(III) LDH and pre-synthesized Co(II)-Co(III) LDH

against *E. coli* and *S. aureus* were tested to understand the dynamic interaction between antibacterial agent and bacterial strains. From the results obtained it can be seen that both *S. aureus* and *E. coli* become completely inactive after a certain point of time, indicating the bactericidal property of the synthesized compounds. *S. aureus*, when treated with Ac@Co-Co LDH took 180 min for their cells to become completely inactive, while it took 210 min when treated with Co(II)-Co(III) LDH. The colony forming unit (CFU) of the bacteria was determined, and a graph of the CFU/ml was plotted against time, as shown in Figure 4.11(e).

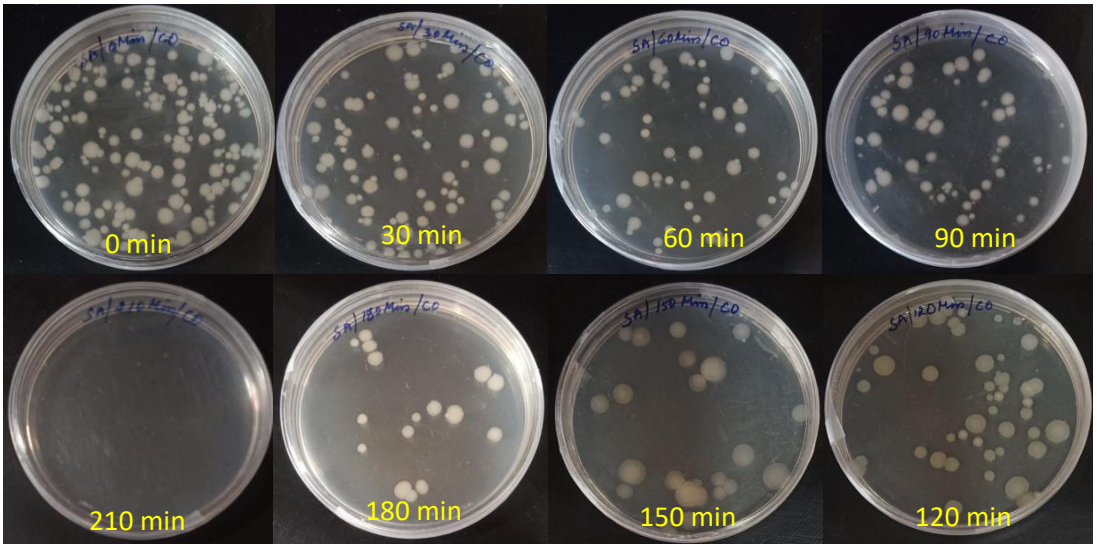

Figure 4.11(a). Colony forming units of *S. aureus* after treatment with Co(II)-Co(III) LDH

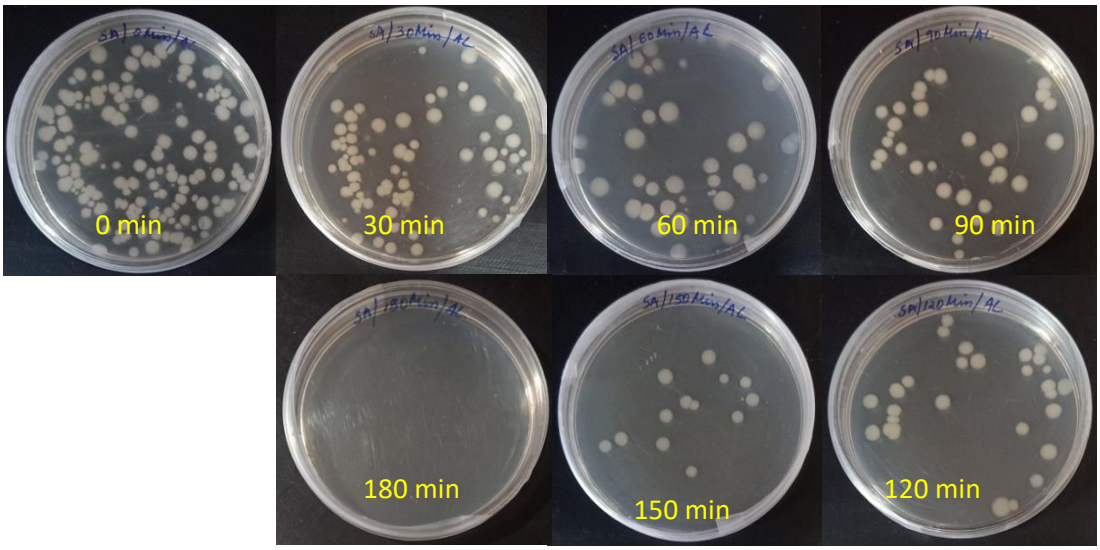

Figure 4.11(b). Colony forming units of *S. aureus* after treatment with Ac@Co(II)-Co(III) LDH

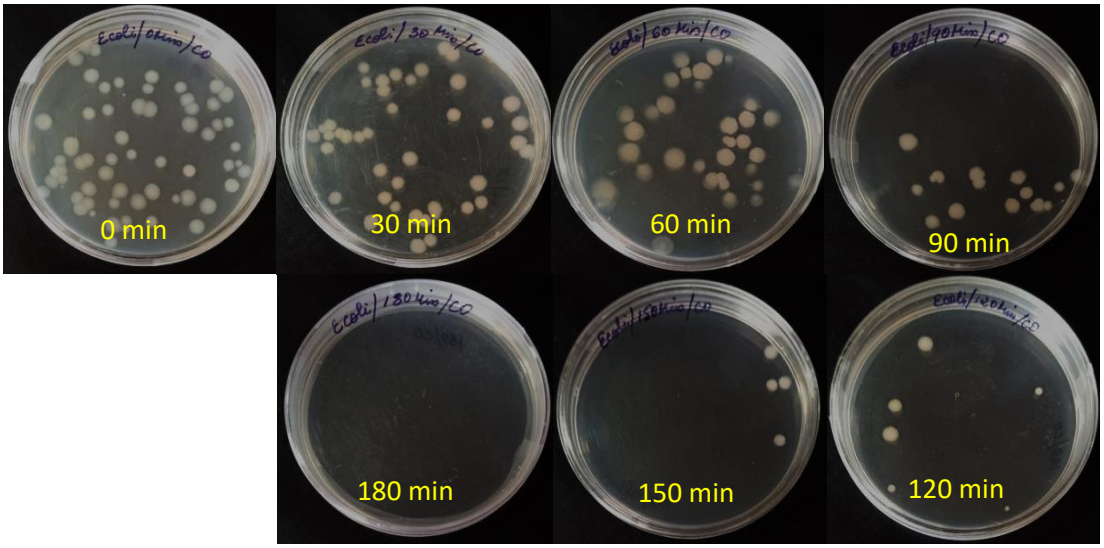

Figure 4.11(c). Colony forming units of *E. coli* after treatment with Co(II)-Co(III) LDH

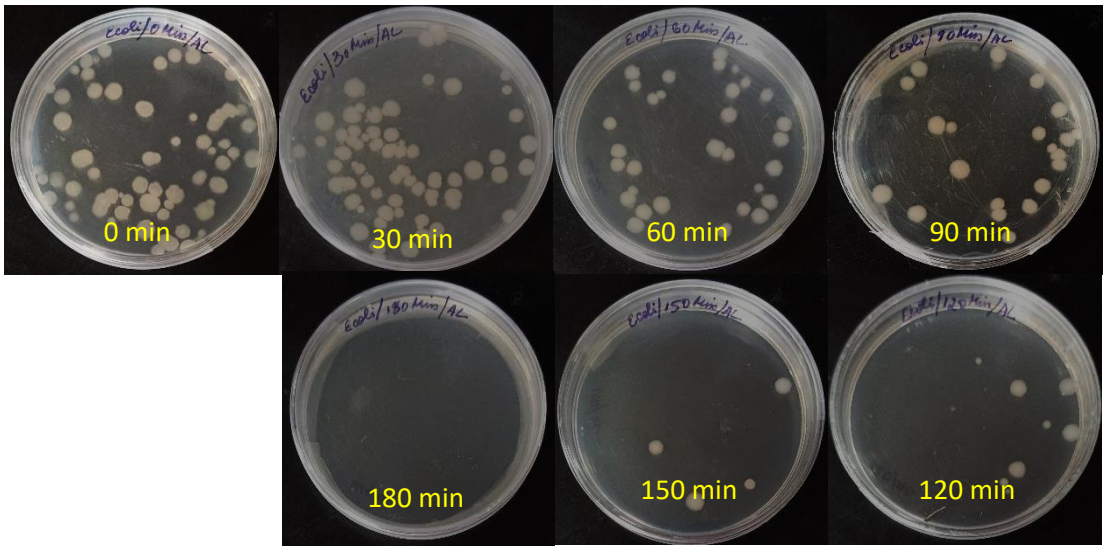

Figure 4.11(d). Colony-forming units of *E. coli* after treatment with Ac@Co(II)-Co(III) LDH

The effect of the killing of bacteria requires the effective control of particle sizes in addition to the bactericidal effect of the compounds used. It is because the smaller the particle size, the easier would be the diffusion of LDH nanoparticles on the host membrane, and the stronger would be the antibacterial effect[7].

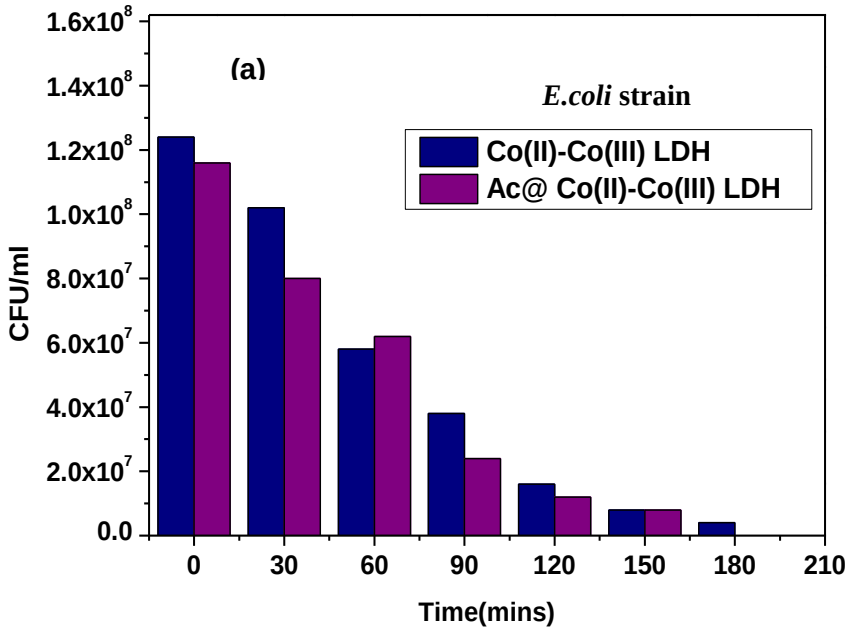

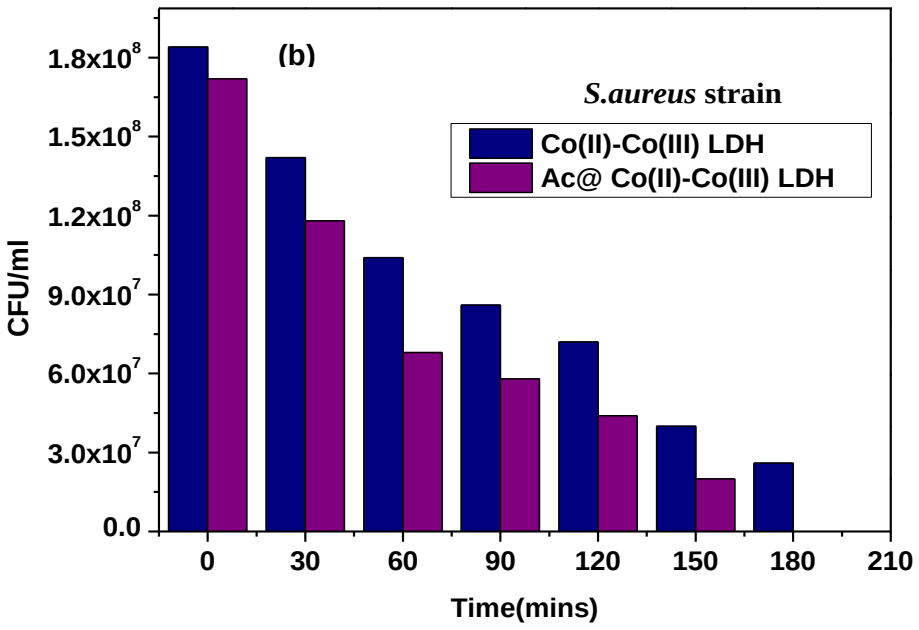

Figure 4.11(e). Colony foming units (CFU) of bacterial strains (a) *E. coli* & (b) *S. aureus*

Mechanistically it can be explained that the cobalt LDH and its nanocomposite, being nanoporous materials, can combat bacterial infection through the destruction of the cell membrane due to oxidative stress or high permeability of reactive cobalt nanoparticles across the cell membrane into the cytoplasm or nucleoplasm of the host cells[1,4]. It is evident that cobalt oxides/cobalt hydroxides or cobalt LDH as nanoparticles produce cobalt radical and reactive oxygen species (ROS) in the form of hydroxyl, peroxide, or superoxides[8]. Fundamentally, the electrostatic interaction of negatively charged (bacteria) with LDH nanoparticles produces a synergistic effect. Consequently, the LDH nanoparticles penetrate the cell membrane of the bacteria due to the strong electrostatic force exerted on the cell surface, and as a result, the cobalt radicals being biocidal agents, toxify the cytoplasm of the bacteria cell. This inhibits the growth and cell division of the cell cycle and, as a result, leads to changes in the shape or size of the host cells resulting in death[9]. It is observed in the study

that the effect inhibition property of nanocomposite has a stronger effect on *E. coli* than on *S. aureus*.

4.8. Conclusion

The synthesized compounds, Co(II)-Co(III) LDH and Ac@Co(II)-Co(III) LDH nanohybrid, were tested as antibacterial agents, and the results showed an effective bactericidal agent against the two *E. coli* (gram-negative) and *S. aureus*(gram-positive) strains, and both were found to be more effective against *E. coli*. The inhibition effect on the two bacteria strains was observed to be more pronounced in the case of Ac@Co(II)-Co(III) LDH nanohybrid than in the parent cobalt LDH.

References

[1] M. Balouiri, M. Sadiki, S.K. Ibnsouda, Methods for invitro evaluating antimicrobial activity: areview, J. Pharm. Anal. (2016). https://doi.org/10.1016/j.jpha.2015.11.005.

[2] I. Wiegand, K. Hilpert, R.E.W. Hancock, Agar and broth dilution methods to determine the minimal inhibitory concentration (MIC) of antimicrobial substances, Nat. Protoc. 3 (2008). https://doi.org/10.1038/nprot.2007.521.

[3] T. Appiah, Y.D. Boakye, C. Agyare, Antimicrobial activities and time-kill kinetics ofextracts of selected ghanaian mushrooms, Evid.-based Complement. Alternat. Med.2017 (2017). https://doi.org/10.1155/2017/4534350.

[4] M. Li, L. Li, S. Lin, Efficient antimicrobial properties of layered double hydroxide assembled with transition metals via a facile preparation method, Chin. Chem. Lett. 31 (2020). https://doi.org/10.1016/j.cclet.2019.09.047.

[5] J.S. Valente, G. Rodriguez-Gattorno, M. Valle-Orta, E. Torres-Garcia,Thermal decomposition kinetics of MgAl layered double hydroxides, Mater. Chem. Phys. 133 (2012). https://doi.org/10.1016/j.matchemphys.2012.01.026.

[6] N.S. Alahmadi, J.W. Betts, F. Cheng, M.G. Francesconi, S.M. Kelly, A. Kornherr, T.J. Prior, J.D. Wadhawan, Synthesis and antibacterial effects of cobalt-cellulose magnetic nanocomposites, RSC Adv. 7 (2017). https://doi.org/10.1039/C7RA00920H.

[7] E.L. Chang, C. Simmers, D.A. Knight, Cobalt complexes as antiviral and antibacterial agents, Pharmaceuticals (2010).

https://doi.org/10.3390/ph3061711.

[8] E. Sánchez-López, D.Gomes, G. Esteruelas, L. Bonilla, A.L. Lopez-Machado, R. Galindo, A. Cano, M. Espina, M. Ettcheto, A. Camins, A.M. Silva, A. Durazzo, A. Santini, M.L. Garcia, E.B. Souto, Metal-based nanoparticles as antimicrobial agents: an overview, Nanomaterials (2020). https://doi.org/10.3390/nano10020292.

[9] R. Wang, B. Zhang, Z. Liang, Y. He, Z. Wang, X. Ma, X. Yao, J. Sun, J. Wang, Insights into rapid photodynamic inactivation mechanism of Staphylococcus aureus via rational design of multifunctional nitrogen-rich carbon-coated bismuth/cobalt nanoparticles, Appl. Catal. B241 (2019). https://doi.org/10.1016/j.apcatb.2018.09.030.

CHAPTER 5

A non-isothermal thermokinetic degradation study of the mesoporous Ni-Co layered double hydroxide using isoconversional approaches

This chapter explores thermokinetic behavior of the mesoporous Ni-Co LDH using various isoconversional approaches. Furthermore, preexponential factors, kinetic degradation models and mathematical deconvolution analysis (MDA) were thoroughly studied.

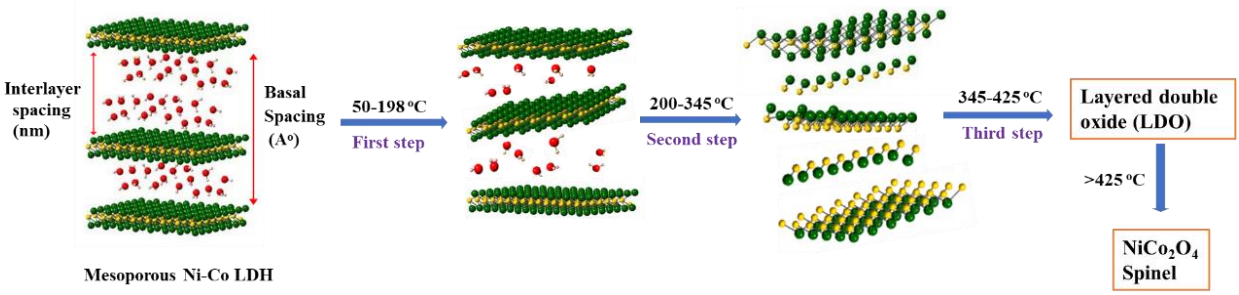

5.1. Introduction

Thermal analysis of materials is considered a fundamental approach to understanding the thermal reactions of solids governed by physical or chemical processes. The earlier studies on thermal applications reported that thermal analysis using TGA or DSC techniques give the materials decomposition process accompanied by their respective mass losses and the thermochemical processes responsible for determining the thermal process viz. stability of materials, melting, crosslinking, crystallization etc. [1]. In modern days, this thermal analysis based on kinetic models is regarded as an advanced approach, which gives important knowledge in practical applications like a supercapacitor [2], reaction model determination such as nucleation, diffusion, power laws etc. [3], production of fuel or clean energy [4], metal oxide precursors [5], catalytic activity [6] etc. Hence, the present study emphasizes thermokinetic investigation of the synthesized compound using Ni-Co LDH as the target of the present study.

Layered double hydroxides (LDHs), also called anionic clays, belong to a general class of clay-like inorganic layered materials characterized by the stacking sequence of metal hydroxide sheets separated by interlayer domains. The interlayer domain contains mainly anionic charged species such as carbonates, halides, oxo-ions, polyatomic ions, water, etc. Speaking of their properties, LDHs exhibit excellent common properties such as catalytic, thermal, adsorbent, ion-exchange, intercalation, etc [7]. Besides, applications of LDHs such as adsorption, electrochemical, antimicrobial, thermal, oxygen evolution reaction (OER) etc. are widely known [8,9]. The chemical composition and structural formula of LDHs can be expressed as; $[M^{2+}_{1-x}M^{3+}_{x}\ (OH)_2]^{x+}\ (A^{n-})_{x/n} \times yH_2O$. The M^{2+} and M^{3+} imply the di- and trivalent metallic cations (M^{2+}= Ni, Mg, Zn, Fe etc.) and (M^{3+}=Al, Co, Fe etc.). A^{n-} and yH_2O represent the interlayer ions and amphoteric molecules like water. In addition, the unique

and most promising properties shown by LDHs are that they undergo a reconstruction process called the 'memory effect' after the entire structural transformation and possess a high ion exchange capacity with other anions like halides, polyatomic anions, macromolecules etc [10].

The present study emphasizes the investigation of the thermokinetic properties of the synthesized compound as the main objective. In recent times, the traditional method of kinetic analysis on LDHs contains information where the evaluation of kinetic parameters were subjected to single heating data or isothermal (ΔT=constant). This inconsistency or unreliability in traditional kinetic procedures may lead to a large deviation in kinetic information [11-13]. Therefore, good care must be taken for the reaction models to be determined. For these reasons, the present study focuses on the use of isoconversional/model-free kinetics approaches to evaluate kinetic parameters. The logical behind for using these approaches is that kinetic parameters could be reliably determined at a constant extent of conversion (α), and it is more convenient to use the non-isothermal TGA/DSC heating data with different heating rates (β), as suggested by ICTAC recommendation [14]. In terms of material undergoing a multi-stage degradation reaction, the isothermal heating process might result in inaccurate estimation for determining kinetic parameters. The major disadvantage of the isothermal heating data is the limited temperature range; sometimes, it might result in an incomplete conversion range at a specified temperature [3,15]. Thus, it does not allow the flexibility of the materials undergoing various degradation stages. The advantages of the isothermal approach seem to be useful when a material undergoes a single step thermal degradation or can be described by one step kinetic model. However, it might not be so reliable in predicting the kinetic parameters, when any materials undergoing multiple reactions or governed by individual

components called a “pseudocomponents", due to unchanged in global temperature or non-flexibility of materials degraded at the undesired temperature. In addition, the recently reported literature on LDHs were made a prediction based on the physical observations or thermal degradation behavior of LDHs but not with all the kinetic information in detail [16-18]. Another insufficient explanation of the thermokinetic behavior of LDHs is the use of kinetic models and, most importantly almost never the explanation of overlapping TGA/DSC curves, which affects the physio-chemical thermal degradation characteristics of LDHs [19-21]. Therefore, we critically analyzed the kinetics of overlapping peak parameters using mathematical deconvolution analysis (MDA) and also the presence of individual peak components called the pseudocomponents, affecting the thermal degradation curves of LDHs [22]. Fundamentally, some literatures had reported that since the area of any kinetic analysis are based on indirect experimental measurement of the reaction rates, and therefore in many cases, the algorithms or mathematical models used are incapable of describing the reaction rates obtained from the experiment and the estimated theoretical rates. Hence, these types of studies are only valid to describe the phenomenological thermokinetic behaviour of some process or models [23]. Accordingly, the present studies also give the knowledge about how a synthesized compound could exhibit a number of degradation reactions or stages that would occur [24]. In such situation, a series of degradation pathway should follow some of the processes, which has to be reliably based on theoretical prediction and similarities with those parameters/values obtained from experimental measurements [25,26].

The mesoporous Ni-Co LDH was used as the representative to understand how commonly occurring LDHs exhibit a thermal degradation characteristic via described by reaction models f(α). The pyrolysis reaction of a mesoporous Ni-Co LDH is crucial in the

present study due to its broader application in different fields such as supercapacitors [27], electrochemical sensors [28], photocatalysts [29], oxygen evolution reactions (OER) [30], adsorption [31], antimicrobial [32], etc. Therefore, the present study still requires Ni-Co LDH as an important precursor for understanding the thermal degradation properties for different applications. Secondly, the evaluation of kinetic parameters in the lower temperature range from 50-198 ^{o}C was omitted due to the presence of physisorbed gas or moisture phases, which cannot be described by kinetic models. Critically, several isoconversional models or model-free methods like Friedman, Flynn-Wall-Ozawa (FWO), Kissinger-Akahira-Sunose (KAS), and advanced non-linear Vyazovkin were chosen to determine the activation energies $E_a(jK.mol^{-1})$ obtained from these models [33]. The calculation of activation energies in the present study were compared experimentally and theoretically. Also, preexponential factors and the kinetic reliability for the determination of reaction models $f(\alpha)$ were determined using the kinetic compensation effect (KCE) and the master plot method. To our knowledge, no known reports were available using our present objectives.

5.2. Experimental

5.2.1. Materials and Synthesis

In the present study, required chemicals like Nickel (II) acetylacetonate and Cobalt (III) acetylacetonate (95 % and 99.9%), Hydrochloric acid (99%), Ammonium hydroxide (≥ 99.99 %), ethanol (96%), acetone (99.5%), Silica (230-400 mesh particle size) were purchased from Sigma Aldrich. All chemicals used in the study were of analytical grade. The synthesis procedure for the mesoporous Ni-Co LDH was according to our previously reported non-aqueous ‘soft chemical’ Sol-Gel route [31].

5.2.2. Characterization techniques

Powder X-ray diffraction (Rigaku Japan, model: Ultima IV, CuKα radiation at λ=0.154 nm, voltage: 20-60 kV) and TGA-DTA (M/S TG-DTA Instrument, model: Q-600, pyrolysis range 50-800 ^{o}C) equipment were used to determine the Ni-Co LDH formation and its thermal degradation properties. The non-isothermal experiment was carried out at four heating rates $\beta = 5$, 10,15, and 20° $C/mins$, respectively.

5.2.3. Computation of activation energies

The theoretical computation of activation energies was carried out to understand the complex numerical integration. The series of activation energies were obtained in the conversion range $\alpha = 57.5 \pm 32.5$. Simultaneously, the various isoconversional models, including non-linear Vyazovkin were performed. MATLAB software was used for the computation of activation energies.

5.2.4. Kinetic models used

Different kinetic models involving nucleation, diffusion, reaction-order model, and geometrical contraction were used to explain the reaction models f(α). Table 5.1 represents the algebraic expressions of kinetic models.

5.2.5. Kinetic Theory

In the present study, various isoconversional or model free-methods, including differential and integral methods viz Friedman, KAS, FWO, and non-linear Vyazovkin were used to evaluate the activation energies of the mesoporous Ni-Co LDH degradation.

Defining the Arrhenius rate constant; $k(T) = Ae^{(-\frac{E}{RT})}$, the solid-state reactions of a single stage give the expression [34]:

$$\frac{d\alpha}{dt} = k(T)f(\alpha) = \ k(T) = Ae^{(-\frac{E}{RT})}\, f(\alpha) \qquad (1)$$

The variables A, E are the kinetic parameters i.e., preexponential factor and activation energy. $'R'$ and $'T'$ represents the gas constant and Arrhenius temperature. $k(T)$= temperature dependence rate constant of the reaction process; $f(\alpha)$= extent of conversion described by the reaction models. α= fraction of a total mass loss in the process and can be expressed as:

$$\alpha = \frac{m_o - m_t}{m_o - m_\infty} \qquad (2)$$

$m_o, m_t,$ and m_∞ represent the initial weight, reactants weight at time $'t'$, and final weight at the end of the pyrolysis process [35].

Equation (1) represents the differential kinetic equation, which applies to both the isothermal ($T = Const$)or non-isothermal ($T = T(t)$ heating programmed. Assuming $\beta = \frac{dT}{dt} = Const(non - isothermal)$, the equation (1) can be re-formulated as:

$$\beta \frac{d\alpha}{dt} = \frac{f(\alpha)}{Ae^{E/RT}} \qquad (3)$$

Integrating equation (3) w.r.t $'dt'$, change in $T = T(t)$as a function of time, becomes

$$g(\alpha) \equiv \int_0^\alpha \frac{d\alpha}{f(\alpha)} = A \int_0^t e^{\left(-\frac{E}{RT}\right)} dt \qquad (4)$$

Equation (4) represents the integral form of the kinetic expression, which can be used to deduce the various integral kinetic parameters at any temperature programmed. Replacing $dt = dT$, and introducing $T = 0\ to\ T$ w.r.t the constant heating rate, the above expression can be written as:

$$g(\alpha) = \frac{A}{\beta} \int_0^T e^{(-\frac{E}{RT})}\ dT \qquad (5)$$

Equation (5) represents the explicit value of the heating rate programmed. However, due to some limitations in the process and approximations, equation (5) does not provide a true

analytical solution. Therefore, the modern integral method replaces the above conditions i.e. it makes use of numerical integration for obtaining the various kinetic parameters called the kinetic triplets $[A, Ea, f(\alpha) or\ g(\alpha)]$ [3].

- ***Isoconversional/Model-free Kinetics***

According to ICTAC kinetic recommendation [15], Isoconversional kinetics analysis not only describes the evaluation of kinetic triplets at a constant extent of conversion but also provides knowledge about the kinetic degradation stages. The reliability of such kinetic analysis uses multiple heating data. The equation (1) through isoconversional principle can be expanded in the form of the partial derivative as:

$$\left[\frac{\partial\, ln(\frac{d\alpha}{dt})}{\partial T^{-1}}\right]_{\alpha} = \left[\frac{\partial\, ln\, k(T)}{\partial T^{-1}}\right]_{\alpha} + \left[\frac{\partial\, ln\, f(\alpha)}{\partial T^{-1}}\right]_{\alpha} \qquad (6)$$

The index$'\alpha'$, designates the constant extent of conversion at multiple heating rates. Differentiating and simplifying equation (6) at $\alpha = const$, the above expression yields

$$\left[\frac{\partial\, ln(\frac{d\alpha}{dt})}{\partial T^{-1}}\right] = \frac{-E_{\alpha}}{R} \qquad (7)$$

Equation (7) represents the general expression for evaluating the various isoconversional activation energies and also the preexponential factor for multiple heating rates without assuming any reaction models.

- ***Friedman isoconversional method***

Friedman's isoconversional method is a differential method. The logarithm derivative of the equation (1) yields:

$$ln\left(\frac{d\alpha}{dt}\right)_{\alpha,i} = \frac{ln[f(\alpha)A_{\alpha}]RT_{\alpha,i} - E_{\alpha}}{RT_{\alpha,i}} = ln[f(\alpha)A_{\alpha}] - \frac{E_{\alpha}}{RT_{\alpha,i}} \qquad (8)$$

For non-isothermal heating rate, defining $\beta = \frac{dT}{dt} = Const$, rearrangement of equation (8) becomes:

$$ln\left[\beta_i \left(\frac{d\alpha}{dt}\right)_{\alpha,i}\right] = ln[f(\alpha)A_\alpha] - \frac{E_\alpha}{RT_{\alpha,i}} \qquad (9)$$

The subscript $'i' and\ T_{\alpha,i}$ denotes the process at various temperature programme, and the temperature at which the extent of conversion is reached under i^{th} temperature program.The linear plot of $\ln\left[\beta_i \left(\frac{d\alpha}{dt}\right)_{\alpha,i}\right]\ Vs \frac{1}{T_{\alpha,i}}$ yields activation energy and preexponential factor $A\ (min^{-1})$ [36].

- ***Flynn-Wall-Ozawa method***

Flynn, Wall, and Ozawa (FWO) is an integral method and it is based on Doyle approximation as [3]:

$$ln(\beta_i) = Const - 1.052\left(\frac{E_\alpha}{RT_\alpha}\right)\ [Doyle\ approximation] \qquad (10)$$

Where, β_i is the heating rate. A linear plot of $ln(\beta_i)$against the reciprocal temperature, yields isoconversional activation energy at the constant extent of conversion (α).

- ***Kissinger-Akahira-Sunose method***

This method uses an integral approximation to evaluate the kinetic parameters. Based on Coats-Redfern formulation, KAS derived the expression as [37]:

$$\ln\left(\frac{\beta}{T_\alpha^2}\right) = \ln\left(\frac{A_\alpha R}{E_{a,\alpha} g(\alpha)}\right) - \frac{E_{a,\alpha}}{RT_\alpha} \qquad (11)$$

A linear plot of$\ln\left(\frac{\beta}{T_\alpha^2}\right) Vs \frac{10^3}{T}$ at the constant extent of conversion yields activation energies

- ***Vyazovkin method (Advanced isoconversional method)***

This method uses the integral expression of estimating activation energies as a function of temperature or time. Explicitly, this method is a non-linear isoconversional

method. For a series of TGA runs at different heating rates, the values of E_α over α dependencies could be determined by minimizing the following equation [38]:

$$\Phi(E_\alpha) = \sum_{i=1}^{n} \sum_{j \neq i}^{n} \frac{I(E_{a,\alpha}, T_{\alpha,i})\beta_j}{I(E_{a,\alpha}, T_{\alpha,j})\beta_j} \qquad (12)$$

The temperature integral (12) can be deduced as:

$$I(E_\alpha, T_\alpha) = \int_0^{T_\alpha} \exp\left(\frac{-E_\alpha}{RT}\right) dT \qquad (13)$$

The integral form of equation (13) can be solved numerically. Minimization is repeated for each set of α to obtain the dependence of E_α on α. The indexes $'\beta', 'i', 'j'$ and $'n'$in equation (13) represents the heating rates, a series of experimental runs performed under different heating rates, and the total number of experiments performed. In the present work, we have chosen a Senum–Yang fourth-degree approximation, where the expression $I(E_\alpha T_\alpha) = \left(\frac{E_{a,\alpha}}{R}\right) p(x)$. The variable $p(x)$ on the right-side term represents the fourth-degree polynomial equation as:

$$p(x) = \frac{\exp(-x)}{x} \cdot \frac{x^3 + 18x^2 + 86x + 96}{x^4 + 20x^3 + 120x^2 + 240x + 120} \qquad (14)$$

The quantity $'x'$ denotes $\frac{E_{a,\alpha}}{RT}$ [39]. The numerical integration in the conversion range $\alpha = 57.5 \pm 32.5$ was performed at the small temperature segments, which yields the effective $E_{a,\alpha}$ values.

Table 5.1. Some important algebraic expressions used in the present study [40]

Model no.	Kinetic models	*f*(α)	*g*(α)
	Nucleation		
1	Power law(P2)	$4\alpha^{3/4}$	$\alpha^{1/4}$
2	Power law(P3)	$3\alpha^{2/3}$	$\alpha^{1/3}$
3	Power law(P4)	$2\alpha^{1/2}$	$\alpha^{1/2}$
4	Power law(P2/3)	$2/3\alpha^{-1/2}$	$\alpha^{3/2}$
5	Avrami-Erofeev(A2)	$2(1-\alpha)[-ln(1-\alpha)]^{1/2}$	$[-ln(1-\alpha)]^{1/2}$
6	Avrami-Erofeev(A3)	$3(1-\alpha)[-ln(1-\alpha)]^{2/3}$	$[-ln(1-\alpha)]^{1/3}$
7	Avrami-Erofeev(A4)	$4(1-\alpha)[-ln(1-\alpha)]^{3/4}$	$[-ln(1-\alpha)]^{1/4}$
	Diffusion		
8	One-Dimensional Diffusion(D1)	$1/2\alpha^{-1}$	α^2
9	Two-Dimensional Diffusion(D2)	$[-ln(1-\alpha)]^{-1}$	$(1-\alpha)ln(1-\alpha)+\alpha$
10	Three-Dimensional Diffusion(D3)	$3/2(1-\alpha)^{2/3}\,[1-(1-\alpha)^{1/3}]^{-1}$	$[1-(1-\alpha)^{1/3}]^2$
	Reaction-order model		
11	Mampel-first order (F1)	$1-\alpha$	$-ln(1-\alpha)$
	Geometrical contraction models		
12	Contracting cylinder(R2)	$2(1-\alpha)^{1/2}$	$1-(1-\alpha)^{1/2}$
13	Contracting sphere(R3)	$3(1-\alpha)^{2/3}$	$1-(1-\alpha)^{1/3}$

- ***Kinetic reliability of master plot methods used for the determination of reaction models f(α)***

The use of various isoconversional or model-free methods, even though calculates kinetic parameters non-isothermally at different heating rates. However, it does not explain reaction models. Therefore, it is important to make use of the Criado master plot method for the overall kinetic factors. The master plot kinetic method uses the integral form of estimating the reaction models f(α), if the activation energies of the process are previously known. Transformation of equation 1 and 5, the following expression can be obtained [41]:

$$\frac{Z(\alpha)}{Z(0.5)} = \frac{f(\alpha)g(\alpha)}{f(0.5)g(0.5)} = \left(\frac{T_\alpha}{T_{0.5}}\right)^2 \frac{\left(d\alpha/dt\right)_\alpha}{\left(d\alpha/dt\right)_{0.5}} \qquad (15)$$

Where 0.5 refers to the conversion at α=0.5

The term $\frac{f(\alpha)g(\alpha)}{f(0.5)g(0.5)}$ can be defined as the reduced theoretical curve, whereas the right side of the term $\frac{(d\alpha/dt)_\alpha}{(d\alpha/dt)_{0.5}}$ can be obtained from experimental values. Comparing both the term tells which kinetic model best describes the degradation process.

- ***Determination of preexponential factor A (min^{-1}) from kinetic compensation effect (KCE)***

Besides, the activation energies (Ea) and reaction models f(α) are known, the preexponential factor (A) can be evaluated using a recommended equation called the kinetic compensation effect(KCE). In recent days, most researchers have reported the preexponential factor subjected to only a single heating rate. Whereas, it applies to multi-heating programme too. In the present study, the compensation effect has been calculated using the equation [42]:

$$lnA_i = \frac{E_i}{RT} + ln\left[\frac{(d\alpha/dt)}{f(\alpha)}\right]_i = aE_i + b \qquad (16)$$

Equation (16) takes the form of equation (1). The variables $'a'$ and $'b'$ represent the compensation parameters, and once the compensation parameters are known,E_i and $A_i$pairs (from equation 16) can be estimated using isoconversional model-free fitting methods for each ith reaction models$f(\alpha)$.Therefore, lnA_i can be evaluated as:

$$lnA_i = a\,E_i + b \qquad (17)$$

- ***Mathematical deconvolution analysis (MDA)***

The thermal decomposition reactions in most solids are, in fact, a complex process. Likewise, layered double hydroxides (LDHs) in general do have degradation reactions that

cannot be described by a single-stage reaction. For this reason, mathematical deconvolution studies have been conducted using the Gaussian, Weibull, and FraserSuzuki multi-peak analysis [43]. According to ICTAC recommendation [15], a series of independent reactions occurring for more than one stage or individual stages under the defined reaction rate can be explicitly expressed as:

$$\frac{d\alpha}{dt} = \sum_{i=1}^{N} \frac{d\alpha_i}{dt} = \sum_{i=1}^{N} \gamma_i A_i \exp\left(-\frac{E_{\alpha i}}{RT}\right) f(\alpha_i) \qquad (18)$$

The letter $'N'$ denotes the number of overlapped Ni-Co LDH peaks called pseudocomponents, $f(\alpha_i)$ denotes physico-geometrical reaction models of the pseudocomponent peaks, and γ_i represents the contribution of ith pseudocomponent to the overall mass loss. Similarly, the deconvolution procedures for the presence of overlapping peaks can be deduced with the help of:

$$y = a_o \exp\left[-\frac{1}{2}\left(\frac{x-a_1}{a_2}\right)^2\right] \qquad (19)$$

The variables $y^o, a_o, a_1 \& a_2$ represent the initial value of the Gaussian distribution function at $x = 0$, the height of the peak or amplitude, center, and width of the curve.

The Weibull function can be expressed as:

$$y = a_o \left(\frac{a_3 - 1}{a_3}\right)^{\frac{(1-a_3)}{a_3}} \left(\frac{x - a_1}{a_2} + \left(\frac{a_3 - 1}{a_3}\right)^{\frac{1}{a_3}}\right)^{a_3 - 1}$$

$$\exp\left[-\left(\frac{x-a_1}{a_2} + \left(\frac{a_3-1}{a_3}\right)^{\frac{1}{a_3}}\right)^{a_3} + \frac{a_3-1}{a_3}\right] \qquad (20)$$

The variables $a_0, a_1, a_2 \& a_3$ represent the amplitude, center, width & shape of the curves. The FraserSuzuki formulation can be expressed as:

$$y = a_o \exp\left[-\ln 2 \left[\frac{\ln\left(1+2a_3\frac{x-a_1}{a_2}\right)}{a_3}\right]^2\right] \qquad (21)$$

Where, a_0, a_1, a_2 & a_3 are the amplitude, position, half-width and asymmetry of the curve, respectively.

Fityk multi-peak fitting program was used in the present study for deconvoluted peaks simulation.

5.3. Result and Discussion

5.3.1. Powder XRD study of mesoporous Ni-Co LDH

The diffractogram profile of the mesoporous Ni-Co LDH is shown in Fig.5.1 (a) and (b) degraded product. It can be seen that the synthesized compound showed the formation of well-hydrolyzed nickel and cobalt hydroxide phases similar to the reported structure (JCPDS:00-040-0216) [44]. The most prominent peak obtained at around θ = 11.56^o corresponds to the formation of α-$Co(OH)_3$ phase, diffracted at (003) plane. Similarly, the alternate peaks were obtained in each 2θ interval at θ=23.12^o, 34.94^o, 37.62^o, 39.38^o, 59.3^o& 60. 84°, relate to the co-existence of di- and trivalent Ni or Co hydroxides, represented by (006), (012), (104), (015), (018), & (110) planes [31].

Fig.5.1(b) shows the formation of nickel cobalt oxide spinel using β=5 $^oC.min^{-1}$ degraded product. The purpose of the thermal degraded product in the study is to observe the formation of the metal oxide spinel phase after the complete pyrolysis reactions. The diffraction peaks obtained at 19.37^{o}C and 39.17^o C correspond to (111) and (222) lattice planes [45].

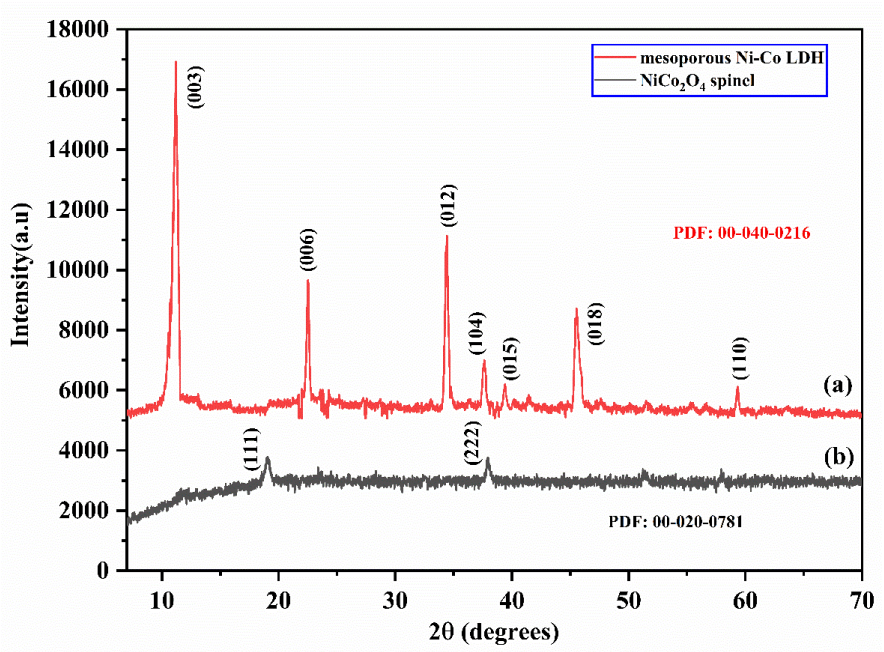

Figure 5.1. Powder diffraction pattern: **(a)** mesoporous Ni-Co LDH and **(b)** $NiCo_2O_4$ spinel (β= 5 °C/min degraded product)

5.3.2. Thermal degradation profile of Ni-Co LDH and effect of heating rates

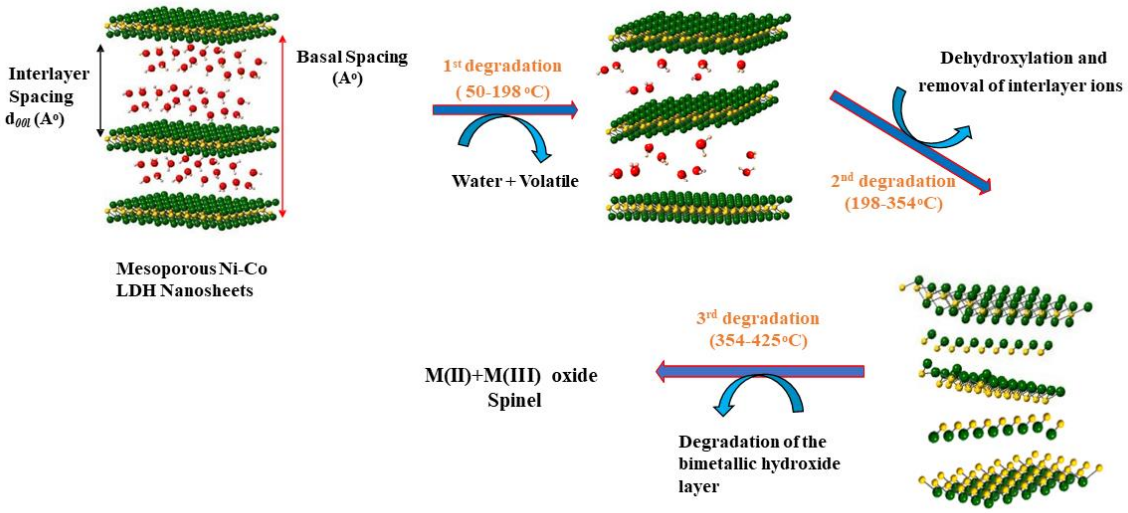

Figure 5.2. Schematic diagram showing the Ni-Co LDH pyrolysis stages

The Ni-Co LDH thermal degradation curves are shown in Fig.5.3(a). It was observed that the Ni-Co LDH thermal behavior shows a general degradation pattern of the frequently

occurring LDHs [46]. The heating curves were obtained at four different heating rates viz, β=5, 10, 15, & 20 $^{o}C.min^{-1}$, respectively. It can be noticed from Fig.5.3(a) and 5.3(b) that the rise in heating rates to maximum produces consistent weight loss curves i.e. independent of heating rates (β), except for the increase in heating rate, resulting in a fast degradation in the lower temperature region. This contribution for the fast degradation at higher heating rates is due to the thermal gradient which results with decrease in mass loss rate and also associated with greater residual mass [24]. In fact, the maximum increase in the β would yield a relatively larger/lower weight loss percent but since the degradation stages follow the same order (curves), and the amount of mass loss (%) differs by only 0.01 or 0.02 %. Hence, it is independent of heating rates for mass loss [23]. Apparently, it can be also be seen that the change or increase in heating rates (β) cause a slight shift in the Ni-Co LDH degradation curves to lower temperature region. Thus, the change in heating rates greatly impacts sample degradation [47].

The Ni-Co LDH degradation curves exhibit three major stages (mass loss). However, due to the presence of feebly adsorbed water molecules, gases, or moisture on the LDH surface, the temperature range from 50-198°C (usually first weight loss) was excluded in the present study. Alternatively, the second and third stages indicate the actual degradation reactions that can be described by the reaction models $f(\alpha)$[19]. The second degradation in the temperature range 198-354 ^{o}C represents substantial mass losses (69%), indicating the dehydroxylation and complete removal of weakly bonded anions (OH or H_2O) in the host Ni-Co LDH layers.

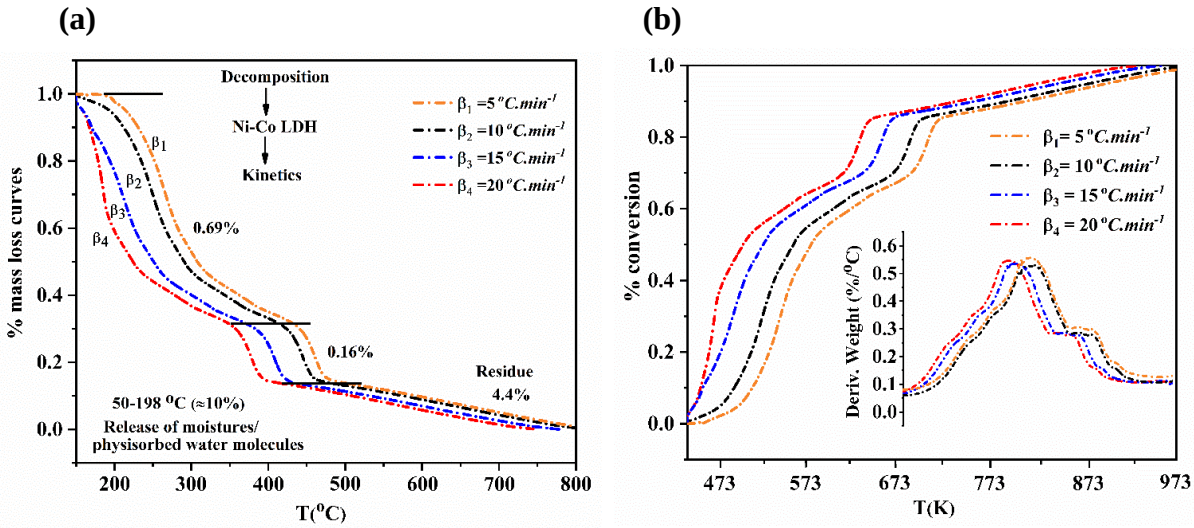

Figure 5.3. Showing **(a)** TGA-DTG thermal degradation pattern of mesoporous Ni-Co LDH(mass loss) at four different heating rates viz. $\beta_1, \beta_2, \beta_3, \beta_4 = 5, 10, 15, 20^o C/mins$, **(b)** Conversion graph at four different heating rates

Similarly, the temperature range from 354-425°C (16 % mass loss) implies the degradation of the main Ni-Co LDH layers. This final stage involves the thermal conversion of bimetallic hydroxide layers into di- and trivalent oxide phases or spinels. The mass loss of 4.4% is the amount of residue that remains after the complete breakdown of the sample during the pyrolysis process.

5.3.3. Experimental and theoretical Isoconversional kinetics calculation and evaluation of activation energies

To determine the reliability in producing the effective activation energies, the numerical integration of the data sets of the models were iterated, which was considered in the isoconversion range from $\alpha = 57.5 \pm 32.5$. Fundamentally, the data obtained from different models were compared experimentally and computationally to increase the accuracy in evaluating the effective activation energies for Ni-Co LDH degradation. Fig.5.

4(a), (b), (c), and (d) show the experimental plots of various isoconversional methods. It can be seen that the methods produce variations in the plots as the conversion range increases.

The computation of effective activation energies (EAE) obtained from various methods is shown in Table 5.2. From Fig.5.5(a) and Table 5.3, It has been observed that the activation energies calculated from the experimental data at the constant extent of conversion were similar to the simulated data (Table 5.2). The series of activation energies obtained under the conversion range from $\alpha = 0.25 - 0.5$ show invariant E_a values (Fig.5.5 a & b).However, the latter conversion range from $\alpha = 55 - 90$ produced inconsistency in Ea values and was found to differ by 9 to 10 % variations, which proved the mesoporous Ni-Co LDH degradation reactions undergo a kinetically complex process. Subsequently, the activation energies decrease within the conversion range $\alpha = 0.8 - 0.9\ degrees$.

Table 5.2. Computation of activation energies obtained by Friedman, Kissinger-Akahira-Sunose, Flynn-Wall-Ozawa &Vyazovkin methods

Sample	Methods	E_a(KJmol^{-1})	Log$_{10}A$/min	Conversion Range (%)	R^2
Ni-Co LDH	KAS	121 ± 27	1.16 ± 0.09	α= 57.5 ± 32.5	0.99481
	Friedman	133 ± 35	1.14 ± 0.06	α= 57.5 ± 32.5	0.99965
	FWO	120 ± 32	1.17 ± 0.01	α= 57.5 ± 32.5	0.99562
	Vyazovkin	132 ± 26	1.2 ± 0.01	α= 57.5 ± 32.5	0.99984

Fundamentally, it is observed that the Friedman and non-linear Vyazovkin produce a consistent trend in activation energy curves with a correlation coefficient comparatively higher than those of KAS and FWO (Table 5.3). Moreover, the theoretical simulation agrees with the experimental results. As mentioned, the series of activation energies undergo a variation at higher conversion ranges. These variations in Ea values, in fact, produce the number of stages or transitions, which are labeled as E1, E2, E3, E4, and E5 (Fig.5.5b).

Hence, the thermal decomposition reactions of Ni-Co LDH is governed by a number of multi-stage reactions.

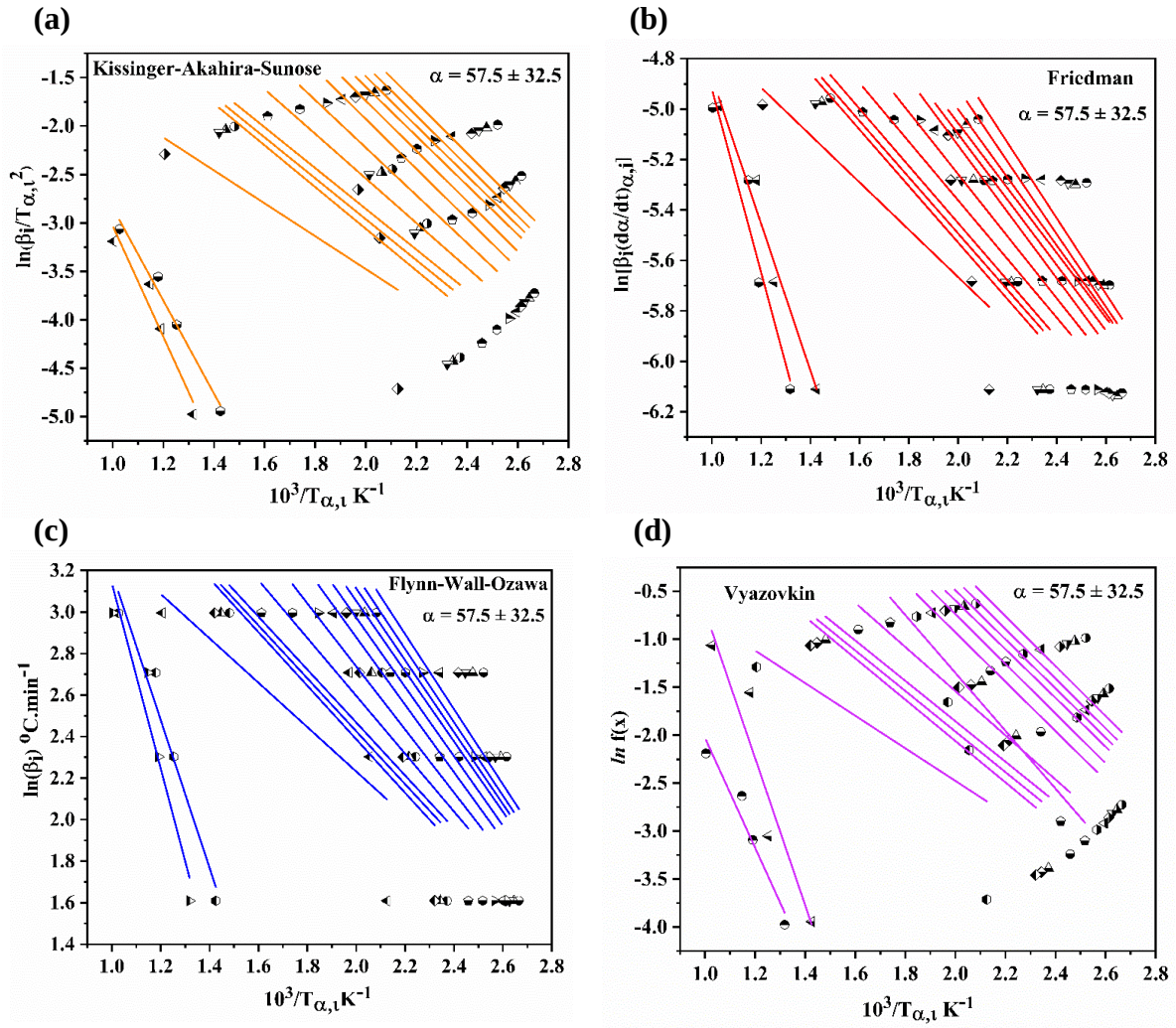

Figure 5.4. Isoconversional kinetic plots: **(a)** Kissanger-Akahira-Sunose, **(b)** Friedman, **(c)** Flynn-Wall-Ozawa, and **(d)** Vyazovkin

Table 5.3. Experimental calculation of activation energies (Ea) obtained by isoconversional methods

Kissinger-Akahira-Sunose(KAS) method			**Friedman Method**			**Flynn-Wall-Ozawa (FWO) method**			**Vyazovkin method**		
Heating rates(β)= 5, 10, 15, 20 °C.min^{-1}, Range(α)=57.5± 32.5											
α	***E_a(kJ.mol^{-1})***	***R^2***	***α***	***E_a(kJ.mol^{-1})***	***R^2***	***α***	***E_a(kJ.mol^{-1})***	***R^2***	***α***	***E_a(kJ.mol^{-1})***	***R^2***
0.25	92.92	0.572	0.25	104.14	0.704	0.25	98.18	0.640	0.25	116.03	0.758
0.30	89.06	0.598	0.30	101.61	0.715	0.3	92.15	0.662	0.3	108.11	0.744
0.35	85.2	0.610	0.35	97.02	0.697	0.35	88.89	0.672	0.35	108.08	0.772
0.40	94.02	0.628	0.4	110.37	0.691	0.4	97.6	0.685	0.4	118.25	0.696
0.45	112.12	0.694	0.45	121.28	0.762	0.45	116.78	0.736	0.45	128.09	0.735
0.5	124.16	0.728	0.5	139.6	0.816	0.5	132.37	0.761	0.5	137.18	0.854
0.55	135.31	0.733	0.55	148.93	0.820	0.55	141.45	0.765	0.55	145.11	0.838
0.6	128.08	0.713	0.6	146.46	0.824	0.6	138.04	0.752	0.6	139.05	0.881
0.65	132.22	0.643	0.65	152.15	0.799	0.65	137.96	0.699	0.65	142.71	0.788
0.7	146.26	0.653	0.7	162.23	0.801	0.7	149.29	0.709	0.7	152.3	0.816
0.75	157.07	0.679	0.75	169.36	0.818	0.75	152.52	0.729	0.75	158.04	0.873
0.8	151.04	0.461	0.8	156.05	0.698	0.8	144.13	0.576	0.8	150.48	0.759
0.85	141.15	0.931	0.85	150.4	0.971	0.85	135.5	0.863	0.85	147.44	0.968
0.9	138.37	0.946	0.9	146.41	0.942	0.9	132.27	0.886	0.9	141.27	0.957
Average (Ea): 123.3557			Average(Ea): 136.1436			Average(Ea):125.5093			Average(Ea): 135.1529		

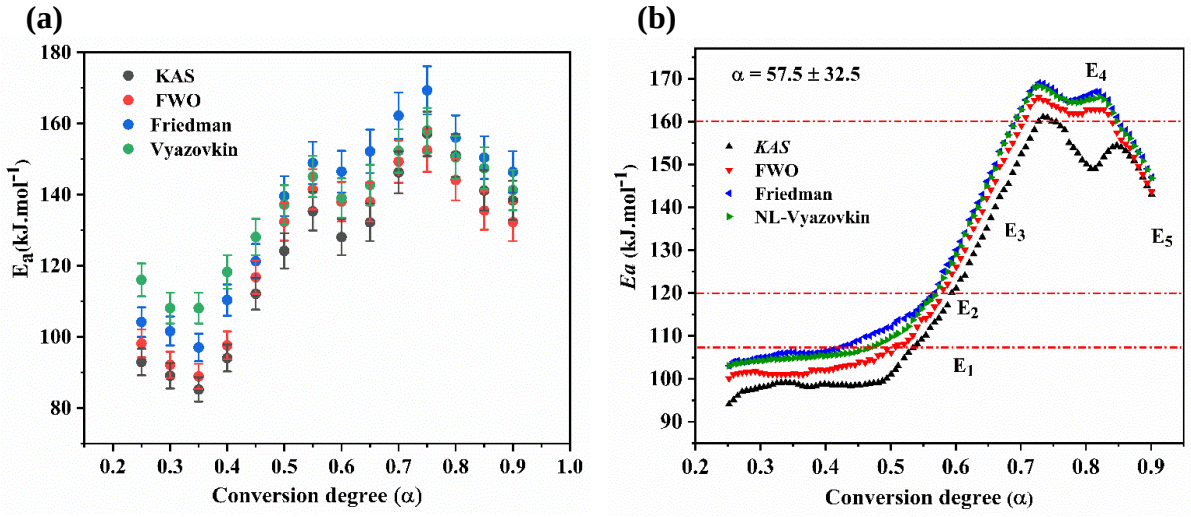

Figure 5.5. Activation energies obtained: **(a)** Experimental and **(b)** Simulation using equation (12)

5.3.4. Determination of preexponential factors $A(min^{-1})$ from kinetic compensation effect

In the present study, the reliability in determining the compensation parameters *a* and *b* were estimated using the Friedman isoconversional method (Table 5.4) into equation (16) w.r.t different reaction models (Table 5.1). Fig.5.6(b) represents the kinetic plot of preexponential factors obtained at 5 $^{o}C.min^{-1}$. The heating rates of 10, 15, and 20 $^{o}C.min^{-1}$ were not shown since the data points obtained produced a similar plot result. It is seen that the preexponential factors of all the used models produce a strong compensation correlation (R^2= >0.995), which yields a straight line in the isoconversion range of 57.5 ± 32.5. Moreover, Table 5.5 shows that the Ea ($kJ.mol^{-1}$) and $logA(min^{-1})$ pair produce a close uniformity despite it might undergo fluctuation in activation energies. These fluctuations differ by 8 to 10%, which confirms that the process is a multi-stage one. According to S.Vyazovkin and N. Sbirrazzuoli ICTAC recommendation [15,43], the determination of the preexponential factor is the one that yields a straight line irrespective of deviations caused

by E_i or A_i pairs and or single-stage or multi-stage kinetic models. Moreover, the closeness in the compensation correlation was found to be much higher in nucleation models viz Avrami-Erofeev and power law models followed by diffusion models.

In conclusion, these observations made in the present study would give a good estimate of preexponential factors for Ni-Co LDH degradation studies.

Table 5.4. Comparisons of compensation parameters at different heating rates using the Friedmanisoconversional method

Heating rates	*a*	*b*	R^2
5 $^oC.min^{-1}$	0.285 ± 0.081	1.197 ± 0.035	0.9995
10 $^oC.min^{-1}$	0.271 ± 0.087	1.199 ± 0.033	0.9992
15 $^oC.min^{-1}$	0.253 ± 0.085	1.195 ± 0.03	0.9997
20 $^oC.min^{-1}$	0.224 ± 0.082	1.191 ±0.034	0.9994

Table 5.5. Evaluation of preexponential factors logA (min^{-1}) obtained using equation (16) for different models (Table 5.1 models)

Models	**Ea(kJ.mol^{-1})**	**Error Ea (kJ.mol^{-1})**	**Log(A/min)**
P2	92.57	2.92×10^{-4}	18.3
P3	113.85	4.46×10^{-4}	31.77
P4	121.51	4.33×10^{-4}	36.11
P2/3	165.01	2.30×10^{-4}	65.01
A2	99.83	3.20×10^{-4}	22.64
A3	149.39	3.27×10^{-4}	54.16
A4	160.08	2.10×10^{-4}	61.28
D1	87.74	4.30×10^{-4}	13.85
D2	139.48	6.12×10^{-4}	48.06
D3	163.18	5.50×10^{-4}	68.03
F1	107.25	7.78×10^{-4}	27.43
R2	79.33	6.99×10^{-4}	8.14
R3	130.02	9.47×10^{-4}	40.88

5.3.5. Master plot determination of kinetic models f(α)

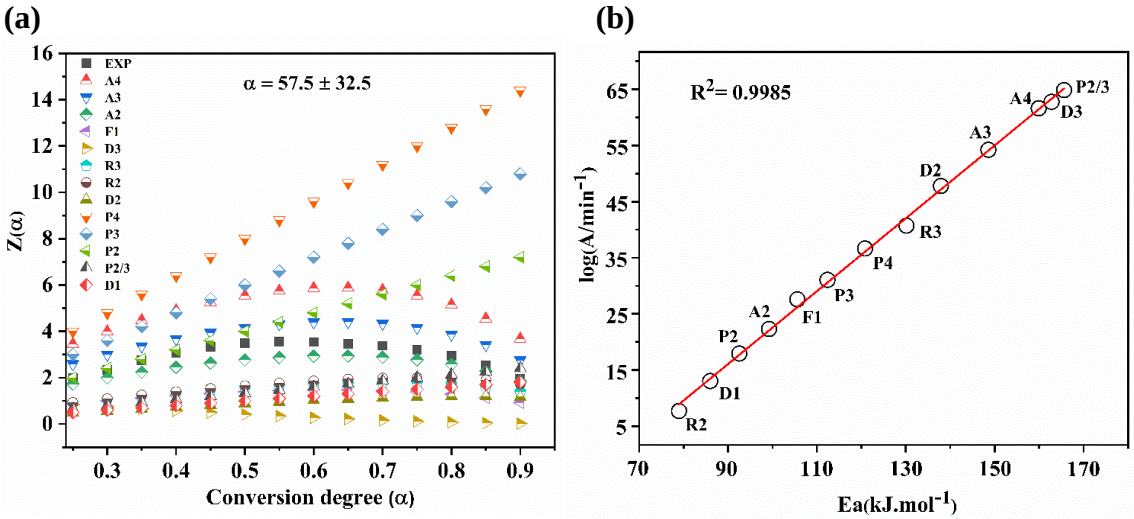

Figure 5.6. **(a)** master plot representing reaction models, **(b)** Preexponential factor using KCE

Once the two kinetic parameters i.e. $E_{a,\alpha}$ $and\ lnA_{\alpha}$ are known, it is important to determine the kinetic models $f(\alpha)$ affecting the overall Ni-Co LDH degradation process (Fig.5.6a). From the isoconversional kinetic master plot of $\frac{Z(\alpha)}{Z(0.5)}$Vs α, the experimental graph overlaps the reduced theoretical curve in the isoconversion range $\alpha = 37.5 \pm 12.5$, which was found to be governed by the $P2$ power-law model. It is known that thermal degradation reactions undergo a complex process when the experimental graph overlaps the reduced theoretical curve above $\alpha = 0.5$ conversion degree [48]. Therefore, the thermal degradation reactions of Ni-Co LDH is controlled by a multiple reaction model. From the mass loss conversion graph shown in Fig.5.3(a), the thermo-kinetic degradation curve of Ni-Co LDH shows a typical sigmoidal shape that agrees with those of the reported literature [3]. Subsequently, the latter conversion segments in the region 72.5 ± 17.5 undergo degradation process controlled by Avrami−Erofeev(A2) model. These two models represent the degradation process dominated by the nucleation models [42].

5.3.6. Mathematical deconvolution analysis of overlapped Ni-Co LDH peaks and kinetics of pseudocomponents

In the present study, three MDA simulation functions, viz. Gaussian, Weibull, and FraserSuzuki were used in the present study to understand the overlapping of the degradation kinetic curves of mesoporous Ni-Co LDH. The deconvolution or presence of additional peaks called 'pseudocomponents' labeled as P1, P2, P3, P4, and P5 with the residual peaks are shown in Fig.5.7 and 5.8 at different heating rates. The short-dashed dot in the figures represents the experimental curves. It can be seen in Fig.5.7 that the fitting parameters in terms of peak position, amplitude, and width of the curves are well fitted in Weibull and FraserSuzuki than in the Gaussian model. These proved that either Weibull or FS function could be reliably used as a well-fitting asymmetric model in the study of thermal degradation of the mesoporous Ni-Co LDH. However, since the correlation coefficient of FS lies almost equal to 1.00 compared to Weibull, which lies between 0.9995-0.9997, the increase in the correlation factors (R^2) follows as FS>Weibull>Gaussian. Therefore, we considered the FS function the accurate model in the present study. The stronger the correlation, the better would be the fitting model.

Furthermore, Fig.5.8 represents the deconvolution of overlapped Ni-Co LDH peaks using a FraserSuzuki simulation function. It can be noticed that the experimental $d\alpha/_{dt}$ reaction rates of Ni-Co LDH are controlled by the presence of additional peaks, which gives the degradation characteristics of the Ni-Co LDH. In the present study, the presence of pseudocomponents for the overall Ni-Co LDH degradation range was assumed under the following conditions: (a)The temperature range from 323- 471 K was considered unreliable or inaccurate in the present study since it involves the escape of weakly adsorbed gases/moistures in the LDH surface; (b) each pseudocomponents denoted as P1, P2, P3, P4,

and P5 represent a series of degradation w.r.t temperature; (c) The peak index as P1, P2 and P3 fall in the second degradation stage; whereas, P4 and P5 fall in the third degradation stage; (d) the second stage corresponds to the complete removal of interlayer anions followed by dehydroxylation; (e) third stage represents the degradation of metal hydroxide layers.

From Fig.5.8 (a),(b) and Table 5.6 i.e. $\beta = 5,\ 10\,^{o}C.min^{-1}$, the presence of pseudocomponents occurs slightly at a higher temperature than those of $\beta = 15,\ 20\,^{o}C.min^{-1}$ as the pyrolysis temperature increases slowly, which results in slow Ni-Co LDH degradations. Moreover, it has been observed that the mass loss for $\beta = 5\,^{o}C.min^{-1}$, in the temperature range of 536-727K (usually second stage;exp T_m = 677 K) undergoes three sub-degradation stages designated as P1, P2, and P3, respectively. Subsequently, the third degradation stage in the temperature range727-803 K undergoes two sub-degradations labeled P4 and P5 (exp T_m=767 K). Similarly, for $\beta = 10\,^{o}C.min^{-1}$, the second stage in the temperature range 536-716 K (exp T_m=665 K), and the third stage in the range 716-779K(expT_m=748).

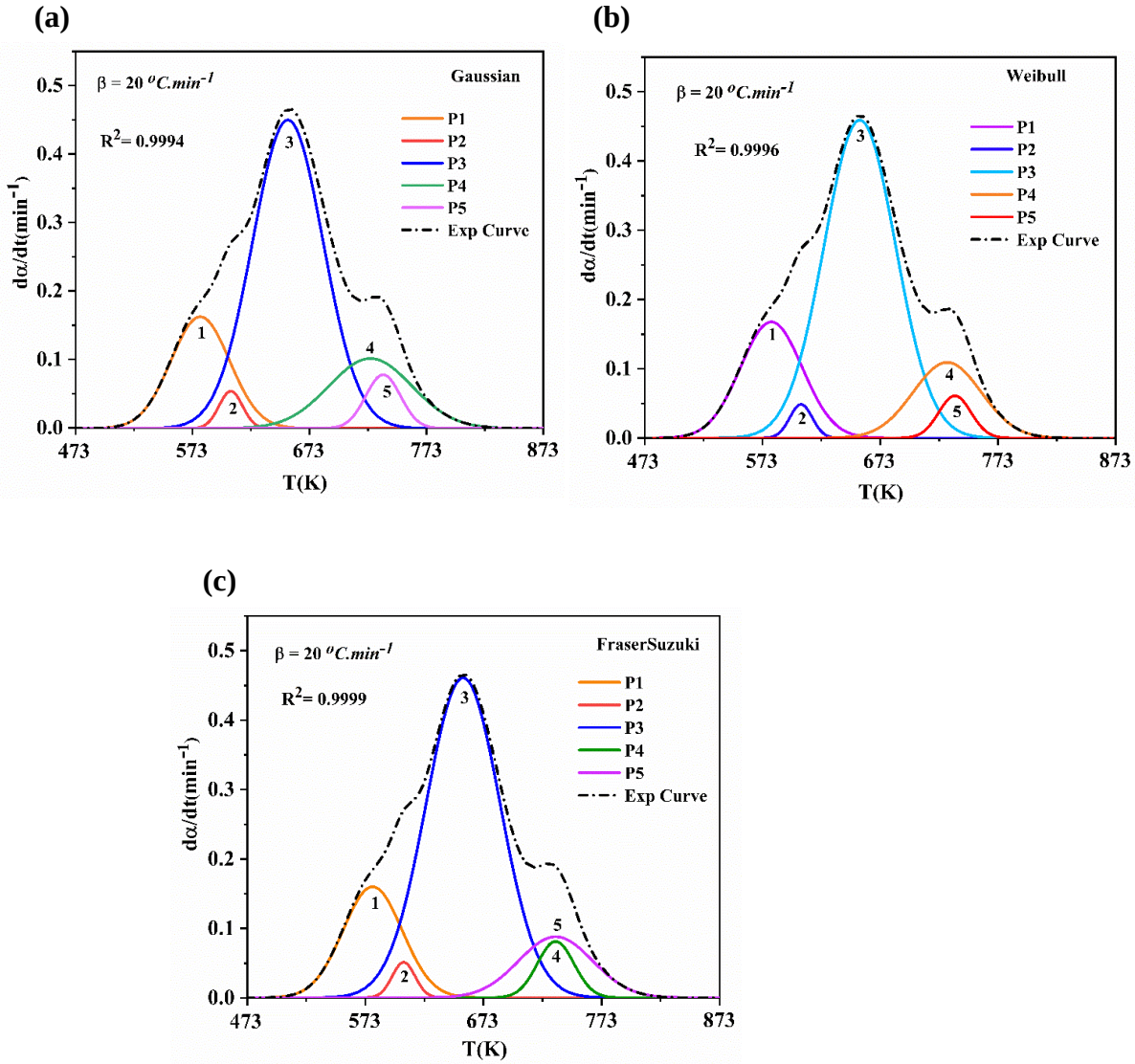

Figure 5.7. Comparison of MDA simulations of **(a)** Gaussian, **(b)** Weibull, and **(c)** FraserSuzuki curves

Moreover, similar transitions were observed for $\beta = 15$, $20\,^{o}C.min^{-1}$, respectively. The heating rate of $\beta = 15\,^{o}C.min^{-1}$, the experimental peak obtained at 652 K in the temperature range 529-710 K has three sub-degradation stages and the third degradation stage, 710-780 K (expT_m=741 K). Furthermore, the temperature range for $\beta = 20\,^{o}C.min^{-1}$, second stage from 527-699 K (exp T_m=656 K), and the third from 699-766 K (T_m=744 K).

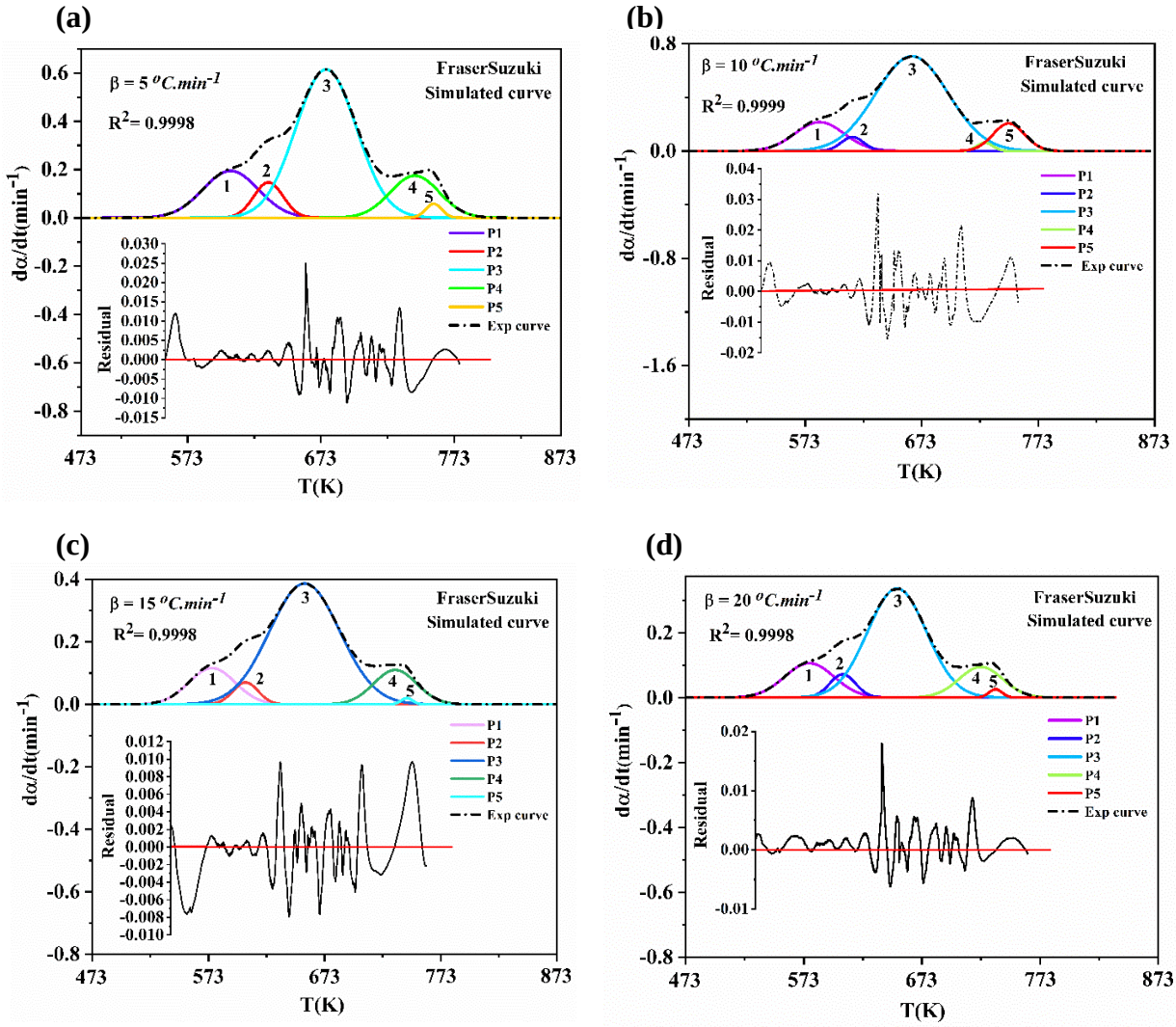

Figure 5.8. Deconvolution of overlapped Ni-Co LDH multi peaks at different heating rates, using Fraser-Suzuki function: **(a)** 5 $^{o}C.min^{-1}$, **(b)** 10 $^{o}C.min^{-1}$, **(c)** 15 $^{o}C.min^{-1}$, and **(d)** 20 $^{o}C.min^{-1}$.

Furthermore, to understand the role of pseudocomponents parameters during Ni-Co LDH degradation, it is important to calculate the activation energies obtained at each conversion with the change in temperature. Fig. 5.5 (a) and (b) represent the activation energies obtained from experimental and simulation results. As discussed, since Friedman and non-linear Vyazovkin produced consistent trends in Ea values, further studies were validated using these two methods. Apparently, it is shown in Fig.5.8 and Table 5.6 that the overall pseudocomponents (P1, P2, P3, P4, and P5, respectively) with the heating rates of

β= 5, 10, 15, 20 $^{o}C.min^{-1}$ from the conversion range from α= 0.25-0.75 undergoes three stage degradation and the activation energies of pseudocomponents denoted as P1, P2 and P3 w.r.t temperature integral were obtained as P1 (103.05-106.92 kJ.mol^{-1}), P2 (107.23-119.41 kJ.mol^{-1}), P3(121.51-168.3 kJ.mol^{-1}). Also, the pseudo peaks denoted as P4 (168.3-165.78 kJ.mol^{-1}) and P5 (165.78-145.68 kJ.mol^{-1}).

Table 5.6. MDA simulation of FraserSuzuki multi-peak analysis

FraserSuzuki	**Peak indexed**	**Peak temperature (T_{max})**	**Standard error**	**RSS**	**Reduced Chi- Sqrt (χ^2)**	**Degrees of freedom**	**R^2**
β= 5 $^{o}C.min^{-1}$, exp T_m= 677 (second stage), and exp T_m= 767 (third stage)	P1	598	0.1950	0.0283	1.403E-5	4441	0.9998
	P2	629	0.0863				
	P3	677	0.0645				
	P4	752	0.0431				
	P5	764	0.0562				
β= 10 $^{o}C.min^{-1}$, exp T_m= 665 (second stage), and exp T_m= 748 (third stage)	P1	585	0.0963	0.0229	1.306E-5	4874	0.9999
	P2	614	0.0677				
	P3	664	0.0328				
	P4	727	0.0735				
	P5	748	0.0851				
β= 15 $^{o}C.min^{-1}$, exp T_m= 652 (second stage), and exp T_m= 741 (third stage)	P1	577	0.0337	0.0317	1.316E-5	4389	0.9998
	P2	605	0.0492				
	P3	651	0.0257				
	P4	723	0.0426				
	P5	735	0.0538				
β= 20 $^{o}C.min^{-1}$,exp T_m= 656(second stage), and exp T_m= 744 (third stage)	P1	576	0.0533	0.0273	1.513E-5	4677	0.9998
	P2	605	0.0588				
	P3	656	0.0252				
	P4	734	0.0731				
	P5	736	0.0483				

Moreover, it has been observed that the maximum activation energies for the second stage were observed in P3, which involves the complete degradation of the interlayer hydroxyl domain, causing the change in Ni-Co LDH crystal symmetry. Similarly, the pseudocomponents for third stage degradation, which affects the entire crystal orientation, corresponding to the degradation of main hydroxide layers i.e., metals bonded to double

hydroxide $M(OH)_2$ start at 168.3-165.78 $kJ.mol^{-1}$ and start decreasing at P4 with the increase in conversion degrees. In summary, it is further validated that the variation in activation energies differs by 8 to 10%, which confirms that the process is a kinetically complex reaction as approved by the experimental calculation. As a result, it can be stated that the pseudocomponents w.r.t heating rates, as well as conversion degrees, follow the degradation order as P3>P1>P2 for the second stage and P4>P5 for the third stage. The overall degradation order follows as P3>P1 or P4>P2>P5. The greater the pseudocomponents, the slower the degradation. Last but not least, when the heating rate increases, the conversion curves of Ni-Co LDH shift slightly to the lower temperature range (Fig.5.3b). As a result, the Ni-Co LDH undergoes a fast degradation process.

5.4. Conclusion

Using the recently synthesized mesoporous Ni-Co LDH, the present study thoroughly investigates how a commonly known Ni-Co LDH exhibits a thermal degradation characteristic described by well-known kinetic models. The evaluation of effective activation energies obtained from various isoconversional methods showed that the overall activation energies required to describe the Ni-Co LDH were best described by either Friedman or non-linear Vyazovkin methods. Also, the estimation of a preexponential factor of Ni-Co LDH degradation showed that the activation energies (E_a) produces a strong linear kinetic compensation effect. Moreover, the experimental and theoretical study revealed that the thermal degradation process of the synthesized mesoporous Ni-Co LDH shows degradation reactions that undergo a process strongly dominated by nucleation models $f(\alpha)$.

From the study point of view, we concluded that thermal characterization of Ni-Co LDH in special reference to kinetic models describing the process is particularly important for understanding the reaction models. The importance of the study doesn't confine only for

obtaining the kinetic triplets but also the basic knowledge of how a material undergoes a transformation, producing thermally transformed di or trivalent metal oxides. Consequently, the M(II) or M(III) LDH oxides produced could be useful for studying applications like solid oxide-based catalysts, temperature dependence electrochemical reactions, ion-exchange reactions, surface adsorption, etc., for other LDHs and Ni-Co LDH in particular.

References

[1] A.W. Coats, J.P. Redfern, Thermogravimetric analysis. A review, Analyst. 88 (1963). https://doi.org/10.1039/AN9638800906.

[2] A. Al-Zubaidi, X. Ji, J. Yu, Thermal charging of supercapacitors: A perspective, Sustain Energy Fuels. 1 (2017). https://doi.org/10.1039/c7se00239d.

[3] S. Vyazovkin, A.K. Burnham, J.M. Criado, L.A. Pérez-Maqueda, C. Popescu, N. Sbirrazzuoli, ICTAC Kinetics Committee recommendations for performing kinetic computations on thermal analysis data, Thermochim Acta. 520 (2011). https://doi.org/10.1016/j.tca.2011.03.034.

[4] M.H. Siddiqi, X. min Liu, T. Qureshi, A.N. Tabish, S. Nawaz, T. Iqbal, Performance analysis of bio-fuel blends for clean energy production: Thermogravimetric analysis, J Clean Prod. 273 (2020). https://doi.org/10.1016/j.jclepro.2020.122936.

[5] X. Zhao, F. Zhang, S. Xu, D.G. Evans, X. Duan, From layered double hydroxides to ZnO-based mixed metal oxides by thermal decomposition: Transformation mechanism and UV-blocking properties of the product, Chemistry of Materials. 22 (2010). https://doi.org/10.1021/cm100383d.

[6] Z. Li, X. Xiang, L. Bai, F. Li, A nanocomposite precursor strategy to mixed-metal oxides with excellent catalytic activity for thermal decomposition of ammonium perchlorate, Appl Clay Sci. 65–66 (2012). https://doi.org/10.1016/j.clay.2012.04.028.

[7] V. Rives, Layered Double Hydroxides: Present and Future, 2001.

[8] M. Laipan, J. Yu, R. Zhu, J. Zhu, A.T. Smith, H. He, D. O'Hare, L. Sun, Functionalized layered double hydroxides for innovative applications, Mater Horiz. 7 (2020). https://doi.org/10.1039/c9mh01494b.

[9] C. Madhusha, K. Rajapaksha, I. Munaweera, M. de Silva, C. Perera, G. Wijesinghe, M. Weerasekera, D. Attygalle, C. Sandaruwan, N. Kottegoda, A Novel Green Approach to Synthesize Curcuminoid-Layered Double Hydroxide Nanohybrids: Adroit Biomaterials for Future Antimicrobial Applications, ACS Omega. 6 (2021). https://doi.org/10.1021/acsomega.1c00151.

[10] F. Li, X. Duan, Applications of layered double hydroxides, Struct Bond. 119 (2005). https://doi.org/10.1007/430_007.

[11] K. Suresh, R.V. Kumar, G. Pugazhenthi, Processing and characterization of polystyrene nanocomposites based on Co–Al layered double hydroxide, Journal of Science: Advanced Materials and Devices. 1 (2016). https://doi.org/10.1016/j.jsamd.2016.07.007.

[12] M. Frunza, G. Lisa, M.I. Popa, N.D. Miron, D.I. Nistor, Thermogravimetric analysis of layered double hydroxides with chloramphenicol and salicylate in the interlayer space, J Therm Anal Calorim. 93 (2008). https://doi.org/10.1007/s10973-007-8381-4.

[13] K. Suresh, M. Kumar, G. Pugazhenthi, R. Uppaluri, Enhanced mechanical and thermal properties of polystyrene nanocomposites prepared using organo-functionalized Ni–Al layered double hydroxide via melt intercalation technique, Journal of Science: Advanced Materials and Devices. 2 (2017). https://doi.org/10.1016/j.jsamd.2017.05.003.

[14] E.C. Moine, M. Tangarfa, M. Khachani, A. el Hamidi, M. Halim, S. Arsalane, Thermal oxidation study of Moroccan oil shale: A new approach to non-isothermal kinetics based on deconvolution procedure, Fuel. 180 (2016). https://doi.org/10.1016/j.fuel.2016.04.076.

[15] S. Vyazovkin, A.K. Burnham, L. Favergeon, N. Koga, E. Moukhina, L.A. Pérez-Maqueda, N. Sbirrazzuoli, ICTAC Kinetics Committee recommendations for analysis of multi-step kinetics, Thermochim Acta. 689 (2020). https://doi.org/10.1016/j.tca.2020.178597.

[16] J.S. Valente, G. Rodriguez-Gattorno, M. Valle-Orta, E. Torres-Garcia, Thermal decomposition kinetics of MgAl layered double hydroxides, Mater Chem Phys. 133 (2012). https://doi.org/10.1016/j.matchemphys.2012.01.026.

[17] S. Velu, V. Ramkumar, A. Narayanan, C.S. Swamy, Effect of interlayer anions on the physicochemical properties of zinc-aluminium hydrotalcite-like compounds, J Mater Sci. 32 (1997). https://doi.org/10.1023/A:1018561918863.

[18] S.W. Rhee, M.J. Kang, Kinetics on dehydration reaction during thermal treatment of MgAl-CO 3-LDHs, Korean Journal of Chemical Engineering. 19 (2002). https://doi.org/10.1007/BF02699312.

[19] P. Saikia, N.B. Allou, A. Borah, R.L. Goswamee, Isoconversional kinetics study on thermal degradation of Ni-Al layered double hydroxide synthesized by 'soft chemical' sol-gel method, Mater Chem Phys. 186 (2017). https://doi.org/10.1016/j.matchemphys.2016.10.028.

[20] Z. Karami, S.M.R. Paran, V.P. Poornima, M.R. Ganjali, M. Jouyandeh, A. Esmaeili, S. Habibzadeh, F.J. Stadler, M.R. Saeb, A comparative study on cure kinetics of layered double hydroxide (Ldh)/epoxy nanocomposites, Journal of Composites Science. 4 (2020). https://doi.org/10.3390/jcs4030111.

[21] Y. Zheng, Y. Chen, Preparation of polypropylene/Mg–Al layered double hydroxides nanocomposites through wet pan-milling: Non-isothermal crystallization behaviour, R Soc Open Sci. 5 (2018). https://doi.org/10.1098/rsos.171070.

[22] N. Koga, S. Vyazovkin, A. K. Burnham, L. Favergeon, N. V. Muravyev, L.A. Perez-Maqueda, C. Saggese, P. E. Sanchez-Jimenez, ICTAC Kinetics Committee recommendations for analysis of thermal decomposition kinetics, Thermochimica Acta 719 (2023). https://doi.org/10.1016/j.tca.2022.179384.

[23] M. A. Amezcua-Allieri, J. Aburto, E. Torres-García, Phenomenological thermokinetic analysis of coffee husk pyrolysis: a study case. *J Therm Anal Calorim* **147** (2022). https://doi.org/10.1007/s10973-022-11392-7.

[24] E. Torres-García, L.F. Ramírez-Verduzco, J. Aburto, Pyrolytic degradation of peanut shell: Activation energy dependence on the conversion, Waste Management. 106 (2020). https://doi.org/10.1016/j.wasman.2020.03.021.

[25] P. Brachi, V. Santes, E. Torres-Garcia, Pyrolytic degradation of spent coffee ground: A thermokinetic analysis through the dependence of activation energy on conversion and temperature, Fuel. 302 (2021). https://doi.org/10.1016/j.fuel.2021.120995.

[26] A. Galano, J. Aburto, J. Sadhukhan, E. Torres-García, A combined theoretical-experimental investigation on the mechanism of lignin pyrolysis: Role of heating rates and residence times, J Anal Appl Pyrolysis. 128 (2017). https://doi.org/10.1016/j.jaap.2017.10.009.

[27] X. Guan, M. Huang, L. Yang, G. Wang, X. Guan, Facial design and synthesis of CoSx/Ni-Co LDH nanocages with rhombic dodecahedral structure for high-performance asymmetric supercapacitors, Chemical Engineering Journal. 372 (2019). https://doi.org/10.1016/j.cej.2019.04.145.

[28] R. Fu, Y. Lu, Y. Ding, L. Li, Z. Ren, X. Si, Q. Wu, A novel non-enzymatic glucose electrochemical sensor based on CNF@Ni-Co layered double hydroxide modified glassy carbon electrode, Microchemical Journal. 150 (2019). https://doi.org/10.1016/j.microc.2019.104106.

[29] S. Li, L. Wang, Y.D. Li, L. Zhang, A. Wang, N. Xiao, Y. Gao, N. Li, W. Song, L. Ge, J. Liu, Novel photocatalyst incorporating Ni-Co layered double hydroxides with P-

doped CdS for enhancing photocatalytic activity towards hydrogen evolution, Appl Catal B. 254 (2019). https://doi.org/10.1016/j.apcatb.2019.05.001.

[30] X. Ma, P. Wei, Y. Yang, H. Kang, D. Guo, L. Liu, One-pot synthesis of Ni-Co layered double hydroxide nanosheets as efficient catalysts for oxygen evolution reaction, Mater Today Commun. 20 (2019). https://doi.org/10.1016/j.mtcomm.2019.100596.

[31] A.R. Sangtam , P. Saikia , R. L.Goswamee , D. Sinha, U.B. Sinha, Green synthesis of mesoporous Ni-Co layered double hydroxide and its application for removal of 2,4-dinitrophenol from water: A theoretical study complemented by the first principle density functional theory-Monte-Carlo approach, Journal of Environmental Chemical Engineering. 10(2022). https://doi.org/10.1016/j.jece.2022.108378.

[32] M. Li, L. Li, S. Lin, Efficient antimicrobial properties of layered double hydroxide assembled with transition metals via a facile preparation method, Chinese Chemical Letters. 31 (2020). https://doi.org/10.1016/j.cclet.2019.09.047.

[33] C.N. Arenas, M.V. Navarro, J.D. Martínez, Pyrolysis kinetics of biomass wastes using isoconversional methods and the distributed activation energy model, Bioresour Technol. 288 (2019). https://doi.org/10.1016/j.biortech.2019.121485.

[34] N. Sbirrazzuoli, L. Vincent, A. Mija, N. Guigo, Integral, differential and advanced isoconversional methods, Chemometrics and Intelligent Laboratory Systems. 96 (2009). https://doi.org/10.1016/j.chemolab.2009.02.002.

[35] B. Janković, B. Adnadević, J. Jovanović, Application of model-fitting and model-free kinetics to the study of non-isothermal dehydration of equilibrium swollen poly (acrylic acid) hydrogel: Thermogravimetric analysis, Thermochim Acta. 452 (2007). https://doi.org/10.1016/j.tca.2006.07.022.

[36] H.L. Friedman, Kinetics of thermal degradation of char-forming plastics from thermogravimetry. Application to a phenolic plastic, Journal of Polymer Science Part C: Polymer Symposia. 6 (2007). https://doi.org/10.1002/polc.5070060121.

[37] T. Akahira, T. Sunose, Method of determining activation deterioration constant of electrical insulating materials, Res Rep Chiba Inst Technol. 16, (1971).

[38] S. Vyazovkin, Advanced isoconversional method, Journal of Thermal Analysis. 49 (1997). https://doi.org/10.1007/bf01983708.

[39] L.A. Pérez-Maqueda, J.M. Criado, Accuracy of Senum and Yang's approximations to the Arrhenius integral, J Therm Anal Calorim. 60 (2000). https://doi.org/10.1023/A:1010115926340.

[40] A. Khawam, D.R. Flanagan, Solid-state kinetic models: Basics and mathematical fundamentals, Journal of Physical Chemistry B. 110 (2006). https://doi.org/10.1021/jp062746a.

[41] J.M. Criado, J. Málek, A. Ortega, Applicability of the master plots in kinetic analysis of non-isothermal data, Thermochim Acta. 147 (1989). https://doi.org/10.1016/0040-6031(89)85192-5.

[42] N. Sbirrazzuoli, Determination of preexponential factor and reaction mechanism in a model-free way, Thermochim Acta. 691 (2020). https://doi.org/10.1016/j.tca.2020.178707.

[43] A. Perejón, P.E. Sánchez-Jiménez, J.M. Criado, L.A. Pérez-Maqueda, Kinetic analysis of complex solid-state reactions. A new deconvolution procedure, Journal of Physical Chemistry B. 115 (2011). https://doi.org/10.1021/jp110895z.

[44] A. MENDIBOURE, R. SCHOELLHORN, ChemInform Abstract: Formation and Anion Exchange Reactions of Layered Transition Metal Hydroxides (Ni1-

xMx)(OH)2(CO3)x/2(H2O)z (M: Fe, Co)., ChemInform. 18 (1987). https://doi.org/10.1002/chin.198723038.

[45] Y. Li, X. Wu, S. Wang, W. Wang, Y. Xiang, C. Dai, Z. Liu, Z. He, X. Wu, Surfactant-assisted solvothermal synthesis of NiCo2O4 as an anode for lithium-ion batteries, RSC Adv. 7 (2017). https://doi.org/10.1039/c7ra06172b.

[46] K. Zhu, Y. Gao, X. Tan, C. Chen, Polyaniline-Modified Mg/Al Layered Double Hydroxide Composites and Their Application in Efficient Removal of Cr(VI), ACS Sustain Chem Eng. 4 (2016). https://doi.org/10.1021/acssuschemeng.6b00922.

[47] B. Wang, F. Xu, P. Zong, J. Zhang, Y. Tian, Y. Qiao, Effects of heating rate on fast pyrolysis behavior and product distribution of Jerusalem artichoke stalk by using TG-FTIR and Py-GC/MS, Renew Energy. 132 (2019). https://doi.org/10.1016/j.renene.2018.08.021.

[48] P.E. Sánchez-Jiménez, L.A. Pérez-Maqueda, A. Perejón, J.M. Criado, Generalized master plots as a straightforward approach for determining the kinetic model: The case of cellulose pyrolysis, Thermochim Acta. 552 (2013). https://doi.org/10.1016/j.tca.2012.11.003.

CHAPTER 6

Summary and conclusion

This chapter presents an overview of the LDHs summary and conclusion. The general scope of the work in terms of current research applications are discussed.

In summary, it can be said that LDHs are well-known nanostructured inorganic layered solids that makeup one of the most well-known polytype families. Moreover, the term 'LDHs' are frequently used as a substitute name to describe any layered materials, such as anionic clays or brucite minerals. The inherent unique properties of the LDHs are that the host metallic layers of the metal hydroxide sheets are composed of positively charged ions with interlayer ions in between them. These interlayer ions are exchangeable in nature and are connected by weak hydrogen, covalent, or Van der Waals interactions. It is well known that LDHs, because of their versatility, flexibility, and tunability, make the material a potential precursor for the study of various chemical applications including environmental chemistry, photochemistry, catalysis, electrochemistry, medicine, intercalation, antibacterial, thermal, biochemistry, sensors, fuel cells, etc. Besides, due to their versatility, LDHs exhibit remarkable properties such as high ion-exchange, optical, catalytic oxidation or reduction, memory effect, etc. The advantages of LDHs, which distinguish them from other materials, are that they are facile to prepare, cost-efficient, generally inexpensive, and less toxic than most hazardous compounds. Therefore, such materials can be potential precursors in advanced nanoscience and material chemistry applications.

Furthermore, the current studies emphasize evaluating the functional properties of some of the selected LDHs in terms of their practical applications like adsorption, intercalation, thermokinetic, and antimicrobial. Moreover, the synthesized LDHs compound can be further used for the study of several nano or material science applications like catalyst precursors, supercapacitors, drug carriers, computational modeling and docking mechanisms, classical mechanics, quantum computation, enhanced water splitting, fuel cells, superconductors, sensors, quantum dots, medicine etc.

6.1. Significant findings of the present research

Layered double hydroxides (LDHs) are multifunctional nanomaterials with broad applicability in nanoscience, clay science, and material science. In the current studies, some of the remarkable findings are listed below:

- The present synthetic protocol using a non-aqueous "soft chemical" Sol-Gel route with ethanol and acetone mixture as "mild organic solvents" have successively been treated as an alternative green approach for synthesizing different LDHs. The advantage of the protocol is the inhibition/solubilization of CO_2 gas (minimizes carbonate formation) or any other unwanted contaminants on the bimetallic LDHs matrix, which could avoid some drawbacks. Moreover, this method is considered economical and cost-effective due to the use of fewer solvents and prevents huge loss of solvents from evaporation. The unique feature of the present method is the control synthesis of particle size, and the LDHs synthesized using this method bears a diverse pores morphology and result in a crystalline LDHs phase.
- The methodology is further enhanced using the metal acetylacetonates as our primary precursors. The superiority or advantage of using such precursors is that it is less toxic, volatile (acetyl group), and can be easily hydrolyzed at moderate temperature (65-95°C) in non-aqueous media compared to LDHs synthesized in the highly alkaline reaction/aqueous phase at the higher temperature. Also, unlike other precursors, there is a formation of acetylacetonate as a by-product, which can be easily separated from filtration and low-temperature distillation.
- The adsorption application study of the mesoporous Ni-Co LDH towards 2,4-dinitrophenol removal revealed that the LDHs are known to be potential adsorbents against various organic or inorganic species. The fascinating property of LDH materials is that they can be regenerated or reused to improve the better adsorption

cycles. The adsorption properties of LDHs can be enhanced by producing a porous structure. Calcination or intercalation of guest molecules/ions could help improve the adsorption properties of LDHs.

- The antibacterial inhibition study of the Co(II)-Co(III) LDH and its intercalated organic LDH nanohybrid ($C_5H_8O_2$@LDH) showed that the LDHs are well known to possess bactericidal properties due to the nature of antimicrobial metallic elements, nanoparticles size and synergistic effects. The better inhibition properties against the microbial species can be observed with the intercalated LDH nanohybrids.
- The thermokinetic investigation of the mesoporous Ni-Co LDH showed that the thermal degradation stages/pathway of LDHs are indeed described by the presence of individual peaks, called the "pseudocomponents". Hence, it undergoes a kinetically complex process. Moreover, the reliability in determining the thermal degradation mechanisms/reactions of LDHs can be increased using non-isothermal TGA/DSC data rather than single isothermal heating data due to flexibility in the temperature range. Basically, one should use isoconversional models/models-free kinetics as fundamental approaches for determining reaction mechanisms or kinetic parameters.

6.2. Future scope of studies

The present studies further extend the usefulness of compounds like intercalation and crystallography applications.

6.2.1. Intercalation chemistry of a novel Co(II)-Co(III) LDH and Ac@ Co(II)-Co(III) LDH nanohybrid

The term “intercalation” means grafting guest ions or molecules into LDHs structure. It is known that intercalation chemistry plays an important role in the ion-

exchange mechanisms. In the current context, the efforts to make the inorganic-organic hybrid are at the pace of developing a new hybrid LDHs nanocomposite and using these to understand the various chemical applications in advanced nanomaterials science. Essentially, it is noteworthy to mention that the development of new hybrid functionalized LDH materials by the intercalation reactions dramatically influences the electronic, optical, thermal, water-splitting, catalytic, and ion-exchange properties of the host LDHs molecule and so on. Nowadays, intercalation chemistry plays a vital role in the delamination or exfoliation of LDHs layer. In such a situation, the introduction or grafting of guest molecules into LDHs matrix results in interposed polymer nanocomposite or delaminated structure. The delamination chemistry is, in fact, a great engineering protocol for obtaining the exfoliated LDHs layer into a single exposed nanosheet. This helps in the synthesis of thin films and has a potential role in polymer chemistry, catalyst, supercapacitors, batteries etc. As aforementioned, LDHs, due to their flexibility or tunability nature and ion-exchange role, a range of various possible ions (organic, inorganic ions or hybrid molecules), also including biomolecules (DNA, RNA, fats, lipids, carbohydrates, proteins, drugs) can be interleaved in the bimetallic hydroxide layers substantially. This is because LDHs have the ability to intercalate/adsorb most chemical species in the interlayer domain resulting in the intercalated complex. However, in some cases, there is a shape or size-selective adsorption of some molecules based on the electrophile or nucleophilic affinity of the guest and the host molecule. There are various available techniques used in the characterization of intercalated LDHs complexes like *in situ* XRD measurements, nuclear magnetic resonance (NMR), Infrared spectroscopy (IR), photoelectron spectroscopy (XPS) etc. In the present study, intercalation studies were carried out to understand the guest-host interaction mechanism of the synthesized LDH compounds and their practical applications. Moreover, the present studies further extend how the intercalation of certain ions or

molecules affects the morphology of LDHs. Additionally, the so-called computational modeling or simulation studies would better help understand the intercalation mechanism. Unfortunately, due to some delay in modeling results, the data obtained has not been presented, and the studies are underway.

6.2.2. Crystallography studies of a novel Co(II)-Co(III) LDH

Crystal structure solution is key for understanding simple or complex crystal systems. In solid-state physics (condensed matter physics) and materials chemistry, X-ray diffraction (XRD) techniques are fundamentally used to describe materials and identification of new materials. Identification of unknown materials using ordinary XRD techniques has been a vast limitation that has so far been encountered throughout the past decades. In the modern era, the determination of newly synthesized compounds using a reliable, sophisticated XRD significantly impacts solving the structural (solids) problem. Therefore, using the recommended structure solution is essential from the viewpoint of the current investigation. In general, certain criteria are required for the crystal structure solution, such as high-quality XRD data, phase identification, indexing, space group determination, refinement, and so on. The use of well-trusted and informative crystal software will increase the reliability of solving a structure problem. Nowadays, a range of software including checkcell, Avogadro, Macmaille, GSAS-II, Jana, Fox, Rietica, Vesta, Atoms, Crystal impact, Powdercell etc. are some of the recommended programs used in indexing, refinement, and visualization of crystal structures. In the present study, some basic information about crystal structure solutions for some of the selected LDHs structures has been thoroughly studied. However, due to some modeling and data analysis delays, the studies have not been completed at the stipulated time. However, the investigations are still underway and will be resumed for further studies in the upcoming days.

APPENDIX

a) Workshop, poster & papers presentation

1. National workshop attended at "*Advanced Techniques in Nano Science and Technology*", Mohali- 160062, Sponsored by Department of Science and Technology, Government of India, 13-16th December 2017.

2. Poster presented at National Seminar on *"Chemistry in Interdisciplinary Research" (NSCIR-2017)*, Organized by Department of Chemistry, Nagaland University, Lumami-798627, 16-17th March 2017.

3. Paper presented at National Seminar on *"Chemistry in Interdisciplinary Research" (NSCIR-2018)*, Organized by Department of Chemistry, Nagaland University, Lumami-798627, 9-10th November 2018.

4. National scientific oral presented at "*Recent Advances in Nano Science and Technology*", Mohali- 160062, Sponsored by Department of Science and Technology, Government of India, 19-21th December 2017.

b) List of Publications

1) **Apuchu R Sangtam**, Pinky Saikia, Rajib Lochan Goswamee, Dipak Sinha, Upasana Bora Sinha, **Green synthesis of mesoporous Ni-Co layered double hydroxide and its application for removal of 2,4-dinitrophenol from water: a theoretical study complemented by the first principle density functional theory-Monte-Carlo approach**. *J. Environ. Chem. Eng.* 10 (2022), 108378. https://doi.org/10.1016/j.jece.2022.108378.

2) **Apuchu R Sangtam**, Kikoleho Richa, Pinky Saikia, Naruti Longkumer, Upasana Bora Sinha, Rajib Lochan Goswamee, **Synthesis and characterization of Co(II)–**

Co(III) LDH and Ac@Co(II)–Co(III) LDH nanohybrid and study of its application as bactericidal agents. *Results in Chemistry* 4 (2022), 100671. https://doi.org/10.1016/j.rechem.2022.100671.

3) **Apuchu R Sangtam**, Pinky Saikia, Rajib Lochan Goswamee, Upasana Bora Sinha, **A non-isothermal thermokinetic degradation study of the mesoporous Ni-Co layered double hydroxide using isoconversional approaches** (Under Revision).